EFFECTS OF TOROIDAL FIELD RIPPLE ON PLASMA ION CONFINEMENT IN A TOKAMAK

（トカマクのプラズマ・イオン閉じ込めに及ぼす
トロイダル磁場リップル効果）

Keiji TANI

EFFECTS OF TOROIDAL FIELD RIPPLE ON PLASMA ION CONFINEMENT IN A TOKAMAK

(トカマクのプラズマ・イオン閉じ込めに及ぼすトロイダル磁場リップル効果)

Keiji TANI

Abstract

Computational studies on the confinement of fast ions in a tokamak with toroidal field ripple have been made by means of a newly developed orbit-following Monte-Carlo code. It is found that collisionless behavior of fast ions relating to ripple trapping, ripple detrapping and ripple-enhanced banana drift is of essential importance in the loss process of fast ions. The collisionless ripple trapping and ripple-enhanced banana drift produce a large number of loss bands in velocity space and enhance the loss of fast ions. The amount of loss particles due to respective loss process is significantly influenced by the effect of finite banana size of fast ions. The ripple-induced loss of fast ions produced by quasi-perpendicular NBI in a reactor grade tokamak is evaluated by using the orbit-following Monte-Carlo code. In order to hold down the ripple loss of fast ions during slowing down to be less than 10 % of the total, the injection angle $|90 - \theta_{inj}| > 20^{\circ}$ and the maximum field ripple $\delta_0 < 0.5\%$ for typical plasma parameters. Ripple-trapped particles enter specific narrow areas of the first wall in the course of their gradient-B drift and cause a significantly large heat loading. Localized heat loads due to

ripple-trapped loss fast ions in the case of quasi-perpendicular NBI may reach a magnitude of 1 MW/m^2 for the next generation tokamak. Even in the presence of ripple, charged fusion products are well confined in a device. The ripple enhanced power loss of alphas during slowing down amounts to 10 % in a reactor grade tokamak with a toroidal field ripple of $\delta_0 \sim 1$ %. Ripple-enhanced banana drift dominates the loss process of alpha particles. The ion heat conductivity in a rippled toroidal field is also investigated numerically by the same code. It is found that the collision frequency transition of the numerical χ_i^{RT} from the collisional to the collisionless regime occurs at the frequency much higher than the theoretical prediction. Consequently, the numerical χ_i^{RT} is about one or two orders of magnitude smaller than the theoretical one in the low collisionality regime. Besides the two reasons for the small heat conductivity which have been assigned previously, the collisionless ripple detrapping and the effectively high drift frequency for particles with $E = 4$ to $6T_i$ which mainly contribute to the ion heat transport, it is found in the present investigation that the singular orbit of barely ripple-trapped particle may reduce the ripple transport. The resulting ripple induced ion heat conductivity has a much weaker temperature dependence of T_i^2 at most. For this reason, rather large value of field ripple ($\delta_0 \sim 5$ %) is required for the control of burning plasma temperature ($T_B \sim 15$ keV).

CONTENTS

§ 1. Introduction

Searching for the energy resources semipermanently available to the mankind, investigations of the controlled thermonuclear fusion have made a rapid progress in the last decade. The machine playing a leading role of the magnetic confinement fusion research is the well-known "tokamak". On the basis of recent studies, large tokamaks are presently under construction in several countries (JT-60 in Japan, TFTR in USA, JET in EC and T-15 in USSR). It is world-widely expected that these large tokamaks are sure to provide the conclusive information on how to obtain the ignition plasma, that is, the establishment of the scientific feasibility of fusion. In the subsequent phase of the research, some experimental reactors (FED in USA, FER in Japan and INTOR by IAEA) are in the design stage with an aim to grasp problems on the establishment of the technological feasibility of fusion.

In the early research of tokamak experiments, there have been discovered many important and unexpected phenomena relating to high temperature plasma ($T_i, T_e > 1\ keV$). These phenomena have been elusidated in many experiments. In addition, theoretical or computational studies have been useful and become indispensable for the interpretation and expectation of those experimental results. Although the scientific foundation for the construction of large tokamaks mentioned above seems to have been established by the co-operation of experimental and theoretical investigations, there still remain several unresolved and unexperienced problems. In the design of those reactor-grade large tokamaks in planning as well as under

construction, there are many scientific or technological considerations such as the energy confinement time, the effective heating method, the ash exhaust, the β limitation, the control of burning plasma temperature, the heat load of the first wall, the tritium breeding, the shielding of neutrons, etc. Concerning these problems, a lot of information beyond the present experimental data is necessary for the design of reactor-grade tokamaks. In order to obtain the required information, computational investigations by means of many kinds of simulation code have been employed. Therefore, computational study is now considered as not only giving the key development of magnetic fusion research but also making the main contribution to the design of fusion devices.

One of the main advantages of tokamak is that its magnetic field is essentially axisymmetric. In a real tokamak system, however, there is no other way but to choose the finite number of toroidal field coils, because of what is feasible in constructing the machine. This results in a non-axisymmetric component of toroidal magnetic field which is called a "ripple". The toroidal field ripple is directly related to some of those considerations mentioned above. For example, the energy confinement of high temperature plasma is greatly influenced by the ripple enhanced transport. The loss processes of injected beam ions and charged fusion products might be dominated by the field ripple. The ripple induced transport has been considered to be available for the control of burning plasma temperature. The ripple enhanced loss of bulk plasma ions, injected beam ions and fusion-produced alpha particles may cause a dangerous heating of the first wall exposed to the plasma. Therefore, the toroidal field ripple has attracted special interest recently, and some theoretical and experimental investigations have been performed.

Influence of the toroidal field ripple on a plasma confinement has been extensively investigated from the view point of ripple diffusion[1),2)]. Charged particles once trapped into a ripple well via Coulomb collisions undergo the gradient-B drift[3)] and move perpendicularly with respect to the torus mid-plane until they are detrapped from the well by pitch angle scattering. In the classical theories, this radial displacement due to collisional ripple-trapping and detrapping has been considered as the basic process of ripple diffusion (the ripple-trapped diffusion). While, the toroidal field ripple can also have a significant effect on banana particles even if they are not trapped in a ripple well. In an axisymmetric field, the radial displacement due to gradient-B drift in the upper and the lower side of the mid-plane completely offset each other. In the presence of ripple, however, they cannot be cancelled and the unbalanced radial displacement causes another kind of ripple induced transport. The theoretical studies[4),5)] subsequent to the above ripple-trapped diffusion have revealed this kind of ripple-enhanced banana-drift diffusion.
According to these theories, the ripple induced transport may result in deleterious effects on the confinement of a high temperature collisionless plasma, so that the extremely low level of the field ripple is required for the design of future tokamaks. Recently, however, a renewed, another attention is paid on the ripple diffusion as a possible tool of the burning plasma control in tokamak fusion reactors. It has been predicted, based on the previous ripple-trapped diffusion theory, that the thermal instability of D-T burning plasmas can be stabilized by the field ripple control[6),7),8)].

On the other hand, few experimental works for the ripple diffusion have been made in the machines Alcator A[9)] and ISX-B[10),11)]. In Alcator A,

the depletion of the high energy component of bulk plasma ions due to ripple was observed by perpendicular charge exchange measurements. In ISX-B, the deterioration of ion energy confinement due to ripple was evaluated by comparing the ion temperature in similar beam-heated discharge with 9 and 18 toroidal field coils. The field ripple δ is generally defined by $\delta \equiv (B_\varphi^{max} - B_\varphi^{min})/(B_\varphi^{max} + B_\varphi^{min})$ where B_φ^{max} and B_φ^{min} are the maximum and minimum values of the toroidal field along a toroidal field line. The ripple δ in ISX-B with 9 TF coils is 1.6% at the plasma center and 10% at the edge (the plasma surface outboard, in the mid-plane), and with 18 TF coils δ = 0.01% at the plasma center and 0.7% at the edge. The uncertainty in ion temperature measurements and the complexity of the ripple effects on plasma ion confinement make the interpretation of experimental results to be very difficult. Consequently, these experiments do not demonstrate conclusively yet that ripple transport agrees with the theoretical prediction.

Another important feature of toroidal field ripple is the reduction of the confinement of suprathermal particles such as perpendicularly injected beam ions and banana-trapped alpha particles. Enhanced beam penetration by ripple, the so-called ripple injection, has also been proposed[12),13)]. A few experimental works were carried out in ISX-B concerning the ripple loss of fast ions produced by neutral beam injection[10),11)]. Concurrently with the experiment of the bulk plasma diffusion by ripple described above, the loss of fast ions was measured by charge exchange analyzer in ISX-B and a sharp decrease in fast neutral flux for 9-TF-coil operation was detected. It was also observed that the central temperature of beam heated plasma (1.1 MW) dropped from 840 eV with 18 TF coils to 460 eV with 9 TF coils. On this problem, however, only a few theoretical or computational works[14),15)] have

been made and the behavior of fast ions in a rippled toroidal field remains unresolved. Hence, the present state of the study on this problem is still open to be investigated for the design of the next-generation tokamaks.

The toroidal field coil system is one of the major components of tokamaks. The maximum allowable toroidal field ripple is a determining factor of the size and number of the coils. In the estimation of allowable field ripple, there are several indispensable considerations. First, the estimation of the ripple enhanced loss of fast ions produced by neutral beam injection must be made. Since ripple-associated loss of fast ions strongly depends on the birth point in velocity space, the allowable or critical injection angle is also a significant problem. Secondly, the ripple loss of suprathermal charged fusion products during slowing down should be investigated carefully, because the machine with low efficiency of alpha particle confinement is very difficult to be a reactor. Thirdly, we must evaluate the ripple induced transport of the bulk plasma ions which might influence greatly the plasma heating scenarios for thermonuclear ignition as well as the control of burning plasma temperature.

Generally, ions in a tokamak move periodically around the magnetic axis, colliding with plasma particles. The theoretical treatment of the collisional process of ions is described by the bounce averaged Fokker-Planck equations. Particles in a field ripple, however, show a very complicated motion[16),17)] which makes it impossible to average the Fokker-Planck equation over a bounce motion. For this reason, we have developed an orbit-following Monte-Carlo simulation code[15),16),17),18)] in which the behavior of ions undergoing Coulomb interactions in a rippled toroidal field is completely described. The purpose of this paper is to investigate

all the problems mentioned above extensively and systematically by using the newly developed Monte-Carlo code. Especially, the effects of ripple-modulated particle orbits on the transport phenomena of plasma ions are carefully studied. Theoretical investigations are also made complementally.

Consequently, in the present studies obtained is a lot of important information on the allowable level of the field ripple for the containment of both injected beam ions and charged fusion products, on the critical injection angle and on the necessary amount of the field ripple to control the burning plasma in a reactor tokamak.

In section 2, calculation model for the orbit-following Monte-Carlo code is described. The basic collisionless behaviors of fast ions in a field ripple discovered in the present investigations are given in section 3. The ripple-associated fundamental properties of fast ions in a collisional plasma are presented in section 4. Ripple loss of fast ions produced by quasi-perpendicular neutral beam injection is described in section 5. Calculation results for the ripple loss of charged fusion products during slowing down are explained in section 6. Some considerations on the ripple diffusion of bulk plasma ions and the feasibility of burn control by using toroidal field ripple are given in section 7. Conclusions of the present investigations are summarized in the last section.

References

1) T.E. Stringer: Nucl. Fusion 12 (1972) 689.

2) J.W. Connor and R.J. Hastie: Nulc. Fusion 13 (1973) 221.

3) L. Spitzer: "*Physics of Fully Ionized Gases*" (2nd Ed. Interscience, New

York, 1967) 6.

4) J.N. Davidson: Nucl. Fusion 16 (1976) 731.

5) K.T. Tsang: Nucl. Fusion 17 (1977) 557.

6) JAERI Fusion Research and Development Center, INTOR Workshop Report, Group 12, JAERI-M 8625 (1980).

7) T.W. Petrie and J.M. Rawls: Nucl. Fusion 20 (1980) 419.

8) M. Sugihara, M. Kasai, T. Tazima, T. Tone, K. Maki: J. Nucl. Sci. Technol. 17 (1980) 729.

9) M. Greenwald, J.J. Schuss, D. Cope: Nucl. Fusion 20 (1980) 783.

10) J.S. Lyon *et al.*: "ISX-B Ripple Studies", Fusion Energy Division Annual Progress Report for Period Ending December 31, 1980, ORNL-5674 (1981)

11) S.D. Scott *et al.*: "Ripple Studies", Fusion Energy Division Annual Progress Report for Period Ending December 31, 1981, ORNL-5843 (1982)

12) D.L. Jassby and R.J. Goldston: Nucl. Fusion 16 (1976) 613.

13) R.J. Goldston and D.L. Jassby: Princeton Plasma Physics Lab. Rep. MATT-1244.

14) G.G. Lister, D.E. Post and R.J. Goldston: *Proc. 3rd Symposium on Plasma Heating in Toroidal Devices, Varenna,* (1976) 303.

15) K. Tani, H. Kishimoto and S. Tamura: *Proc. 9th European Conf. on Controlled Fusion and Plasma Physics, Oxford,* Vol. 1 (1979) 157.

16) K. Tani, H. Kishimoto and S. Tamura: *Proc. 8th Int. Conf. Plasma physics and Controlled Nuclear Fusion Research, Brussels,* 1980, Vol. 1 IAEA, Vienna (1981) 631.

17) K. Tani, M. Azumi, H. Kishimoto, S. Tamura: J. Phys. Soc. Japan 50 (1981) 1926.

18) K. Tani, T. Takizuka, M. Azumi, H. Kishimoto: Nucl. Fusion 23 (1983) 657.

§ 2. Basic Model for Numerical Analysis

2-1. Introduction

The thermalization process of fast ions is described by the drift kinetic equations with Fokker-Planck collision terms of Landau form. In an axisymmetric system, the projection chart of the collisionless guiding center orbit on a poloidal cross section shows a completely closed contour. This enables us to solve analytically the above mentioned equations after linearizing and averaging them over the bounce time of fast ions. Many authors have adopted this method to solve the slowing-down process of fast ions produced by NBI[1)-4)] or charged fusion products[5)]. In the presence of ripple, however, the guiding center orbit never closes and consequently the loss process of fast ions is seriously affected by the unclose collisionless orbits. This makes it very difficult to apply the theoretical method to solve the relaxation process of fast ions in a non-axisymmetric system. To make a precise treatment of this kind of problem, an orbit-following Monte-Carlo simulation code has been newly developed, in which the calculation of Coulomb collisions is executed at every several time steps of orbit calculation (1/10~1/50 bounce time) until the test particle slows down to the local ion temperature of bulk plasma.

For the convenience of calculations, following assumptions are made in our orbit-following Monte-Carlo code. The plasma is assumed to be circular in cross section with minor radius a and all the magnetic surfaces are

concentric circles. The effects of electric potential in a plasma as well as the finite β on ion orbits might be important. However, the main purpose of the present investigation is to make it clear the primary influence of ripple on the confinement of fast ions. Accordingly, these problems are beyond our scope and left for future studies. The background plasma parameters are assumed to be immutable during the slowing-down time τ_s.

In the present section, the model magnetic field with ripple for the calculation of ion trajectory, the equations of guiding center orbit and the Coulomb collision model using Monte-Carlo techniques are explained.

2-2. Model magnetic field in a tokamak with toroidal field ripple

The magnetic field in a tokamak with finite number of toroidal field coils can be described by

$$\vec{B} = B_r(r,\theta,\varphi)\vec{e}_r + B_\theta(r,\theta,\varphi)\vec{e}_\theta + B_\varphi(r,\theta,\varphi)\vec{e}_\varphi \ , \qquad (2\text{-}1)$$

where r, θ are polar co-ordinates in the minor cross section of the torus, φ is the toroidal angular co-ordinate along the magnetic axis as shown in Fig.2-1 and $\vec{e}_r$, $\vec{e}_\theta$, $\vec{e}_\varphi$ are the respective unit vectors. The toroidal, poloidal and radial components of the magnetic field are given by

$$B_\varphi = \bar{B}_\varphi(r,\theta) + \tilde{B}_\varphi(r,\theta,\varphi) \ , \qquad (2\text{-}2\text{-}1)$$

$$B_\theta = \bar{B}_\theta(r,\theta) + \tilde{B}_\theta(r,\theta,\varphi) \ , \qquad (2\text{-}2\text{-}2)$$

$$B_r = \tilde{B}_r(r,\theta,\varphi) \ . \qquad (2\text{-}2\text{-}3)$$

Here $\bar{B}_\varphi$ and $\bar{B}_\theta$ are the axisymmetric components of the toroidal and poloidal magnetic field, respectively, and are taken as

$$\bar{B}_\varphi = \frac{R_t}{R} B_t \ , \tag{2-3-1}$$

$$\bar{B}_\theta = \frac{R_t}{R} B_p(r) \ , \tag{2-3-2}$$

with R_t the major radius, B_t the toroidal magnetic field on the magnetic axis, $R = R_t + r\cos\theta$, and B_p the poloidal field produced by plasma current in a cylindrical model. For the calculation of ripple components of the magnetic field in eqs. (2-2-1) ~ (2-2-3), $\tilde{B}_\varphi$, $\tilde{B}_\theta$ and $\tilde{B}_r$, we consider a model toroidal coil current which is a sheet current on a torus as shown in Fig.2-2. The distribution of the current is of the form

$$j_t(\theta,\varphi) = \frac{I_0}{2\pi} \frac{1}{R_t + r_c(\theta)\cos\theta} (1 + \Delta\cos N_t\varphi) \ , \tag{2-4}$$

where $r_c(\theta)$ is the distance from the magnetic axis to the toroidal field coil, I_0 the total ampere turns, Δ the proportion of the ripple current, and N_t the number of toroidal field coils.

With the model current described above, the respective field ripple can be derived by the method of Biot-Savart as follows;

$$\tilde{B}_\varphi = \cos N_t\varphi \frac{\mu_0}{4\pi} \oint_{\varphi,\theta} \frac{\tilde{j}_t'}{|\vec{r} - \vec{r}'|^3} [(Z_c - r\sin\theta)\cos\varphi' \alpha_x + (R_t + r\cos\theta - R_c\cos\varphi')\alpha_y] \cos N_t\varphi' ds' \ , \tag{2-5-1}$$

$$\tilde{B}_\theta = \sin N_t\varphi \frac{\mu_0}{4\pi} \oint_{\varphi,\theta} \frac{\tilde{j}_t'}{|\vec{r} - \vec{r}'|^3} [(R_t\cos\theta - Z_c\sin\theta + r)\alpha_x + R_c\sin\theta\alpha_y] \sin\varphi' \sin N_t\varphi' ds' \ , \tag{2-5-2}$$

$$\tilde{B}_r = \sin N_t\varphi \frac{\mu_0}{4\pi} \oint_{\varphi,\theta} \frac{\tilde{\jmath}'_t}{|\vec{r} - \vec{r}'|^3} [(R_t \sin\theta + Z_c \cos\theta)\alpha_x + R_c \cos\theta \alpha_y] \sin\varphi' \sin N_t\varphi' ds' , \qquad (2\text{-}5\text{-}3)$$

where

$$\tilde{\jmath}'_t = \frac{I_0}{2\pi} \frac{\Delta}{R_t + r_c(\theta')\cos\theta'},$$

$$R_c = R_t + r_c(\theta')\cos\theta' ,$$

$$Z_c = r_c(\theta')\cos\theta' ,$$

$$\alpha_x = [\chi(\theta')\cos\theta' - \sin\theta'] / \sqrt{1+\chi^2(\theta')} ,$$

$$\alpha_y = [\chi(\theta')\sin\theta' + \cos\theta'] / \sqrt{1+\chi^2(\theta')} ,$$

$$ds' = r_c(\theta') \sqrt{1+\chi^2(\theta')} [R_t + r_c(\theta')\cos\theta'] d\theta' d\varphi' ,$$

$$\chi(\theta') = \frac{1}{r_c(\theta')} \frac{dr_c(\theta')}{d\theta'} ,$$

$$\vec{r} = (r, \theta, \varphi) ,$$

$$\vec{r}' = (r_c(\theta'), \theta',, \varphi') ,$$

and μ_0 is the permeability in the vacuum. The proportion of the ripple current Δ is approximately estimated from the first term of the Fourier expansion of toroidal coil current with respect to toroidal angle, that is,

$$\Delta \sim \frac{4}{N_t\varphi_c} \sin\frac{N_t\varphi_c}{2} ,$$

where φ_c is the average sector angle of a toroidal coil. With these expressions, the peak-to-average field ripple δ in tokamaks can be defined as

$$\delta\ (r,\theta) = \frac{\tilde{B}_\varphi\ (r,\theta,0)}{\bar{B}_\varphi\ (r,\theta)}. \qquad (2\text{-}6)$$

The ripple size proper to the machine δ_0 which indicates the maximum field ripple in a plasma in usual tokamaks, is given by

$$\delta_0 = \delta\ (a,0)\ ,$$

where a is the plasma minor radius. Contours of constant field ripple δ calculated by eq.(2-6) is shown in Fig.2-3 for the model coil system shown in Fig.2-2 with eighteen ($N_t = 18$) toroidal field coils which is appropriate to JT-60 (JAERI large tokamak). The result agrees well with the numerically derived one in actual coil system[6].

2-3. Guiding center equations

Ion trajectories are followed by numerical integration of the standard guiding center equations of motion[7] in a rippled toroidal field described in the last subsection. The guiding center equations are

$$\vec{v}_g = \frac{1}{Z_t e}\left(\mu_m + \frac{m_t}{B} v_{g\parallel}^2\right)\frac{\vec{B}}{B}\times\frac{\nabla B}{B} + \frac{\vec{B}}{B} v_{g\parallel}\ , \qquad (2\text{-}7\text{-}1)$$

$$\frac{dv_{g\parallel}}{dt} = -\frac{\mu_m}{m_t}\frac{\partial B}{\partial l}\ , \qquad (2\text{-}7\text{-}2)$$

where $v_{g\parallel}$ and $v_{g\perp}$ are the guiding center velocities parallel and perpendicular to the magnetic field line, l the length along the field line, m_t the charged particle mass, Z_t the charge number , $e = 1.6\times10^{-19}C$,

$$\mu_m = \frac{m_t v_\perp^2}{2B} ,$$

$$B = \sqrt{(\bar{B}_\varphi+\tilde{B}_\varphi)^2 + (\bar{B}_\theta+\tilde{B}_\theta)^2 + \tilde{B}_r^2}, \qquad (2\text{-}8)$$

respectively. In usual tokamak ordering

$$\frac{\tilde{B}_\varphi}{B} \sim \frac{\tilde{B}_\theta}{B} \sim \frac{\tilde{B}_r}{B} \sim \Delta^2, \text{ and}$$

$$\frac{\bar{B}_\theta}{B} \sim \frac{r}{R_t q} \sim \Delta ,$$

where $\Delta \sim 10^{-1}$ and q is the safety factor. Under these conditions magnetic field B in eq.(2-8) can be approximately given by

$$B \simeq \bar{B} \left(1 + \frac{\bar{B}_\varphi \tilde{B}_\varphi}{\bar{B}^2} \right) ,$$

with

$$\bar{B} = \sqrt{\bar{B}_\varphi^2 + \bar{B}_\theta^2} ,$$

and the guiding center equations (2-7-1) and (2-7-2) are rewritten in the forms

$$\frac{dr}{dt} \simeq W_{r0} + W_{r1}\cos N_t\varphi + W_{r2}\sin N_t\varphi + \tilde{b}_r v_{g\parallel} + O(\Delta^4) , \qquad (2\text{-}9\text{-}1)$$

$$\frac{d\theta}{dt} \simeq W_{\theta 0} + W_{\theta 1}\cos N_t\varphi + W_{\theta 2}\sin N_t\varphi + \frac{(\bar{b}_\theta+\tilde{b}_\theta)}{r} v_{g\parallel} + O(\Delta^4) , \qquad (2\text{-}9\text{-}2)$$

$$\frac{d\varphi}{dt} \simeq W_{\varphi 0} + W_{\varphi 1}\cos N_t\varphi + W_{\varphi 2}\sin N_t\varphi + \frac{\bar{b}_\varphi}{R} v_{g\parallel} + O(\Delta^4) , \qquad (2\text{-}9\text{-}3)$$

$$\frac{dv_{g\parallel}}{dt} \simeq W_{v0} + W_{v1}\cos N_t\varphi + W_{v2}\sin N_t\varphi + O(\Delta^4) , \qquad (2\text{-}9\text{-}4)$$

where

$$W_{r0} \simeq -U_A \bar{b}_\varphi \frac{\sin\theta}{R} ,$$

$$W_{r1} \simeq U_A \bar{b}_\varphi^2 \left(\bar{b}_\varphi^2 \tilde{b}_\varphi \frac{\sin\theta}{R} - \frac{1}{\bar{B}} \frac{\partial \tilde{B}_\varphi}{r\partial\theta} \right) ,$$

$$W_{r2} \simeq U_A \bar{b}_\theta \bar{b}_\varphi \frac{1}{\bar{B}} \frac{\partial \tilde{B}_\varphi}{R\partial\varphi} ,$$

$$W_{\theta 0} \simeq U_A \frac{\bar{b}_\varphi}{r} \left(-\frac{\cos\theta}{R} + \bar{b}_\theta^2 \frac{1}{B_p} \frac{dB_p}{dr} \right) ,$$

$$W_{\theta 1} \simeq U_A \frac{\bar{b}_\varphi^2}{r} \left(\bar{b}_\varphi^2 \tilde{b}_\varphi \frac{\cos\theta}{R} + \frac{1}{\bar{B}} \frac{\partial \tilde{B}_\varphi}{\partial r} \right) ,$$

$$W_{\theta 2} \simeq O(\Delta^4) ,$$

$$W_{\varphi 0} \simeq -U_A \frac{\bar{b}_\theta}{R} \left(-\frac{\cos\theta}{R} + \bar{b}_\theta^2 \frac{1}{B_p} \frac{\partial B_p}{\partial r} \right) ,$$

$$W_{\varphi 1} \simeq -U_A \frac{\bar{b}_\theta \bar{b}_\varphi}{R} \left(2\bar{b}_\varphi^2 \tilde{b}_\varphi \frac{\cos\theta}{R} + \frac{1}{\bar{B}} \frac{\partial \tilde{B}_\varphi}{\partial r} \right) ,$$

$$W_{\varphi 2} \simeq U_A \frac{1}{R} \left(\tilde{b}_r \frac{\sin\theta}{R} + \tilde{b}_\theta \frac{\cos\theta}{R} \right) ,$$

$$W_{v0} \simeq U_B \bar{b}_\theta \frac{\sin\theta}{R} ,$$

$$W_{v1} \simeq U_B \bar{b}_\theta \bar{b}_\varphi \left(\frac{1}{\bar{B}} \frac{\partial \tilde{B}_\varphi}{r\partial\theta} + \frac{1}{\bar{B}} \frac{\partial \tilde{B}_\theta}{R\partial\varphi} - \frac{\sin\theta}{R} \tilde{b}_\varphi \right)$$

$$W_{v2} \simeq U_B \frac{1}{R} \left(\bar{b}_\varphi^2 \frac{1}{\bar{B}} \frac{\partial \tilde{B}_\varphi}{\partial\varphi} + \tilde{b}_\theta \sin\theta - \tilde{b}_r \cos\theta \right)$$

$$U_A = \frac{1}{Z_t e} \left(\mu_m + \frac{m_t}{B} v_{g\parallel}^2 \right) ,$$

$$U_B = -\frac{\mu_m}{m_t} \bar{B} ,$$

$$\tilde{b}_r = \frac{\tilde{B}_r}{\bar{B}} ,$$

$$\bar{b}_\theta = \frac{\bar{B}_\theta}{\bar{B}} , \qquad \tilde{b}_\theta = \frac{\tilde{B}_\theta}{\bar{B}} ,$$

$$\bar{b}_\varphi = \frac{\bar{B}_\varphi}{\bar{B}} , \qquad \tilde{b}_\theta = \frac{\tilde{B}_\varphi}{\bar{B}} ,$$

respectively.

The coefficients W_{r0}, W_{r1}, $\cdots$, W_{v2} , in eqs. (2-9-1) $\sim$ (2-9-4) are computed at every mesh point in the plasma and tabulated in advance of the main calculation. For the calculation of guiding center orbit, the time derivatives of eqs. (2-9-1) $\sim$ (2-9-4) are given by the linear interpolation with those tabulated values. This method can effectively save the computational time. The integration of orbit equations is executed by a kind of P-C method (predictor and corrector method). The algorism of the P-C method is as follows:

1) The guiding center position (r,θ,φ) and $v_{g\parallel}$ after $1/2\Delta t$ is predicted with time derivatives at time t.

$$\vec{X}_p = \vec{X}(t) + d\vec{X}/dt \mid_t \Delta t/2 .$$

2) The time derivatives at $\vec{X} = \vec{X}_p$ is defined.

$$d\vec{X}/dt \mid_{t+1/2\Delta t} .$$

3) The new (r,θ,φ) and $v_{g\parallel}$ at $t + \Delta t$ is calculated by

$$\vec{X}(t+\Delta t) = \vec{X}(t) + d\vec{X}/dt \mid_{t+1/2\Delta t} \Delta t.$$

The velocity components of fast ion parallel and perpendicular to the magnetic field line are given by

$$v_\parallel = v_{g\parallel} ,$$

$$v_\perp = \sqrt{2\mu_m B} .$$

The calculation results from the above P-C method have been examined by comparing them with those from the Runge-Kutta method, and a very good agreement, $\mid r_{P\text{-}C} - r_{R\text{-}K} \mid /a < 10^{-5}$ after a bounce of motion, is obtained.

The orbit calculation with this level of error is accurate enough for the orbit-following Monte-Carlo code, because the simulation step of Coulomb collision interrupts the orbit calculation at every 1/10 ~ 1/50 bounce time.

2-4. Collision model using Monte-Carlo techniques

The collisional process of fast ions has been simulated by a technique of Monte-Carlo. Provided that a test particle change its velocity components parallel and perpendicular to the magnetic field line from $(v_{\parallel}, v_{\perp})$ to $(v_{\parallel}', v_{\perp}')$ by collision with field particles as shown in Fig.2-4, relations among these velocity components are given by

$$v_{\parallel}' = v_{\parallel} + \Delta v_l \frac{v_{\parallel}}{v} - \Delta v_t \frac{v_{\perp}}{v} \sin\Omega \ , \tag{2-10}$$

$$v_{\perp}' = [(v + \Delta v_l)^2 + \Delta v_t^2 - v_{\parallel}'^2]^{1/2} \ , \tag{2-11}$$

where $v \ (= \sqrt{v_{\parallel}^2 + v_{\perp}^2})$ is the total velocity of the test particle, Ω the Larmor phase, Δv_l the longitudinal component of the velocity change, and Δv_t the transverse component, respectively. The velocity changes Δv_l and Δv_t result from the slowing-down and pitch-angle scattering of the test particles due to Coulomb collision with field particles. Under the assumption that the field particles have a Maxwellian velocity distribution, the mean values and mean square deviations of Δv_l and Δv_t are given by[8)]

$$\frac{<\Delta v_l>}{v_\beta} = -\frac{3}{2}\sqrt{\pi}\, M_t \frac{\Delta t}{\tau_s} \sum_p Z_p^2 \frac{m_p + m_t}{m_t} \frac{n_p'}{T_p'} \frac{\mu(\chi_p)}{2\chi_p} \ , \tag{2-12}$$

$$\frac{<\Delta v_t>}{v_\beta} = 0.0 \tag{2-13}$$

$$\frac{<\Delta v_l^2>}{v_\beta^2} = \frac{3}{2}\sqrt{\pi}\, M_t \frac{\Delta t}{\tau_s} \sum_p Z_p^2 \frac{m_p^{1/2}}{m_t^{1/2}} \frac{n_p'}{T_p'^{1/2}} \frac{\mu(\chi_p)}{2\chi_p^{3/2}} \ , \tag{2-14}$$

$$\frac{<\Delta v_t^2>}{v_\beta^2} = \frac{3}{2}\sqrt{\pi}\, M_t \frac{\Delta t}{\tau_s} \sum_p Z_p^2 \frac{m_p^{1/2}}{m_t^{1/2}} \frac{n_p'}{T_p'^{1/2}} \left[\mu(\chi_p) + \frac{d\mu(\chi_p)}{d\chi_p} - \frac{\mu(\chi_p)}{2\chi_p} \right] \frac{1}{\chi_p^{1/2}} \ , \tag{2-15}$$

where Z_p is the charge number of the respective plasma species denoted by p ($= e, i \cdots$), m_e the electron mass, m_t the test particle mass, Δt a time interval,

$$M_t = (m_t/m_e)^{3/2} (1+m_t/m_e)^{-1} \ ,$$

$$\chi_p = \frac{m_p}{m_t} \frac{v^2}{v_\beta^2} \frac{1}{T_p'} \ ,$$

$$\mu(\chi_p) = Erf(\sqrt{\chi_p}) - 2\sqrt{\chi_p/\pi}\, exp(-\chi_p) \ ,$$

$$v_\beta = \sqrt{2kT_{e0}/m_t} \ ,$$

and τ_s is the slowing-down time of test particles with mass number A_t and charge number Z_t at plasma center defined by

$$\tau_s = 0.125 (A_t/Z_t^2) [T_{e0}(keV)^{3/2}/n_{e0}(10^{19}m^{-3})] \ . \tag{2-16}$$

The summation $\sum$ in eqs. (2-11), (2-13) and (2-14) is taken for all the plasma species. The plasma parameters such as temperature T_p' and plasma density n_p' in the above expressions are normalized by the electron temperature T_{e0} and the electron density n_{e0} at the plasma center.

In the present Monte-Carlo simulation, Δv_l and Δv_t are computed by generating normal random numbers with the mean values and the mean square

deviations given by eqs. (2-12) ~ (2-15). The Larmor phase Ω in eq. (2-10) is given by a uniform random number between zero and 2π.

The validity of the collision model described above has been confirmed by comparing the numerical result with analytical one. If the velocity of fast ions v exists between the ion thermal velocity and the electron thermal velocity, that is, $v_{iT} \ll v \ll v_{eT}$, the two dimensional Fokker-Planck equation[1)-4)] in a fully ionized plasma without electric field can be written in the form

$$\frac{\partial f}{\partial t} = \frac{1}{v^2}\frac{\partial}{\partial v}\left(\frac{1}{2\tau_s}\frac{m_e}{m_t}\frac{v_e^3}{v}(v_e^3 + v_c^3\frac{[Z]}{<Z>})\frac{\partial f}{\partial v}\right) + \frac{1}{v^2}\frac{\partial}{\partial v}\left(\frac{1}{\tau_s}(v^3 + v_c^3)f\right)$$

$$+ \frac{1}{2\tau_s}\frac{v_c^3}{v^3}\frac{Z_{eff}}{<Z>}\frac{\partial}{\partial \eta}(1-\eta^2)\frac{\partial f}{\partial \eta} + S(\vec{v}, t), \qquad (2\text{-}17)$$

where

$$E_c = \frac{m_t}{2}v_c^2 \simeq 14.8<Z>^{2/3}T_e ,$$

$$Z_{eff} = \sum_p Z_p^2 n_p/n_e ,$$

$$<Z> = \sum_p Z_p^2 n_p/n_e \cdot m_p/m_t ,$$

$$[Z] = \sum_p Z_p^2 n_p/n_e \cdot m_p/m_t \cdot T_p/T_e ,$$

$$\eta = \frac{v_{\parallel}}{v} = \sin\zeta ,$$

and ζ is the pitch angle, respectively. The first term of eq. (2-17) describes the velocity diffusion, the second the slowing down, the third the pitch angle scattering and the fourth the fast ion source, respectively. If the velocity diffusion term is eliminated, the analytical

solution of eq.(2-17) with

$$S(\vec{v},t) = \frac{I_B}{e}\delta(t-0)\delta(v-v_0)\delta(\eta-\eta_0) \tag{2-18}$$

can be given by

$$f(v,\eta,t) = \frac{3I_B\tau_s}{2\pi e}\sum_n (n+1/2)[1+u_c^3\{1-\exp(3t/\tau_s)\}]^{c(n)}$$

$$\times P_n(\eta_0)P_n(\eta)\delta[u^3-\{(1+u_c^3)\exp(-3t/\tau_s)-u_c^3\}] \tag{2-19}$$

where $\delta(x_1-x_2)$ is the delta function, P_n the Legendre function, I_B the source current of fast ions, $u = v/v_0$, $u_c = v_c/v_0$ and

$$c(n) = \frac{n(n+1)}{6}\frac{Z_{eff}}{<Z>} .$$

The numerically derived pitch angle scattering process using 500 test particles with $\eta_0 = 1.0$ (in eq.(2-18)) is shown in Fig.2-5 for various t/τ_s. The pitch angle distribution of fast ions given by the v-integration of eq.(2-19) is also shown in Fig.2-5 by the dashed curve. It is clearly seen from Fig.2-5 that the numerical result fairly agrees with the theoretical one.

2-5. Charge-exchange model using Monte-Carlo techniques

The charge-exchange process of fast ions is also simulated by Monte-Carlo techniques. The charge-exchange probability during a small time interval Δt is given by

$$P_{cx}(\Delta t) = 1 - exp(-n_0 <\sigma v>_{cx} \Delta t) \qquad (2\text{-}20)$$

$$\sim n_0 <\sigma v>_{cx} \Delta t$$

where n_0 is the neutral density, $<\sigma v>_{cx}$ the charge-exchange reaction rate of fast ions with back ground neutrals. To simulate the charge-exchange process, a simple hit-or-miss Monte-Carlo method is employed. The charge-exchange probability eq.(2-20) is calculated at every time step Δt for all the test particles, that is,

$$P_{cx}(\Delta t, i) \quad (i=1,2,\ldots\ldots,N_p) \ ,$$

where N_p is the total number of test particles. Simultaneously, N_p uniform random numbers $(\chi^{cx}_{random}(i), i=1,2,\ldots\ldots,N_p)$ are also generated at every Δt. Comparing $P_{cx}(\Delta t, i)$ with $\chi^{cx}_{random}(i)$ for all the test particles, we switch on the calculation of charge-exchange process for only the particles whose $P_{cx}(\Delta t, i)$ is greater than $\chi^{cx}_{random}(i)$. Once a fast ion is charge-exchanged, it becomes a fast neutral and makes a straight flight in a plasma until it is reionized by the field particles or lost to the first wall. The reionization probability is described by

$$\cdot P_{ion}(s) = \int_0^s exp(-\lambda/\lambda_{ion})\, d\lambda/\lambda_{ion} \ , \qquad (2\text{-}21)$$

where λ is the flight length, λ_{ion} the ionization mean free path. The above integration is executed up to

$$\chi^{ri}_{random} = P_{ion}(s),$$

where χ^{ri}_{random} is another uniform random number between zero and unity. If a fast neutral hits the first wall without being reionized, it is labeled as a charge-exchange loss particle.

Since the main purpose of the present paper is to investigate the ripple-associated loss process, the charge-exchange process described above is "switched-off" in the following sections without notice.

References

1) J.A. Rome *et al.*: Nucl. Fusion 14 (1974) 141.

2) J.G. Cordey: Nucl. Fusion 16 (1976) 499.

3) J.D. Callen, R.J. Colchin, R.H. Fowler, D.G. McAlees, J.A. Rome: Presented at 5th IAEA Conf. on Plasma Physics and Controlled Nuclear Fusion Research, Tokyo (1974), paper IAEA CN-33/A16-3.

4) J.W. Connor, J.G. Cordey: Nucl. Fusion 14 (1974) 185.

5) L.M. Hively, G.H. Miley: Nucl. Fusion 20 (1980) 969.

6) S. Nishio, M. Ohkubo, K. Kawasaki, N. Miki: JAERI-M 7846 (1978).

7) T.G. Northrop: *The Adiabatic Motion of Charged Particles* (Wiely, New York, 1963)

8) B.A. Turbnikov: *Particle Interactions in a Fully Ionized Plasma*, Rev. Plasma Phys., Vol.1 (1965) 105.

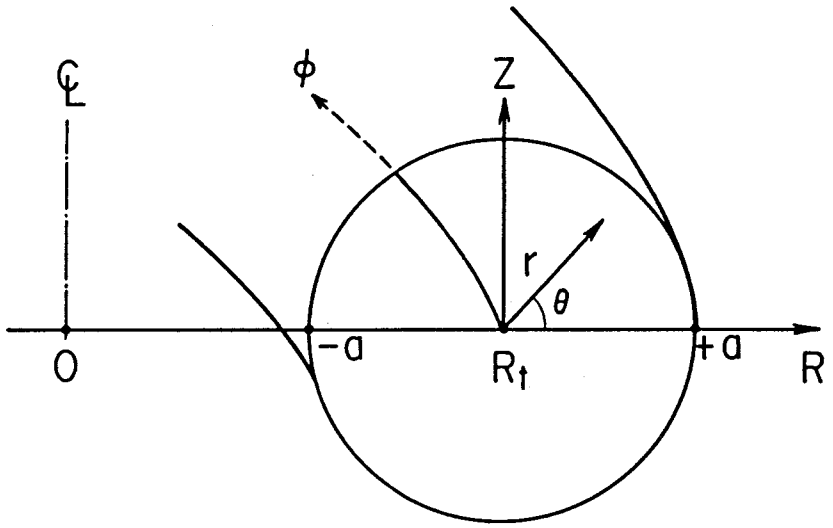

Fig.2-1 System of co-ordinates.

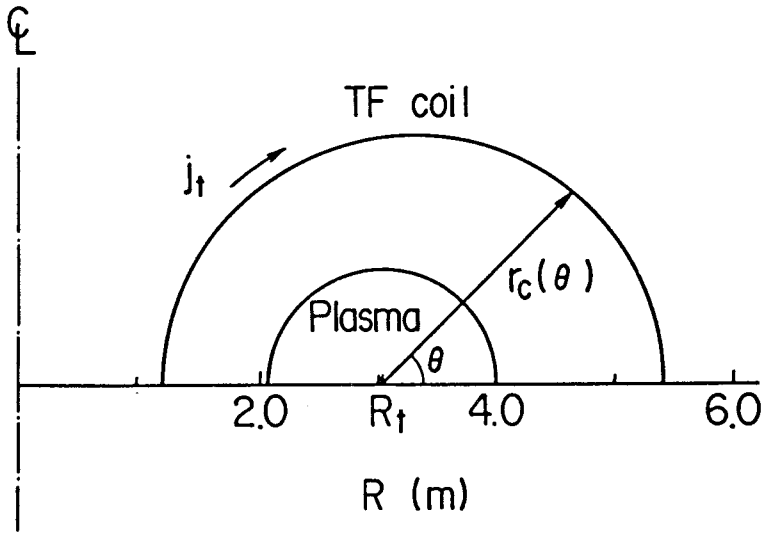

Fig.2-2 Simplified model of toroidal field coil system for the calculation of ripple field divergence-free as well as curl-free.

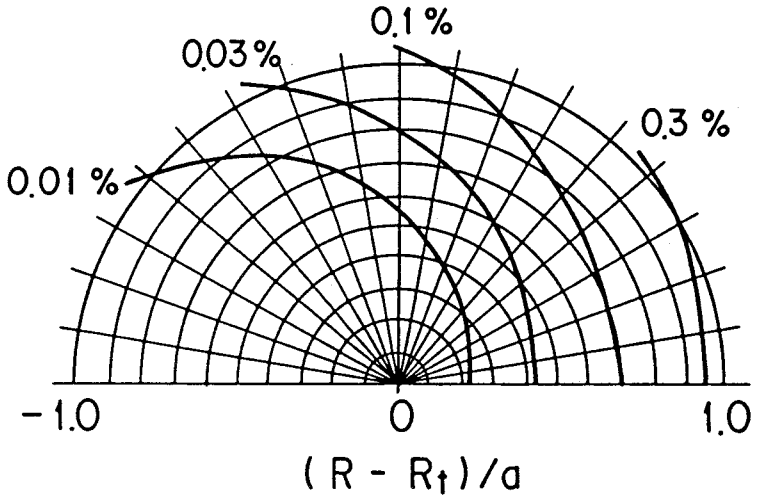

Fig.2-3 Constant contours of field ripple in JT-60.

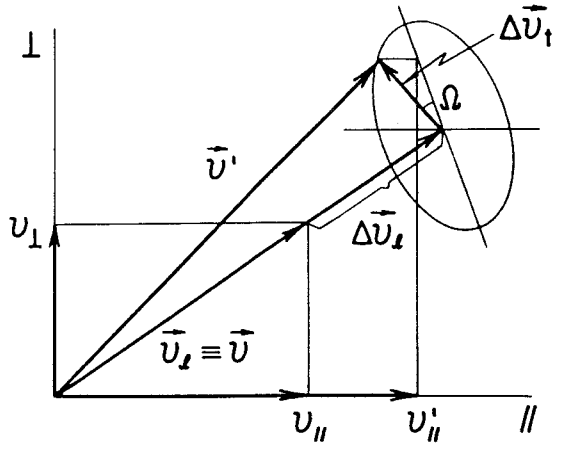

Fig.2-4 Velocity change due to Coulomb collision.

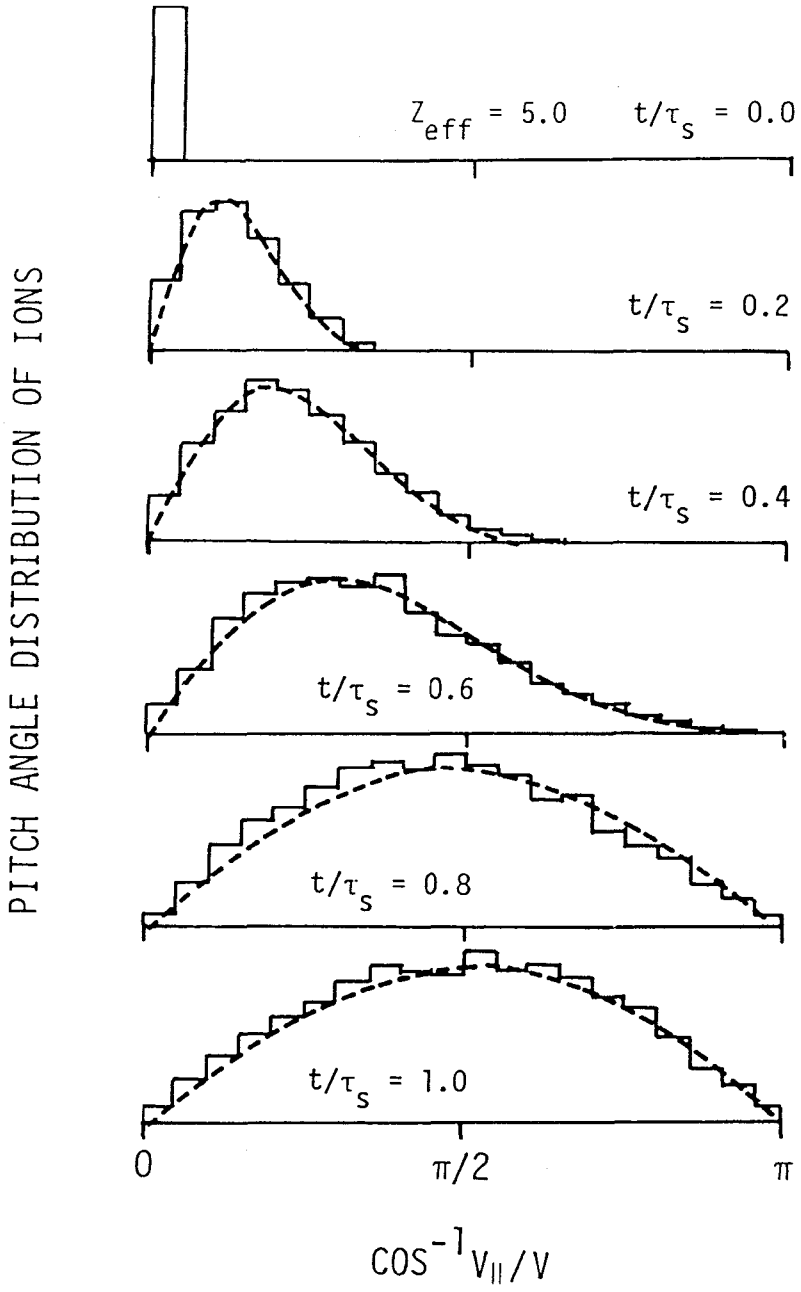

Fig.2-5 Simulation of pitch angle scattering. The solid lines indicate the Monte-Carlo results using 500 test particles and the dashed curves the thoeretical ones.

§ 3. Collisionless Behavior of Fast Ions in Ripple

3-1 Introduction

Guiding center orbits in a magnetic field with toroidal ripple have essential importance in the behavior of fast ions during their slowing down process, so that we exclude the collisional process of fast ions with field particles in this section. Three kinds of processes are the typical features of fast ion collisionless behavior in ripple as pointed out by the authors[1),2),3)]:

(a) collisionless ripple trapping,

(b) collisionless ripple detrapping, and

(c) ripple-enhanced banana drift.

These processes have been investigated by solving numerically the guiding center orbit eqs. (2-7-1) and (2-7-2). The above mentioned behaviors of fast ions depend on the collisionless orbits near banana tips, accordingly, those orbits are solved analytically in order to understand the numerical results. Parameters for the present calculations are taken as those appropriate to JT-60 which are summarized in Table 3-I. The toroidal coil system of JT-60 has been designed so that the maximum toroidal field ripple at the plasma edge δ_0 is less than 0.5 % of the toroidal magnetic field strength as shown in Fig.2-3. The main purpose of the present investigation in this section, however, is to make it clear the ripple effect on the collisionless behavior of fast ions, we set the field ripple δ_0 at 1 % in this and in the next section.

3-2 Collisionless ripple trapping

If we employ the usual tokamak ordering, $\overline{b}_\theta$ is much less than $\overline{b}_\varphi$, therefore W_{v1} in eq. (2-9-4) is much less than W_{v2} and the variation in φ along the magnetic field line is much greater than that in θ. Under these condition, we can find a toroidal angle φ which makes $\partial B/\partial l$ or $dv_{g\parallel}/dt$ to be zero if

$$| W_{v0}/W_{v2} | < 1.0.$$

The above condition is the well-known condition for a ripple well to occur and

$$\alpha = W_{v0}/W_{v2}$$

$$\sim \frac{\overline{B}_\theta \sin\theta}{N_t \tilde{B}_\varphi + \tilde{B}_r \cos\theta - \tilde{B}_\theta \sin\theta}, \tag{3-1}$$

$$\sim \frac{r\sin\theta}{N_t R q(r,\theta)\delta(r,\theta)} . \tag{3-2}$$

is the ripple-well parameter, where $q(r,\theta)$ is the safety factor. The effective ripple well depth can be written in the form

$$\delta_{eff} = 2\,\delta(r,\theta)A(\alpha), \tag{3-3}$$

where

$$A(\alpha) = \sqrt{1.0 - \alpha^2} - |\alpha| \left(\frac{\pi}{2} - \sin^{-1}|\alpha| \right). \tag{3-4}$$

When ions exist within the ripple well region defined by $|\alpha| < 1.0$, they

have a chance to be trapped in a ripple well.

It must be noted that, taking account of the finite size of the banana orbit (which has been neglected in the classical ripple diffusion theory), ions can be collisionlessly trapped in a ripple well even if they are initially free from ripple wells. In order to describe this process, let us consider a particle passing just over the top of a magnetic field corrugation. This particle stays in the ripple well near a banana tip for a comparatively long time and moves into a different ripple well region due to the gradient-B drift. The drifting particle can be trapped in the ripple well, if the ripple encountered has a higher corrugation. This situation of the particle motion is illustrated in Fig.3-1.

The collisionless ripple-trapping zones are obtained by the numerical integration of the guiding center equations and are shown in Fig.3-2 in the space of initial pitch angle ζ and toroidal angle φ for fast ions born at $r = 0.9a$ and $\theta = 0^\circ$. The central zone in this figure corresponds to the direct ripple-trapping region defined by a well-known relation

$$(v_\parallel / v)^2 < \delta_{eff}.$$

The finite banana size effect makes this zone asymmetric with respect to both ζ and φ. In addition to this central zone, a series of collisionless ripple-trapping bands due to the finite banana size effect appear as shown in Fig.3-2.

According to an analytical study (see Appendix), the ripple trapping band width $\Delta\zeta$ can be represented in terms of the initial pitch angle ζ on the mid-plane, and given by

$$\Delta\zeta = \frac{N_t \delta(r_{bt}, \theta_{bt})}{2} \Delta\varphi \left(\alpha - \sin N_t \varphi_{bt} \right) \cos\zeta , \qquad (3\text{-}5)$$

where $\Delta\varphi$ is the toroidal angle difference between the banana tips with zero and finite banana size and (r_{bt}, θ_{bt}, φ_{bt}) is the banana tip point with zero banana size, respectively (see Fig.A-1). As shown in Appendix, $\Delta\varphi$ is proportional to the gradient-B drift velocity

$$v_d = \frac{m_t\, v_\perp^2}{2eZ_tB_tR_t} ,$$

therefore the width of these side bands becomes broad with the increase of the banana size.

3-3 Collisionless ripple detrapping

Fast ions trapped in a ripple well undergo the gradient-B drift with velocity v_d. In general, the ripple well depth δ_{eff} is not constant along the gradient-B drift trajectory. If ripple-trapped particles get into a lower ripple region, they can be detrapped collisionlessly from the well when they reach the point where

$$\delta_{eff} < (v_\parallel / v)^2 .$$

In the usual toroidal field coil system, the ripple well δ_{eff} has its peak on the mid-plane and decreases with the distance from the mid-plane. Under some conditions of the spatial change of ripple size and the radial distribution of plasma current density, δ_{eff} can have the minimum $(\delta_{eff})_{min}$ on the drift trajectory and it can fall within the plasma region. The contours of $(\delta_{eff})_{min}$ in JT-60 with a parabolic current density distribution are also shown in Fig.3-3. The particle trapped in the region ① cannot be detrapped without collision. On the other hand, particles initially

trapped in the region ②, ③ or ④ with

$$|v_{\parallel}| > v\sqrt{(\delta_{eff})_{min}}$$

are detrapped from the ripple well on their way toward the lines $(\delta_{eff})_{min}$. Deeply trapped particles with

$$|v_{\parallel}| < v\sqrt{(\delta_{eff})_{min}}$$

are never detrapped collisionlessly and escape out of the plasma. It is apparent that all of the particles trapped in the region ⑤ are detrapped during their gradient-B drift. As described above, the collisionless ripple-detrapping process limits the radial excursion of the ripple-trapped particles and prevents their loss. Consequently this process plays an important role on the loss of fast ions and the ripple-associated diffusion of bulk plasma ions.

3-4 Ripple-enhanced banana drift

Collisionless banana drift enhanced by ripple has been discussed by K. T. Tsang and he has estimated the diffusion coefficient by taking account of the radial component $\tilde{B}_r$ of the toroildal field ripple. The $\tilde{B}_r$ banana drift is not significant for fast ions. Another ripple-induced banana drift which originates in the finite banana size, is more important for particles with higher energy. In the presence of ripple, the banana orbit of a ripple untrapped particle is seriously disturbed. As is shown in Fig.3-4, the ripple untrapped particles, especially barely untrapped particles, undergo a large radial drift at the ripple peak point near their banana tip. The radial excursion of the guiding center after a half bounce

of banana is plotted in Fig.3-5 as a function of the initial pitch angle for 75 keV fast ions born initially at r/a = 0.9 on the mid-plane. The white blanks in Fig.3-5 correspond to the collisionless ripple trapping regions described in § 3-2 .

The discontinuous step size of the radial drift Δr is given by

$$\Delta r = \tau_{rb}\, v_d \sin\theta_{bt} \ , \tag{3-6}$$

where τ_{rb} is the resident time of a barely untrapped particle in the ripple well at a banana tip and is approximately given by

$$\tau_{rb} = \frac{2.83\, R}{N_t v_\perp \delta^{1/2}}\, t_{rp} \ , \tag{3-7}$$

for a small value of $|\alpha|$ ($|\alpha| < 0.5$) where t_{rp} is a numerical factor having a value of about 10 in case of large safety factor q. It must be noted that the radial drift Δr is inversely proportional to $\sqrt{\delta}$ and this nature of the banana drift is essentially different from $\tilde{B}_r$ banana drift.

The hatched regions in Fig.3-5 indicate the loss regions. If the ripple amplitude is reduced to zero keeping other parameters unchanged, these loss regions disappear. This indicates that new prompt loss regions are induced by the toroidal field ripple.

3-5 Collisionless loss region in velocity space

Collisionless behaviors of fast ions described above produce new prompt loss region associated with toroidal field ripple in the velocity space, in addition to the well-known loss region due to the loss orbits in

an axisymmetric toroidal field, hereafter referred to simply as banana loss cone, and the direct ripple trapping loss cone ($|v_{\parallel}/v| < \sqrt{\delta_{eff}}$).

Collisionless loss regions in the velocity space are shown in Fig.3-6 for protons whose initial point is (0.9a, 0.0, π/N). Figure 3-6-(a) shows the prompt loss region in an axisymmetric tokamak. Collisionless loss region in the presence of ripple are shown in Fig.3-6-(b), (c) and (d), where collisionless orbits are followed for 0.5, 1.0 and 5.0 bounce time of banana motions, respectively. The banana loss cone and the direct ripple trapping loss cone are easily recognized in Fig.3-6-(b). One should note that one of the boundaries of the banana loss cone is strongly disturbed by the ripple. Loss bands begin to appear in both sides of the direct ripple trapping loss cone after one bounce time of banana and their number increases with the bounce time. These loss bands result from the collisionless ripple-trapping and ripple-enhanced banana drift.

Most of the loss bands appear in the pitch angle region $|\zeta| < \zeta_\alpha$, where ζ_α is the pitch angle defined by

$$\cos^2\zeta_\alpha = \frac{R_t + r_0\cos\theta_a}{R_t + r_0} \tag{3-8}$$

with θ_α the poloidal angle on the line $|\alpha| = 1.0$ at $r = r_0$ and r_0 the initial minor radius. The banana tip of the fast ion with this pitch angle just touches the boundary line of the ripple well region.

Although collisionless ripple trapping does not occur in the pitch angle region $|\zeta| < \zeta_\alpha$, the radial drift of fast ions is still enhanced by ripple. This ripple-enhanced radial excursion disturbs the boundary of the banana loss cone in the region $\zeta < -\zeta_\alpha$.

3-6 Concluding remarks

Collisionless process of fast ions have been investigated by following the collisionless guiding center orbits. It has been found that there are three kinds of collisionless behaviors as typical features of fast ions in a rippled toroidal field;

(a) collisionless ripple trapping,

(b) collisionless ripple detrapping, and

(c) ripple-enhanced banana drift.

The collisionless ripple-trapping occurs in an uneven distribution of the toroidal field ripple and the pitch angle width of the trapping region is proportional to the banana size of fast ions. The radial excursion step size due to the ripple-enhanced banana drift is also proportional to the banana size of fast ions and is inversely proportional to the square root of the local ripple size at the banana tip point in the region $|\alpha| < 1.0$. The collisionless ripple trapping as well as the ripple-enhanced banana drift produce a large number of loss bands in velocity space and strongly disturb the well-known banana loss cone.

References

1) K. Tani, H. Kishimoto and S. Tamura: *Proc. 9th European Conf. on Controlled Fusion and Plasma Physics*, Oxford, Vol.1 (1979) p.157.

2) JAERI Fusion Research and Development Center, INTOR Workshop Report,

Group 1, JAERI-M 8621 (1980).

3) K. Tani, H. Kishimoto and S. Tamura: *Proc. 8th Int. Conf. on Plasma Physics and Controlled Nuclear Fusion Research*, Brussels, 1980, Vol.1, IAEA, Vienna (1981) p.631.

4) T.E. Stringer: Nucl. Fusion 12 (1972) 689.

5) J.A. Rome *et al.*: Nucl. Fusion 14 (1974) 141.

Table 3-I Calculation parameters

major radius	$R_t = 3.03\ m$
minor radius	$a = 0.95\ m$
toroidal field	$B_t = 4.5\ T$
plasma current	$j_p(r) = j_0(1-(r/a)^2)$
	$j_0 = 4.73/q_a \quad MA/m^2$
safety factor	$q_a = 3.5$
plasma ion species	H^+
number of toroidal field coils	$N_t = 18$
maximum toroidal field ripple	$\delta_0 = 0.01$
energy of fast ion	$E = 75\ keV$
fast ion species	H^+

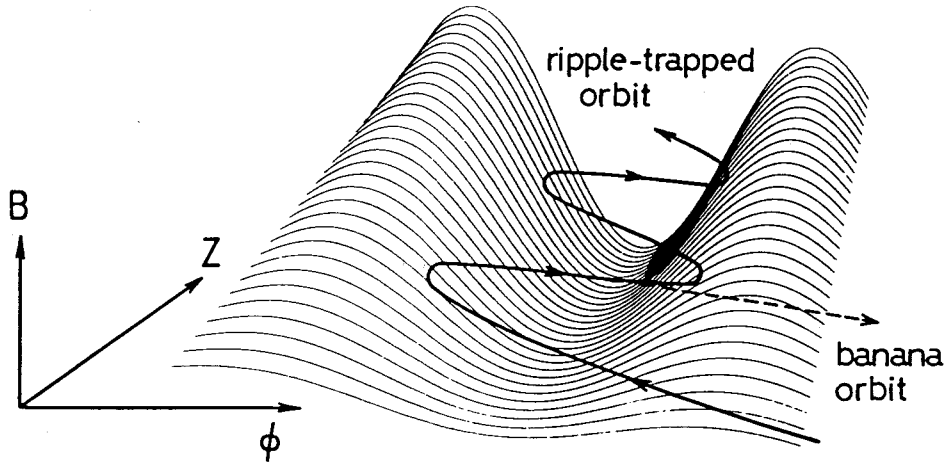

Fig.3-1 Schematic of collisionless ripple-trapping due to finite banana size effect in an inhomogeneous field ripple.

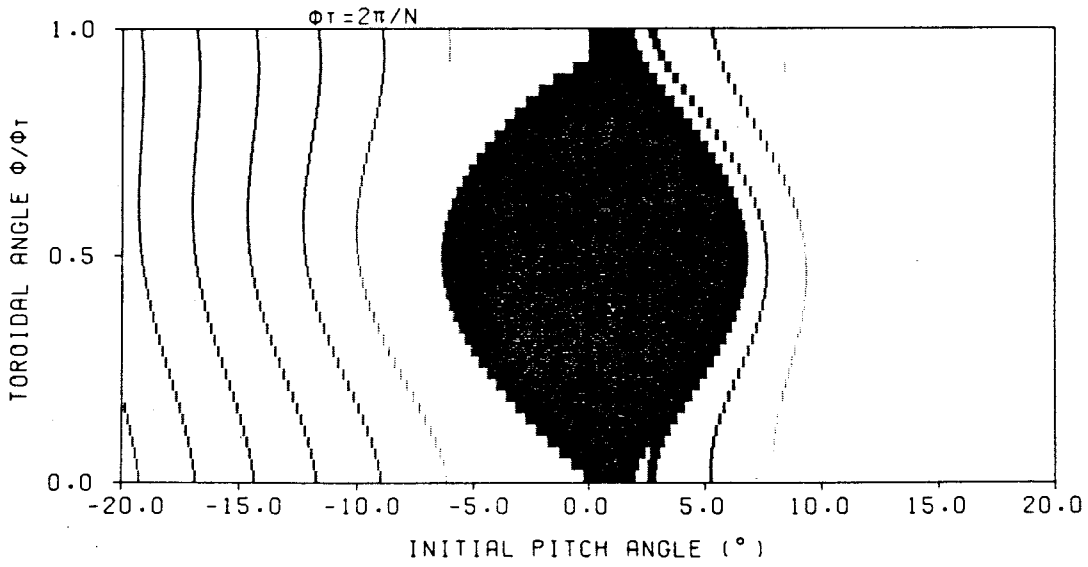

Fig.3-2 Collisionless ripple-trapping zones in a space of initial pitch angle and toroidal angle of fast ion. Calculation parameters as in Table 3-I.

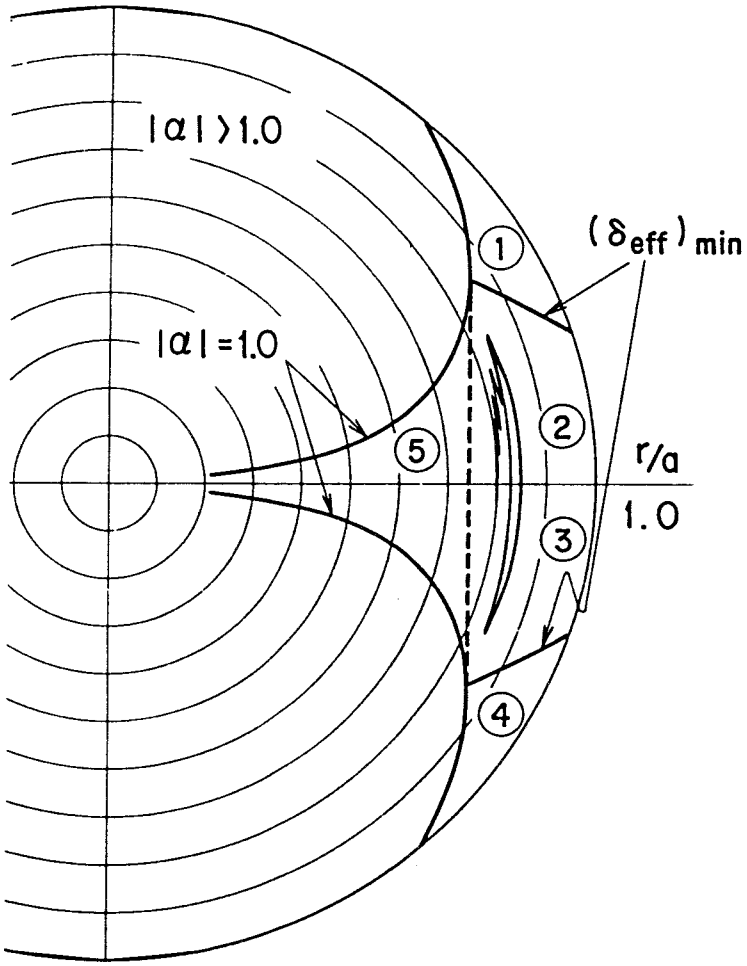

Fig.3-3 Collisionless ripple-detrapping process and ripple well structure.

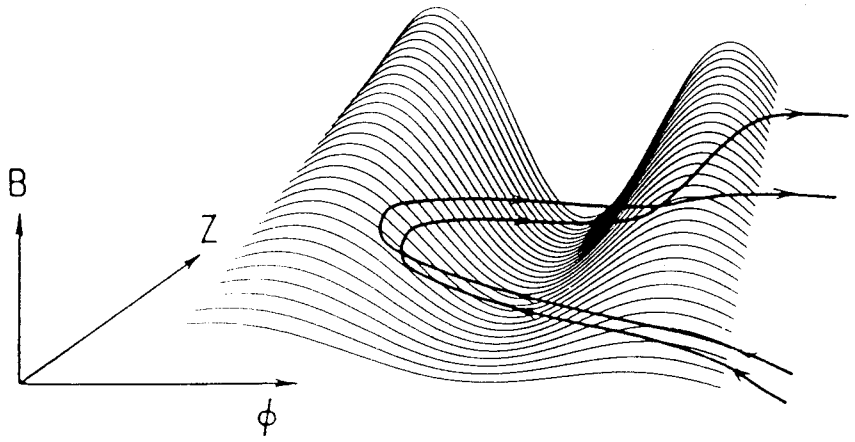

Fig.3-4 Schematic of ripple-enhanced banana drift in the vicinity of a banana tip.

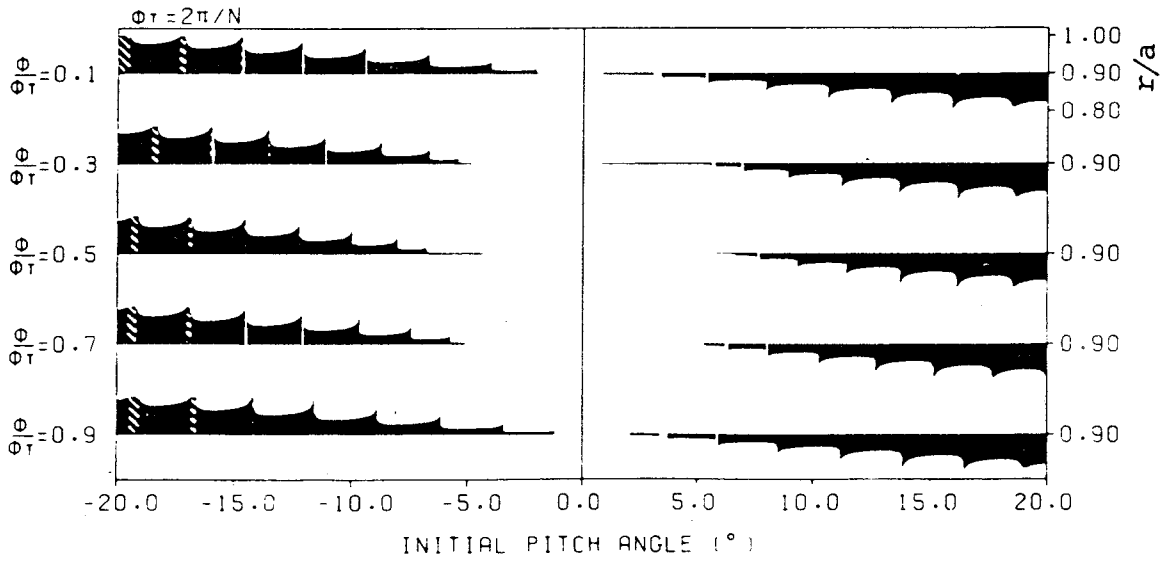

Fig.3-5 Radial drift of guiding center of fast ion against initial pitch angle for various initial toroidal angles. Calculation parameters as in Table 3-I.

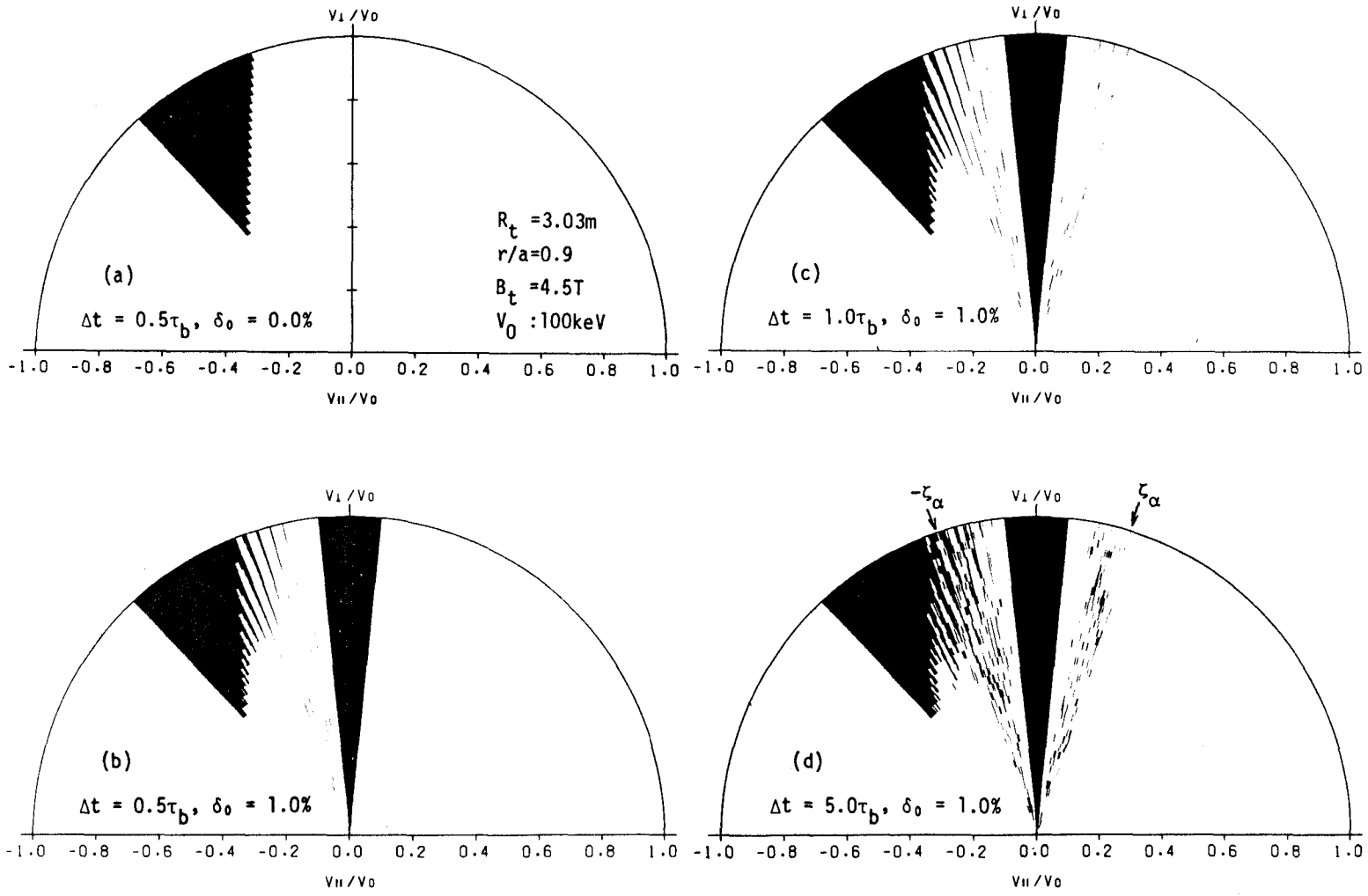

Fig.3-6 Collisionless loss region in velocity space.

§ 4. Collisional Behavior of Fast Ions in Ripple

4-1. Introduction

As described in the last section, there exist two kinds of fast ion loss processes associated with the toroidal field ripple; ripple trapping and ripple-enhanced banana drift[1),2)]. Owing to the collisional as well as collisionless ripple-detrapping processes, it is difficult to distinguish between ripple-trapped loss and banana-drift loss. Here, however, we classify the loss particles by their final state; that is, if the fast ions are trapped in a ripple well when they hit the first wall, we count them as ripple-trapped loss particles and if they are not trapped, banana-drift loss particles. Typical orbits during slowing down are shown in Fig.4-1; (a), (b) for ripple-trapped loss particles and (c), (d) for ripple-enhanced banana-drift loss particles.

In this section the loss of fast ions during slowing-down process is investigated in the case where fast ions are originated at a specific point within the plasma region ($r_0 = 0.9a$). The fast ions are assumed to have a uni-directional velocity and mono-energy ($75\,keV$). Plasma temperatures and density are given to be spatially uniform as summarized in Table 4-I.

In order to investigate the ripple-associated loss process we estimate the total energy loss time of fast ions τ_{ls} . The first interest in τ_{ls} lies in its dependence on the initial pitch angle of fast ions, which is shown in Fig.4-2. Only the positive side of the initial pitch angle is considered to exclude the effects of ripple free loss orbits (loss orbits

in an axisymmetric field). The loss time τ_{ls} shows sharp changes at the pitch angles $\zeta = \zeta_d$ and ζ_α. The pitch angle ζ_d is given by $\sqrt{\delta_{eff}}$ and the fast ions whose initial pitch angle is less than ζ_d are directly trapped in a ripple well. The other critical pitch angle ζ_α is given in § 3-5. Three regions of the initial pitch angle are recognized clearly in Fig.4-2;

1) direct ripple-trapping region $|\zeta| < \zeta_d$,

2) intermediate region $\zeta_d < |\zeta| < \zeta_\alpha$, and

3) collisional region $|\zeta| > \zeta_\alpha$.

4-2. Direct ripple-trapping region ($|\zeta| < \zeta_d$)

Fast ions with initial pitch angle less than ζ_d are trapped directly in a ripple well and lost to the first wall in a very short time. The loss time agrees with z_s/v_d where z_s is the vertical length from the ripple-trapped point to the first wall.

4-3. Intermediate region ($\zeta_d < |\zeta| < \zeta_\alpha$)

It is noticeable that the loss time τ_{ls} in this pitch angle region is smaller by two orders of magnitude than the slowing-down time τ_s as shown in Fig.4-2. It has been considered that the ripple-associated loss cone is the direct ripple-trapping region described in the last subsection. This result indicates that a kind of loss cone is effectively formed also in this pitch angle region.

As discussed in § 3, the finite banana size gives rise to the colli-

sionless ripple trapping as well as the ripple-enhanced banana drift. They produce a lot of loss bands in this pitch angle region as shown in Fig.3-6. Fast ions are easily scattered into these loss bands via small pitch angle scattering with plasma particles. Therefore, fast ions in this pitch angle region are lost to the wall through cooperative process of these collisionless behaviors and Coulomb interactions with field particles.

In the following, we investigate the ripple-trapped loss process and the ripple-enhanced banana-drift loss process, individually.

4-3-1. Ripple-trapped loss

In Fig.4-2 the ripple-trapped loss time τ_{rt}/τ_s, the energy loss time of ripple-trapped loss particles, is also plotted. The dotted curve shows the ripple-trapped loss time for fast ions whose banana size is artificially reduced to zero until they are trapped in a ripple well, that is, only the collisional effect is taken into consideration for the ripple-trapping process. What is evident on comparing the above two lines is that the ripple-trapped loss is enhanced significantly by the finite banana size effect in the intermediate region.

To investigate the ripple-trapping process, we consider the ripple-trapping time τ_t, the time defined as the reciprocal of the ripple trapping rate. There is a series of pitch angle ζ_k measured on the mid-plane with which fast ions are reflected at one of the ripple vertices. The difference between the two adjacent pitch angles $\Delta\zeta_k (= \zeta_{k+1} - \zeta_k)$ can be given by

$$\Delta\zeta_k \sim \frac{r_{bt}\,\sin\theta_{bt}}{R_t + r_{bt}} \frac{2\pi}{N_t q} \frac{1}{\sin 2\zeta_k} . \qquad (4\text{-}3)$$

The collisional pitch angle change of fast ions in one banana bounce time τ_b is approximately given by

$$\Delta\zeta_{bc} \sim \frac{\pi}{2}\sqrt{\tau_b/\tau_d},$$

where τ_d is the deflection time. If $\Delta\zeta_{bc}$ is comparable to $\Delta\zeta_k$, it can be considered that the pitch angle of fast ions is sufficiently spread over the pitch angle width $\Delta\zeta_k$ in a bounce time. This condition is usually satisfied for the fast ions produced by neutral beam injection in tokamaks. For fast ions to be trapped in a ripple well, the finite banana size effect on ripple trapping or a sufficient pitch angle scattering while they pass through a ripple well is required. Here we estimate the ripple trapping due to each process.

Under the condition of $\Delta\zeta_k \sim \Delta\zeta_{bc}$, the collisionless ripple trapping time due to the finite banana size effect is simply given by

$$\tau_t^{FB} = \frac{\Delta\zeta_k}{\Delta\zeta}\tau_b \ , \qquad (4\text{–}4)$$

where $\Delta\zeta$ is the pitch angle band width of collisionless ripple trapping given by eq. (3–5). On the other hand if only the pitch angle scattering in the ripple well at a banana tips contributes to the ripple trapping, the collisional ripple trapping rate τ_t^C is given by

$$\tau_t^C \sim \sqrt{\tau_d/\tau_{rb}}\ \Delta\zeta_k'\tau_b \ , \qquad (4\text{–}5)$$

where τ_{rb} is the time interval given by eq. (3–7) and $\Delta\zeta_k'$ is the pitch angle corresponding to $\Delta\zeta_k$ observed at the ripple peak point near a banana tip defined by

$$(\Delta\zeta_k')^2 = 2\Delta\zeta_k \sin\zeta_k \sqrt{(R_t + r_{bt})/(R_t + r_{bt}\cos\theta_{bt})}.$$

Figure 4-3 shows the dependence of τ_t/τ_s on B_t calculated by the Monte-Carlo simulation code for q_a ($= aB_t/R_tB_p(a)$) = 3.5. It is shown that τ_t/τ_s has a proportional increase with B_t in a low B_t range. The ripple-trapping time in this region agrees well with τ_t^{FB} given by eq. (4-4). In order to clarify the effect of the finite banana size, the ripple-trapping time of fast ions with zero banana size is also shown in Fig.4-3, in which case only the collisional ripple-trapping process is taken into consideration. In the high B_t range, the banana size becomes small and the collisional trapping turns to be dominant. The numerically derived ripple-trapping time in this region also fairly agrees with the collisional ripple-trapping time τ_t^C described by eq. (4-5). The agreement of the numerical ripple-trapping rate with analytical one in both large and small banana size region supports the evidence that our orbit-following Monte-Carlo code well describes the behaviors of fast ions undergoing Coulomb collisions in a rippled toroidal field.

The ripple-trapped loss time τ_{rt} is also plotted in Fig.4-3. If the ripple-detrapping process is not accounted, τ_{rt} may be given by $\tau_t + z_s/v_d$ where z_s is the vertical length from the ripple-trapped point to the plasma surface. The loss time τ_{rt} is somewhat larger than $\tau_t + z_s/v_d$ especially in the high B_t range. This difference comes from the ripple-detrapping process which prevents the fast ions from escaping directly out of the plasma region.

4-3-2. Ripple-enhanced banana-drift loss

Even if fast ions are not trapped in the ripple well near a banana tip, they can take a large radial drift as shown in Fig.3-5. This kind of radial drift cannot be cancelled in a bounce time. In a top-bottom symmetric ripple field, however, outward and inward drift are balanced in many bounces, therefore, ripple transport of fast ions may be described by a diffusive process, which is much different from the convective one in a top-bottom asymmetric ripple field[3].

In order to estimate the diffusion coefficient, we consider a simple model of the banana drift instead of the saw-tooth-shaped one as shown in Fig.4-4. The random walk step size Δr_{BD} ($= C_{BD}\Delta r$) and the effective collision time Δt ($= \tau_b \Delta \zeta_k' / \Delta \zeta_{BD}$) are calculated by means of a least square method. The diffusion coefficient of the ripple-enhanced banana drift is represented by

$$D^{BD} \sim \frac{<\Delta r_{BD}^2>}{\Delta t} \sim \frac{C_{BD}^2}{(\Delta \zeta_k' / \Delta \zeta_{BD})} \frac{(\Delta r)^2}{\tau_b} . \qquad (4\text{-}6)$$

The analytical calculation described in Appendix shows that $C_{BD}^2/(\Delta \zeta_k' / \Delta \zeta_{BD})$ is about 0.02 for all the value of $|\alpha|$ less than unity.

The energy loss time τ_{ro} calculated by the orbit-following Monte-Carlo code is shown in Fig.4-5 as a function of B_t. In the low B_t region, τ_{ro}/τ_s is proportional to B_t^2. This nature of the B_t dependence of τ_{ro} is well described by the diffusion process mentioned above, and the loss time defined by the diffusion coefficient (eq.(4-6)) agrees well with that of Monte-Carlo calculation.

As the toroidal field becomes high, τ_{ro}/τ_s changes its B_t dependence. In order to understand this nature of τ_{ro}, we count the number of particles undergoing more than one sequential process of ripple-trapping and detrapping. The number ration of these particles to the total banana-drift loss particles N'/N is plotted against B_t in Fig.4-5. In the high B_t region ($B_t > 5T$), N'/N is so large that the virtual banana drift due to the sequential process of ripple-trapping and detrapping process predominates over the collisionless ripple-enhanced banana drift described in § 3-4 . This kind of radial drift has been considered as the basic process of ripple-trapped diffusion[4] of bulk plasma ions which is discussed in §7. The histories of the banana-drift loss particles with $N'/N = 0$ and $N'/N > 1.0$ are shown in Fig.4-1 (c) and (d), respectively.

4-4. Collisional region ($|\zeta| > \zeta_\alpha$)

Fast ions in this pitch angle region can be lost to the wall by diffusing into the intermediate region as well as into the ripple-modulated loss cone due to the ripple-enhanced banana drift described in § 3-5.

Particles scattered into the intermediate region escape from the plasma region through the processes described in § 4-3. Therefore the collisional process is essential for the loss of fast ions in this pitch angle region, and the loss time τ_{ls} is less affected by the finite banana size of fast ions as shown in Fig.4-2.

Concerning the loss of fast ions scattered into the banana loss cone, it should be noted that the loss cone is strongly disturbed by the toroidal field ripple as shown in Fig.3-6. This ripple-modulated loss cone signifi-

cantly enhances the loss of fast ions with initial pitch angle less than $-\zeta_\alpha$.

4-5. Concluding remarks

Collisional behaviors of fast ions coupled with the guiding center motions in a rippled toroidal field ripple have been investigated for fast ions which originate in a specific point in a plasma with uni-directional velocity and mono-energy. There are three initial pitch angle regions with respect to the loss process of fast ions;

1) direct ripple-trapping region $|\zeta| < \zeta_d$,

2) intermediate region $\zeta_d < |\zeta| < \zeta_\alpha$, and

3) collisional region $|\zeta| > \zeta_\alpha$.

Most of fast ions with pitch angle $|\zeta| < \zeta_\alpha$ are lost in a time interval much shorter than the slowing-down time. Therefore, a kind of loss cone is effectively formed in this pitch angle region. Under the condition $\Delta\zeta_k < \Delta\zeta_{bc}$, the ripple trapping time due to finite banana size effect is simply given by

$$\tau_t^{FB} = \frac{\Delta\zeta_k}{\Delta\zeta}\,\tau_b .$$

The diffusion coefficient of ripple-enhanced banana drift for fast ions in the intermediate region can be approximately given by

$$D^{BD} \sim 0.02\,\frac{(\Delta r)^2}{\tau_b}$$

which is independent of the collisionality.

References

1) K. Tani, H. Kishimoto, S. Tamura : *Proc. 9th European Conf. on Controlled Fusion and Plasma Physics, Oxford*, Vol. 1 (1979) p. 157.

2) K. Tani, M. Azumi, H. Kishimoto, S. Tamura : J. Phys. Soc. Japan 50 (1981) 1726.

3) R.J. Goldston, D.L. Jassby : Princeton Plasma Physics Lab. Rep. MATT-1244.

4) T.E. Stringer : Nucl. Fusion 12 (1972) 689.

Table 4-I Calculation parameters

major radius	$R_t = 3.03\ m$
minor radius	$a = 0.95\ m$
toroidal field	$B_t = 4.5\ T$
plasma temperature	$T_e(r) = 1\ keV$ (uniform)
	$T_i(r) = T_e(r)$
plasma density	$n_e(r) = 2.0 \times 10^{19}\ m^{-3}$ (uniform)
plasma current	$j_p(r) = j_0(1-(r/a)^2)$
	$j_0 = 4.73/q_a\ \ MA/m^2$
safety factor	$q_a = 3.5$
plasma ion species	H^+
effective Z	$Z_{eff} = 1.5$ (uniform)
charge number of impurity ion	$Z_{imp} = 8.0$ (oxygen)
number of toroidal field coils	$N_t = 18$
maximum toroidal field ripple	$\delta_0 = 0.01$
energy of fast ion	$E = 75.0\ keV$
initial position of fast ion	$r/a = 0.9 \quad \theta = 0.0$

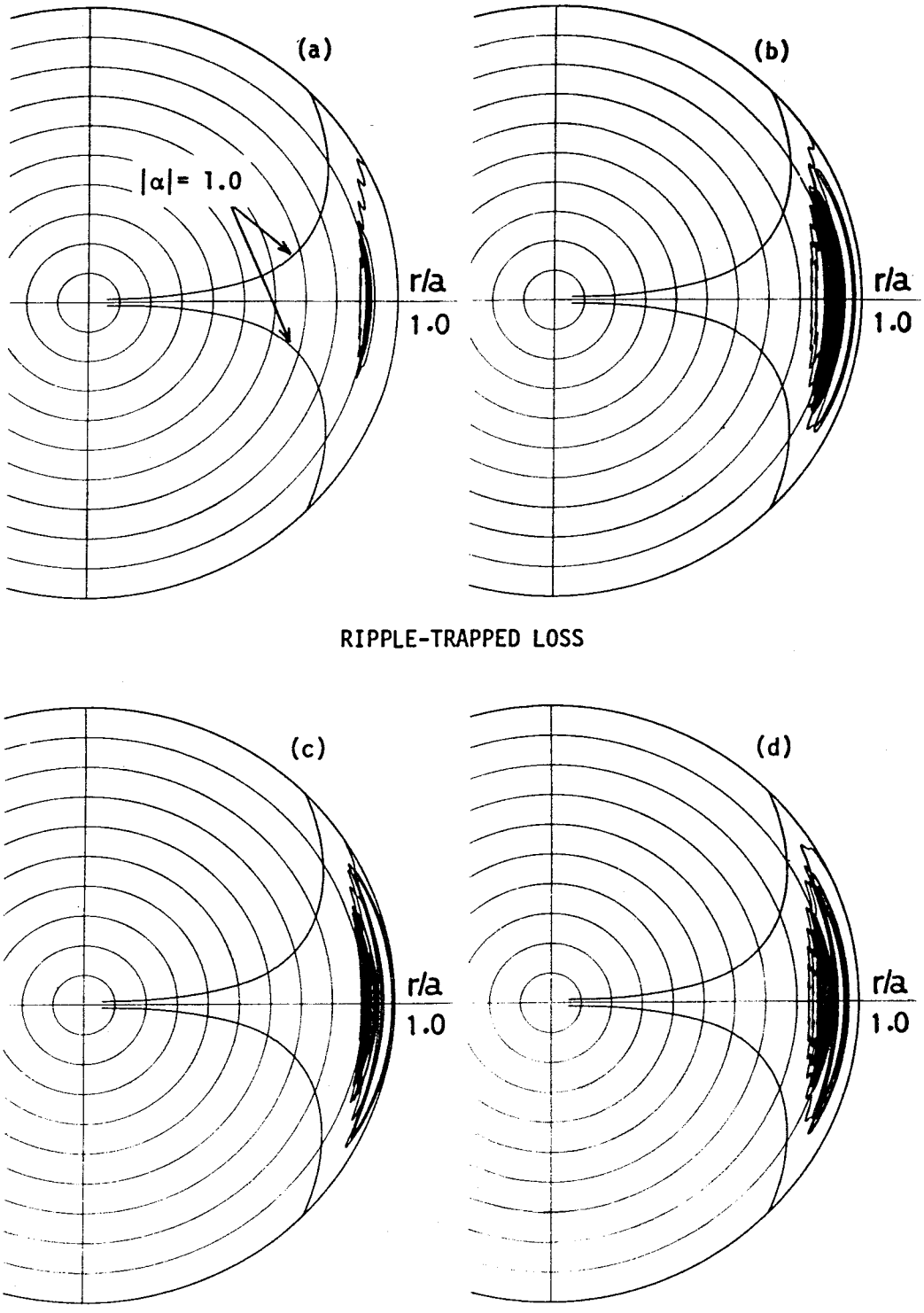

Fig.4-1 Guiding center orbits of loss particles in the slowing down process; (a), (b) for ripple-trapped loss particles and (c), (d) for ripple-enhanced banana-drift loss particles.

Fig.4-2 Relative energy loss time to slowing down time versus initial pitch angle. The total loss time τ_{ls}/τ_s (—●—) and loss time of ripple-trapped loss particles τ_{rt}/τ_s (—○—) for fast ions with finite banana size. The dotted curve (--×--) is the one for fast ions whose banana size is artificially reduced to zero until they are trapped in a ripple well. Calculation parameters as in Table 4-I.

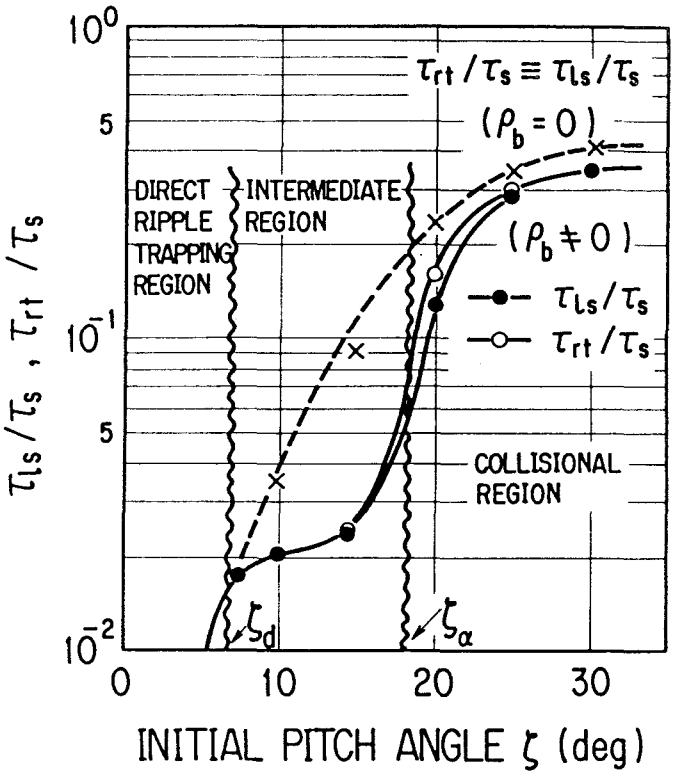

Fig.4-3 Ratio of ripple-trapping time and ripple-trapped loss time to slowing down time, τ_t/τ_s , and τ_{rt}/τ_s , versus toroidal field strength B_t . Calculation parameters as in Table 4-I with initial pitch angle ζ = 10°

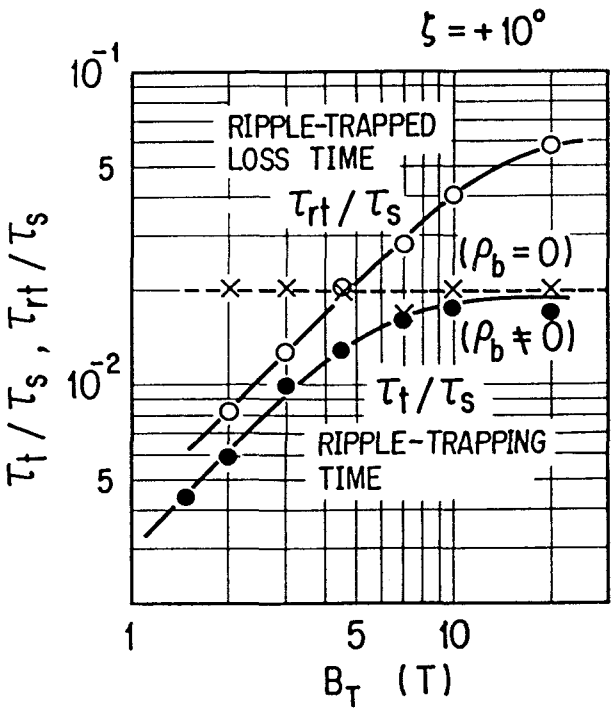

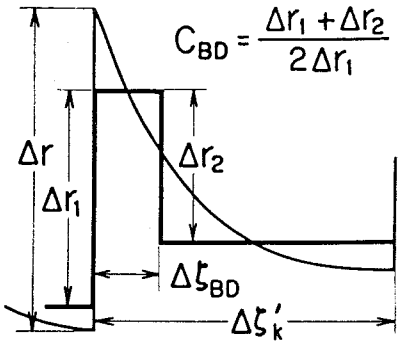

Fig.4-4 Simplified banana drift model for analysis.

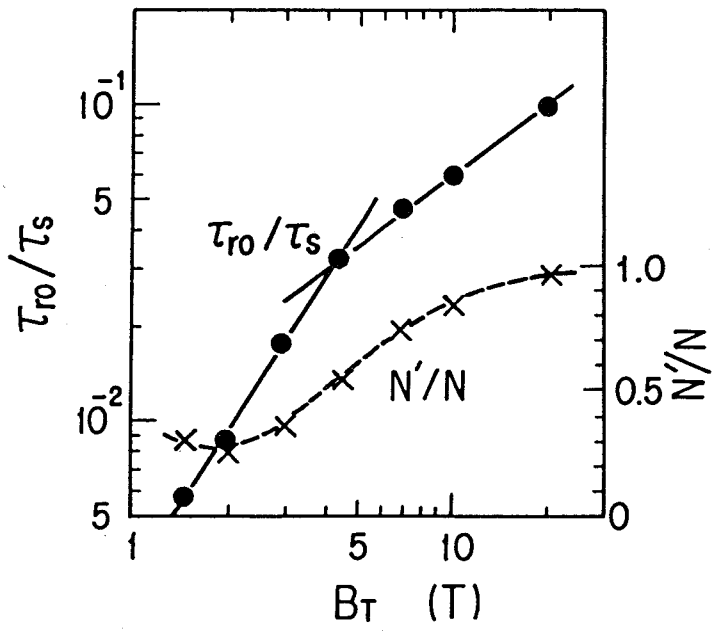

Fig.4-5 Banana-drift loss time normalized by slowing down time τ_{ro}/τ_s and relative number of particles undergoing more than one sequential process of ripple-trapping and detrapping among banana drift loss particles N'/N versus B_t. Calculation parameters as in Table 4-I with initial pitch angle ζ = 10° .

§ 5. Ripple Loss of Fast Ions Produced by Quasi-perpendicular NBI

5-1. Introduction

Neutral beam injection is the most promising plasma heating method which has been demonstrated in many fusion devices[1)-7)]. As the machine becomes large in size, the beam energy should be improved for the sufficient beam penetration. The acceleration voltage, however, is limited within about 150~200 keV for deuteron beam due to the deterioration of the neutralization efficiency of energetic ions. This leads us to choose the quasi-perpendicular neutral beam injection to save the beam path length from the plasma surface to the center. As the injection angle approaches perpendicular with respect to the magnetic axis, the birth point of fast ions is brought close to the effective ripple loss cone described in § 4-3 and the ripple-associated loss of fast ions is increased. Therefore, the ripple loss of fast ions produced by neutral beam injection strongly depends not only on the field ripple but also on the injection angle.

The consideration on the ripple loss of injected beam ions is important from the view point not only of the beam energy confinement but also of the protection of the first wall from the loss particles. The ripple-trapped loss particles undergo a gradient-B drift and may lost to the specific narrow area on the first wall. This kind of particle loss results in an enhancement of the local heat loading.

The loss of the beam power due to the toroidal field ripple[8)] as well as the consequent local heat deposition on the first wall[9)] are the essen-

tial problems in the design of the neutral beam injection for reactor grade large tokamaks. The main objective of the development of our orbit-following Monte-Carlo code is to obtain a lot of useful information on the design of NBI and on the plasma heating scenario in a large tokamak by evaluating the ripple loss of fast ions produced by NBI.

5-2. Birth distribution of fast ions

Fast neutral atoms injected into an ohmically heated plasma are ionized or charge exchanged by interactions with field plasma ions and electrons. The fraction of neutral beams which is trapped in a plasma can be described by[10]

$$S = \sum_k \gamma_k \int_0^{L_{max}} \int_0^{2\pi} \int_0^{a_b} f(r_b, \theta_b) \exp\left[-\int_0^{L_b} n_e(r)\sigma_i(E_b/k)dL\right] \times n_e(r)\sigma_i(E_b/k) r_b dr_b d\theta_b dL_b, \quad (5\text{-}1)$$

where r_b, θ_b are polar co-ordinates in the beam cross section perpendicular to the beam line, L_b the beam path length, L_{max} the maximum beam path length which intersects the plasma column, a_b the neutral beam radius, E_b the primary beam energy, γ_k the density fraction of beam atoms with energy of E_b/k, σ_i the total ionization cross section, and $f(r_b, \theta_b)$ the normalized distribution of beam density which gives

$$\int_0^{a_b} \int_0^{2\pi} f(r_b, \theta_b) r_b dr_b d\theta_b = 1.0 .$$

Provided that the cross section for ionization of atomic hydrogen by stripped impurity ions is of the form[11),12)]

$$\sigma_z = Z_{imp}^{1.4}(\sigma_p + \sigma_{cx}),$$

where σ_p is the ionization cross section of atomic hydrogen by protons, σ_{cx} the cross section for charge exchange by protons in atomic hydrogen[13] and Z_{imp} the charge number of impurity ions. Then the total ionization cross section is given by

$$\sigma_i = \sigma_e + (\sigma_p + \sigma_{cx})[f_i + (1 - f_i)^{0.6}(Z_{eff} - f_i)^{0.4}],$$

where σ_e is the cross section for ionization of atomic hydrogen by electrons, Z_{eff} the effective Z and $f_i = n_i/n_e$.

Here we consider a circular cross-sectional neutral beam with

$$f(r_b, \theta_b) = \frac{c_g}{\pi a_b^2} \exp[1 - (r_b/a_b)^2], \tag{5-2}$$

where $c_g = e/(e-1)$. Introducing new variables

$$r_b' = \sqrt{c_g[1-exp(-(r_b/a_b)^2)]}$$
$$\theta_b' = \theta_b/2\pi$$
$$L_b' = L_b/L_{max}$$

and substituting eq. (5-2) into eq. (5-1), we obtain

$$S = 2L_{max}\sum_k \gamma_k \int_0^1\int_0^1\int_0^1 \exp\left[-L_{max}\int_0^{L_b} n_e(r)\sigma_i(E_b/k)dL\right] \times n_e(r)\sigma_i(E_b/k)r_b' dr_b' d\theta_b' dL_b'. \tag{5-3}$$

Since the total number of test particles is limited within about 2000 due to the long computational time, the Monte-Carlo integration method is again adopted to calculate S numerically, in which five uniform random numbers corresponding to r_b, θ_b, L_b, beam ion species k, and co-injection fraction

are generated for every sampling point (≡ test particle).

For example, the above method is adopted to the calculation of birth profile of fast ions produced by neutral beam injection in JT-60. The quasi-perpendicular NBI system for JT-60 is shown in Fig.5-1. Calculation results, projections of birth points on the minor cross section, are shown in Fig.5-2 for various plasma densities; (a) for $n_{e0} = 3\times10^{19}\ m^{-3}$, (b) for $n_{e0} = 1\times10^{20}\ m^{-3}$ and (c) for $n_{e0} = 2\times10^{20}\ m^{-3}$, respectively. As shown in Fig.5-2, the neutral beam in JT-60 comes at an angle with respect the mid-plane (an oblique injection), in which case the initial pitch angle of fast ions is described by

$$\zeta = \cos^{-1}\left[\sqrt{(R_t+r\cos\theta_0)/(R_t+r)}\,\cos\zeta_{bm}\right] ,$$

$$\sim \zeta_{bm} + \cot\zeta_{bm}\,\frac{r}{2(R_t+r)}\,(1-\cos\theta_0) , \qquad (5\text{-}4)$$

where θ_0 is the poloidal angle of birth point and ζ_{bm} is the angle of the beam line with respect to the plane which is vertical to the magnetic axis and contains the birth point. In an oblique beam injection described above, the pitch-angle of fast ions measured in the the mid-plane becomes somewhat greater than ζ_{bm} . Therefore, an oblique NBI is favourable to prevent the ripple loss of injected beam ions.

We see from Fig.5-2 that the radial profile of initial beam-power density depends on plasma deposition. The fraction of fast ions deposited in the plasma periphery where the field ripple is large in size, increases with the plasma density. Consequently, the ripple loss of fast ions produced by NBI may be a strong function of the bulk plasma density.

5-3. Ripple loss of fast ions during slowing down

As described in § 4-1, the ripple-associated loss can be categorized into two groups: ripple-trapped and ripple-enhanced banana-drift loss particles. In the present paper, the fraction of power loss due to ripple-trapped loss particles during slowing down is denoted by G_{rt}, that due to ripple-enhanced banana-drift loss particles by G_{ro} and the total loss by G_t.

First, to estimate the allowable field ripple and injection angle, the mapping of ripple-induced power loss of fast ions produced by neutral beam injection is investigated. In order to deal with generalities, the injection geometry is chosen so that the beam line is on the same level with the mid-plane. Constant contours of the power loss fraction G_t in space of the maximum field ripple δ_o and the complementary injection angle $|90 - \theta_{inj}|$ are shown in Fig.5-3. The injection angle θ_{inj} is defined by an angle between the magnetic axis and the beam line. In a plasma with small aspect ratio ($R_t/a < 10.0$), a geometrical effect makes the angle $|\zeta_{bm}|$ somewhat greater than than $|90 - \theta_{inj}|^\circ$, especially near the plasma periphery. Furthermore, in an oblique injection the initial pitch angle becomes greater than $|\zeta_{bm}|$ as shown in eq. (5-4). The geometrical θ_{inj} in JT-60 is about $90 \pm 12^\circ$, however, the effective injection angle corresponding to the initial pitch-angle of fast ions near the plasma periphery is $\theta_{inj} = 90 \pm (20 \sim 25)^\circ$. Parameters of the neutral beams used in the present investigations are summarized in Table 5-II. For example, in JT-60 with the maximum field ripple δ_0 0.4% to 0.5% and the effective injection angle $\theta_{inj} \sim 90 \pm (20 \sim 25)^\circ$, the loss of injected beam ions is estimated to be only $\sim$ 10% of the total power.

Next, the details of the ripple-associated loss of fast ions , G_{rt} and G_{ro} , against injection angle $90 - \theta_{inj}$ for $\delta_0 = 0.5\%$ are shown in Fig.5-4. To make it clear the effect of the toroidal field ripple on the loss of fast ions, the banana orbit loss in an axisymmetric magnetic field G_{so} is also plotted in Fig.5-4. The difference between G_t and G_{so} can be considered as the contribution of ripple. It is noted that in a toroidal field ripple banana-orbit loss is remarkably enhanced even in the co-injection scheme. Consequently, in the presence of ripple, the total loss of fast ions has no significant difference between the counter- and the co-injection of neutral beams with a quasi-perpendicular injection angle. From a view point of reducing the fast ion loss, the co-injection scheme is somewhat preferable to the counter-injection in the larger injection angle region. However, the ripple-enhanced banana-drift loss G_{ro} does not decrease sufficiently with an increase of the complementary angle of θ_{inj} in the co-injection side. At the injection angles of JT-60, the power loss fraction of injected beams is estimated to be about 8 to 11% for co-injection and 12 to 14% for counter-injection with the parameters used here. In an axisymmetric toroidal field, power loss fractions of 1.5% for co-injection and 5.5% for counter-injection are estimated. Therefore, the loss of fast ions is enhanced by the toroidal field ripple by a factor of 3.

The ripple loss of injected beam ions depends also on their radial birth profile which is briefly shown in § 5-1. Hence, the plasma density dependence of ripple loss is an important consideration to estimate the maximum plasma density in neutral beam injection heating. Various power loss fractions associated with beam injection are shown in Fig.5-5 as a function of the average plasma density $\bar{n}_e$. In Fig.5-5, G_{cx} denotes the

charge-exchange loss of fast ions during slowing down and G_{sh} the loss of injected neutral beams due to shine through. The neutral particle density for the calculation of charge-exchange loss described in § 2-4 is obtained by solving a Boltzmann equation with respect to neutrals which is three dimensional in velocity space and one dimensional in real space[14]. Both ripple-induced losses G_{ro} and G_{rt} are roughly proportional to the average plasma density. In high density plasma ($\bar{n}_e > 2\sim3\times10^{19}\ m^{-3}$), the ripple loss dominates the loss process of fast ions produced by a quasi-perpendicular neutral beam injection.

5-4. Localized heat loading on the first wall due to ripple-trapped loss particles

As discussed in § 3-2, the ripple well is formed in the region defined by

$$|\alpha| < 1.$$

In this region, the corrugated field has a minimum at $N_t\varphi_1 = 2n\pi + \sin^{-1}\alpha$ with the adjacent maximum at $N_t\varphi_2 = (2n + \alpha/|\alpha|)\pi - \sin^{-1}\alpha$, where n is any integer less than N_t.

From the guiding center equation (2-7-2), we obtain a relation for ripple-trapped particles:

$$\frac{1}{2} m_t \left(R \frac{d\varphi}{dt} \right)^2 + \psi = \psi_t . \qquad (5\text{-}5)$$

Here

$$\psi = \mu_m B\delta N_t (\alpha\varphi + \cos N_t\varphi/N_t), \qquad (5\text{-}6)$$

and $\psi_t = \psi(\varphi_t)$, where φ_t is the toroidal angle at the turning point of a ripple-trapped oscillation. The ripple well depth is given by

$$\Delta\psi = \psi(\varphi_2) - \psi(\varphi_1)$$

$$= \Delta\psi_0 \left[\sqrt{1-\alpha^2} - |\alpha| \left(\frac{\pi}{2} - \sin^{-1}|\alpha|\right)\right], \qquad (5\text{-}7)$$

where $\Delta\psi_0 = 2\mu_m B\delta$ is the ripple well depth at $|\alpha| = 0$.

For a particle trapped barely in the ripple well ($\psi_t = \psi(\varphi_2)$), the oscillation width in the toroidal angle becomes $\Delta\varphi = |\varphi_k - \varphi_2|$, where φ_k is determined by

$$\alpha N_t\varphi_k + \cos N_t\varphi_k = (2n + \alpha/|\alpha|)\pi\alpha - \alpha\sin^{-1}\alpha + \sqrt{1 - \alpha^2}.$$

Any ripple trapped particles exist within the region bounded by (φ_2 , φ_k) during their gradient-B drift. It is noted that the oscillation band width $\Delta\psi$ becomes small with the increase of $|\alpha|$ toward unity, and $\Delta\varphi = 0$ and $\Delta\psi = 0$ at $|\alpha| = 1$.

In a reactor-grade tokamak, various kinds of ions, such as thermal plasma ions, beam injected ions, and alpha-particles, can be lost out of the plasma region under the influence of ripple. Particles whose banana tips are in the ripple-well region ($|\alpha|<1$), can be rapidly trapped by ripple or undergo large radial banana drift as shown in the last section. Even if the banana tips exist outside the ripple-well region, some fraction of those ions can be scattered into the region and lost by ripple trapping or ripple-enhanced banana drift.

In the present investigation, the fast ions produced by neutral beam injection is typically considered. The parameters used here are summarized in Table 5-I and 5-II. From the Monte-Carlo calculations with these parameters, we evaluate the fraction of loss power against the injected beam power: 3.5% for ripple-trapped loss and 8% for banana drift loss.

The deposition of the loss ions is mapped on the plasma surface $r = a$ as shown in Fig.5-6. We see that the ripple-trapped loss ions are distributed within the region (φ_2, φ_k). Furthermore, they are also concentrated in a narrow region of the poloidal angle. This poloidal localization comes from the trapping process which means that ions are scattered from the region free of ripple well into the shallow well region, $|\alpha| \sim 1$, and are ripple-trapped before diffusing into the deeper well region, $|\alpha| \ll 1$. Fast neutrals due to charge-exchange loss distribute almost uniformly on the $r = a$ surface, and no noticeable localization was observed. The ripple-trapped loss particles hit the first wall of the containment vessel and the banana-drift loss particles may enter the material limiter or the neutralizer plate in a divertor system.

The feature of ripple-trapping seems to be important for the localization of loss particles. The well depth for ripple trapped particles is given by

$$[\Delta\psi]_{tr} = \psi_t - \psi(\varphi_1),$$

and $[\Delta\psi]_{tr}$ becomes equal to $\Delta\psi$ for barely trapped particles. The mapping of ripple-trapped loss ions on the $\alpha - \sqrt{[\Delta\psi]_{tr}}$ plane is shown in Fig.5-7. It is found that fast ions are barely trapped in the shallow well, and this tendency becomes pronounced with the increase of the ion energy.

The poloidal profiles, Γ_θ, as well as the toroidal ones, Γ_φ,

are shown in Fig.5-8 for the heat deposition of loss particles, where

$$\Gamma_\theta = R \int_0^{2\pi/N_t} g(\theta, \varphi)\, d\varphi$$

and

$$\Gamma_\varphi = a \int_{-\pi}^{\pi} g(\theta, \varphi)\, d\theta$$

with the loss power density $g(\theta, \varphi)$ on the $r = a$ surface. The loss power associated with the ripple-trapped loss ions is concentrated in a region $30^\circ < \theta < 45^\circ$ and $10^\circ < \varphi < 15^\circ$ of every toroidal coil section, which is less than 1% of the plasma surface area. The banana drift-loss power has a rather broad profile in the poloidal direction but is localized toroidally. This toroidal localization of banana-drift loss power is accounted for the ripple-enhanced banana drift which becomes significantly large near the rippled field maximum at φ_2.

The heat load on the first wall due to ripple-trapped loss ions reaches 0.7~0.8 MW/m^2 at its peak under the conditions investigated here. The power density of the banana-drift loss ions on the limiter or the neutralizer plate basically depends on their geometrical configuration. However, the heat load is estimated to be tens of MW/m^2 on the usual poloidal limiter or neutralizer plate.

The situation concerning the localization of heat deposition is the same for the ripple loss of bulk plasma ions, r.f. heated ions and alpha particles. Hence, the heat loading is enhanced further by these particles in tokamak reactor. Effective protection against the localized heat deposition due to ripple may be essential in the first-wall thermal design.

5-5. Concluding remarks

Ripple-associated loss of fast ions produced by a quasi-perpendicular neutral beam injection has been investigated numerically by use of the orbit-following Monte-Carlo code. Conclusions obtained in the present investigations are summarized as follows:

1) The ripple enhanced loss dominates the loss of fast ions produced by a quasi-perpendicular neutral beam injection in a reactor-grade tokamak.
2) In order to hold down the ripple loss of fast ions to be less than 10% of the total, $|90 - \theta_{inj}| > 20^{\circ}$ and $\delta_0 < 0.5\%$ for the typical plasma parameters summarized in Table 5-I.
3) Banana-drift loss of fast ions is significantly enhanced by the field ripple not only in the counter-injection but also in the co-injection. Consequently, no remarkable advantage of co-injection can be expected for a quasi-perpendicular injection in the presence of ripple.
4) One of the essential features of the ripple-trapped loss is the localization of the loss particles in a specific narrow area on the first wall. This causes a serious heat load problem of the first wall, especially for a long pulse neutral beam injection heating.

References

1) L.A. Berry *et al.*: *Proc. 5th Int. Conf. on Plasma physics and Controlled Nuclear Fusion Research*, Tokyo, 1974, Vol.1, IAEA, Vienna

(1975) p. 101.

2) EQUIPE TFR : Nucl. Fusion 16 (1976)

3) L.A. Berry *et al.*: *Proc. 5th Int. Conf. on Plasma physics and Controlled Nuclear Fusion Research*, Berchtesgaden, 1976, Vol.1, IAEA, Vienna (1977) p. 49.

4) M. Murakami *et al.*: *Proc. 8th Int. Conf. on Plasma physics and Controlled Nuclear Fusion Research*, Brussels, 1980, Vol.1, IAEA, Vienna (1981) p. 377.

5) N. Suzuki *et al.*: *Proc. 8th Int. Conf. on Plasma physics and Controlled Nuclear Fusion Research*, Brussels, 1980, Vol.1, IAEA, Vienna (1981) p. 525.

6) F. Wagner *et al.* : Presented at 9th IAEA Conf. on Plasma Physics and Controlled Nuclear Fusion Research, Baltimore (1982), paper IAEA-CN-41/A-3

7) S. Yamamoto *et al.* : Presented at 9th IAEA Conf. on Plasma Physics and Controlled Nuclear Fusion Research, Baltimore (1982), paper IAEA-CN-41/A-5

8) K. Tani, H. Kishimoto, S. Tamura : J. Phys. Soc. Japan 50 (1981) 1726.

9) K. Tani, H. Kishimoto : Nucl. Fusion 22 (1982) 1108.

10) M. Ohtsuka, K. Tani, H. Kishimoto, R. Shimada, H. Yoshida, K. Hoshino, S. Tamura :"*Fast Ion Spatial Distribution in Neutral Beam Injection into a Tokamak*", JAERI-M 7551 (1978)

11) R.E. Olson, A. Salop : *Stripped Ion Collision of Interest in MFE plasma Research, Stanford Research Institute Annual Report* (1977).

12) Y. Nakai *et al.* : KAKUYUGO KENKYU, 39 (1978) p. 241.

13) A.C. Riviere : Nucl. Fusion 11 (1971) 363.

14) T. Kobayashi, T. Tazima, K. Tani, S. Tamura: JAERI-M 7014.

Table 5-I Plasma parameters

major radius	$R_t = 3.03 \ m$
minor radius	$a = 0.95 \ m$
toroidal field	$B_t = 4.5 \ T$
plasma temperature	$T_e(r) = T_{e0}(1-(r/a)^2$
	$T_i(r) = T_e(r)$
	$T_{e0} = 1.0 \times 10^4 \ eV$
plasma density	$n_e(r) = n_{e0}(1-(r/a)^4)$
	$n_{e0} = 1.0 \times 10^{20} \ m^{-3}$
plasma current	$j_p(r) = j_0(1-(r/a)^2)$
	$j_0 = 4.73/q_a \ MA/m^2$
safety factor	$q_a = 3.5$
plasma ion species	H^+
effective Z	$Z_{eff} = 1.5$ (uniform)
charge number of impurity ion	$Z_{imp} = 8.0$ (oxygen)
number of toroidal field coils	$N_t = 18$
maximum toroidal field ripple	$\delta_0 = 0.005$

Table 5-II Parameters of neutal beams in JT-60

beam energy	$E = 75\ keV$
beam power	$P = 20\ MW$
power ratio of neutral beam components	$P_E : P_{E/2} : P_{E/3} = 0.6 : 0.3 : 0.1$
effective injection angle	θ_{inj} about +70 *deg.* (co) +110 *deg.* (counter)
injection scheme	$P_{co} : P_{counter} = 1 : 1$
beam particle species	H^0

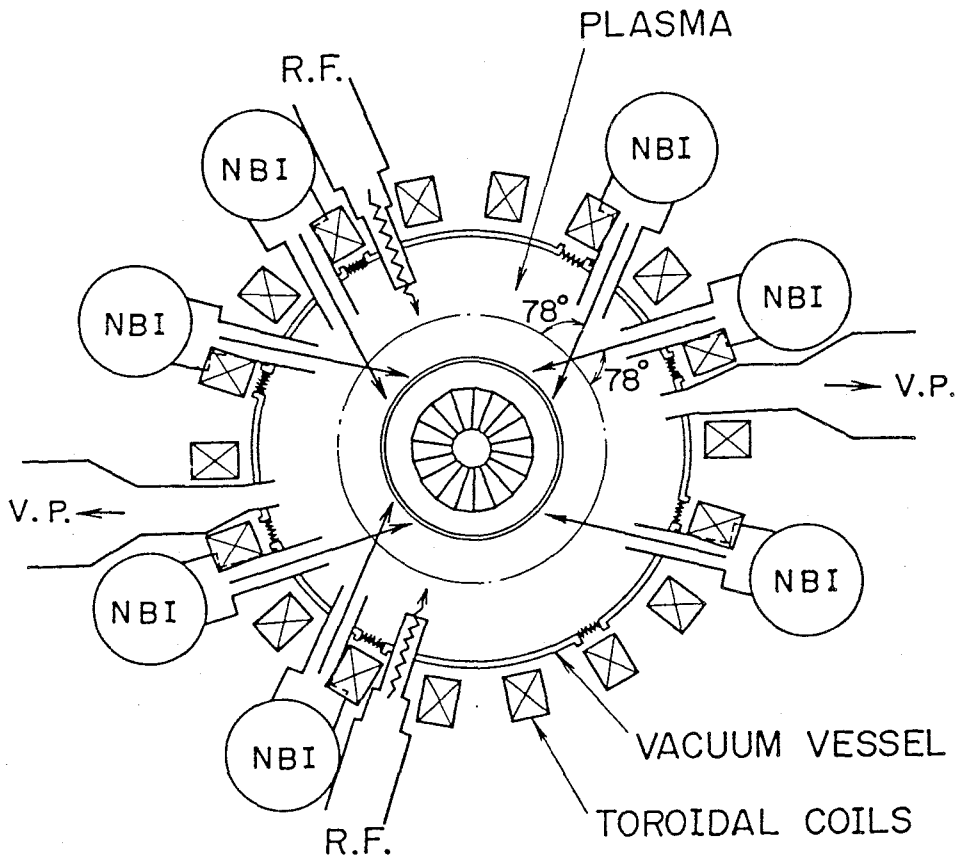

Fig.5-1 Neutral beam injection system in JT-60.

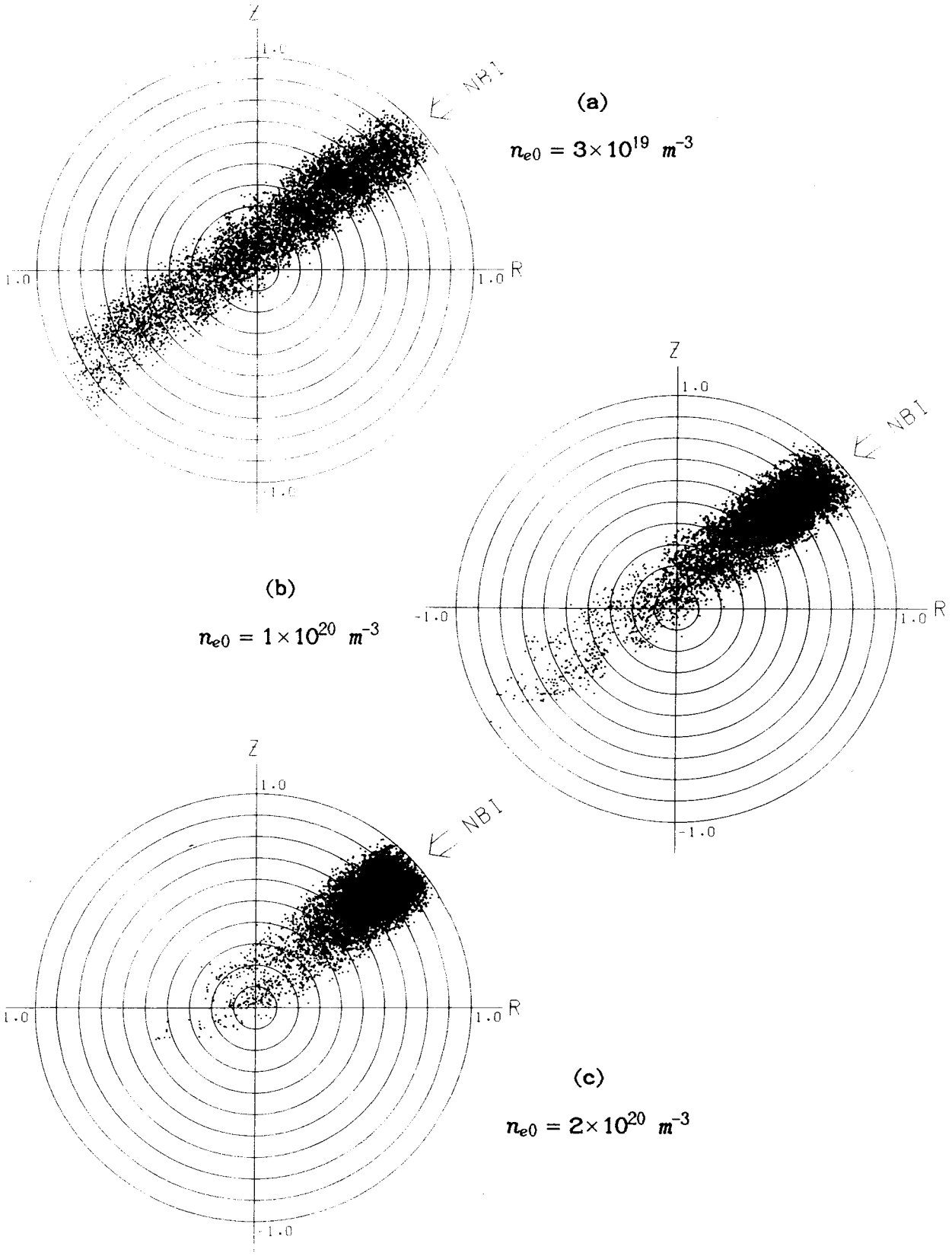

Fig.5-2 Radial profile of beam-power density for various plasma density: $n_e(r) = n_{e0}\,[1 - (r/a)^4]$.

Fig.5-3 Constant contours of power loss fraction in space of maximum field ripple and injection angle. Calculation parameters as in Table 5-I and 5-II.

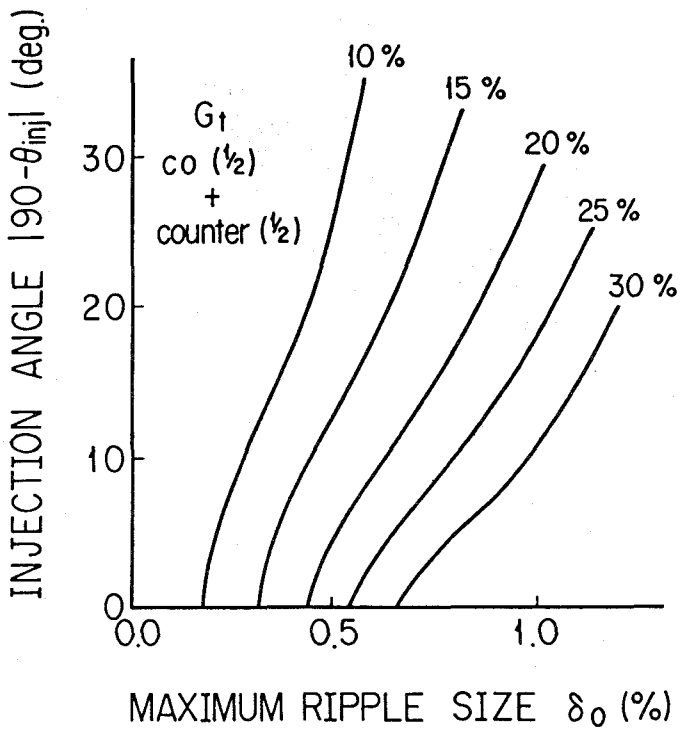

Fig.5-4 Power loss fraction of fast ions produced by NBI in JT-60 against injection angle. G_{rt} and G_{ro} are the ripple-trapped loss and the banana-drift loss. G_{so} is the banana orbit loss in an axisymmetric field. G_t is the sum of G_{rt} and G_{ro}. Calculation parameters as in Table 5-I and 5-II.

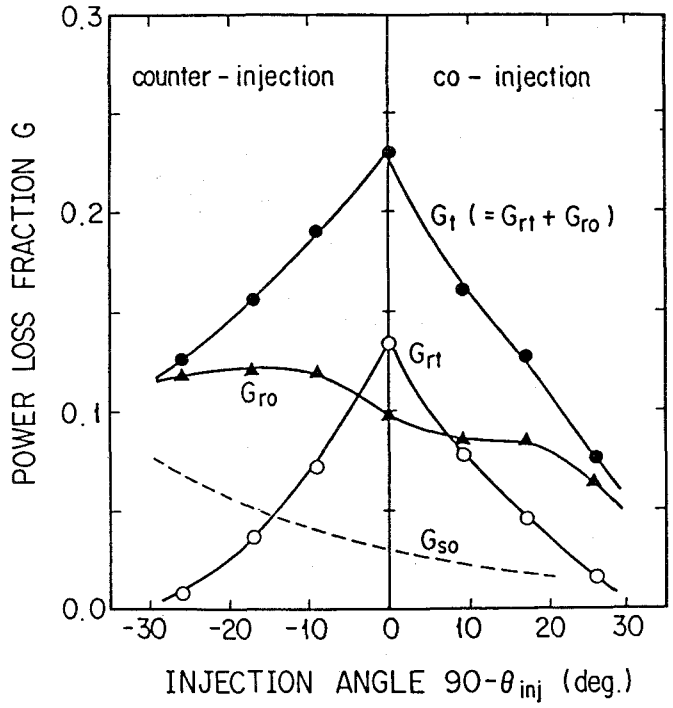

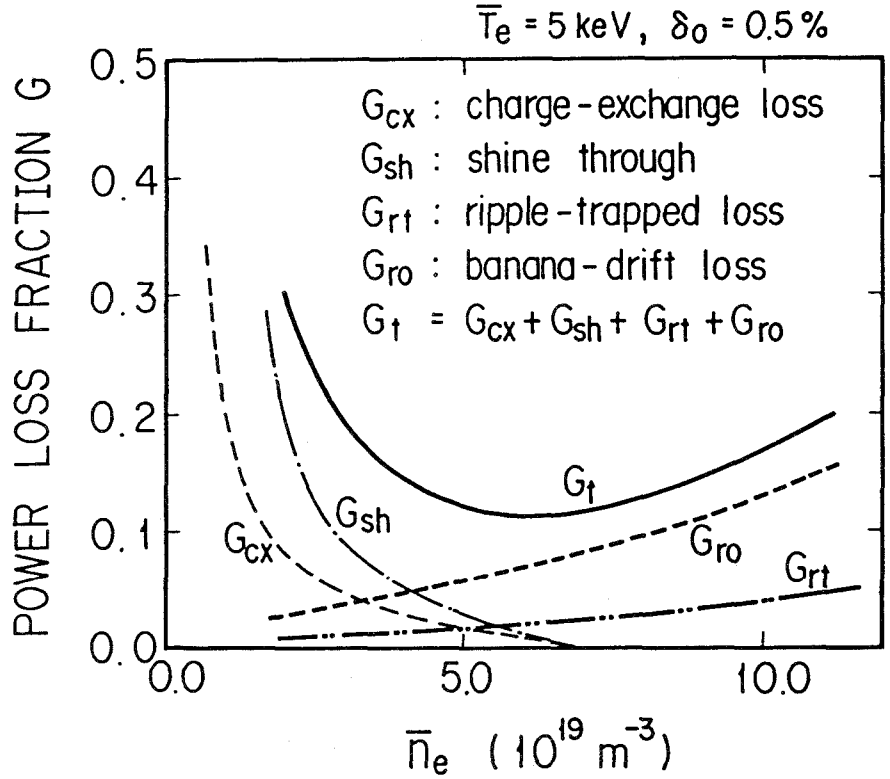

Fig.5-5 Power loss fraction of injected beam versus average plasma density. G_{cx} is the charge-exchange loss during slowing down and G_{sh} is the loss due to shine through. G_t is the sum of G_{sh} ,G_{cx} ,G_{ro} and G_{rt} . Calculation parameters without notice are as in Table 5-I and 5-II.

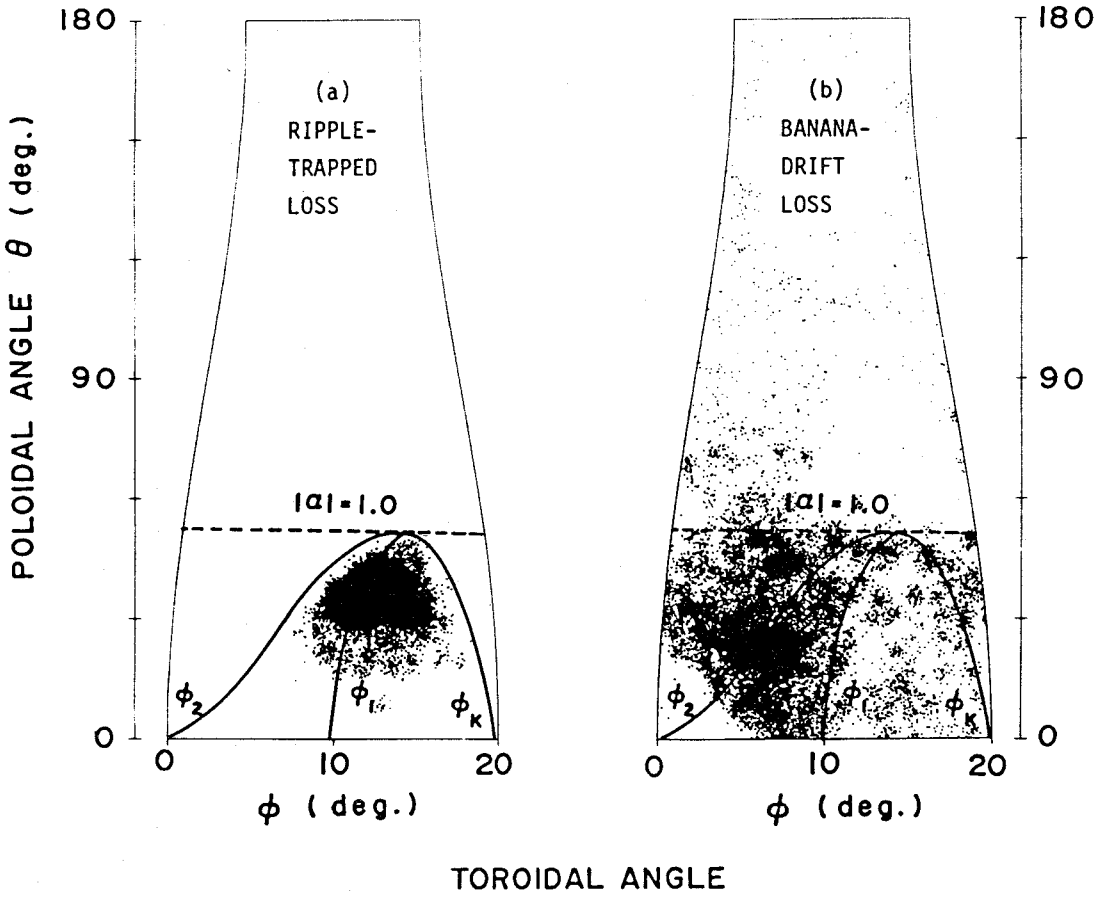

Fig.5-6 Mapping of ripple-induced loss particles on plasma surface.

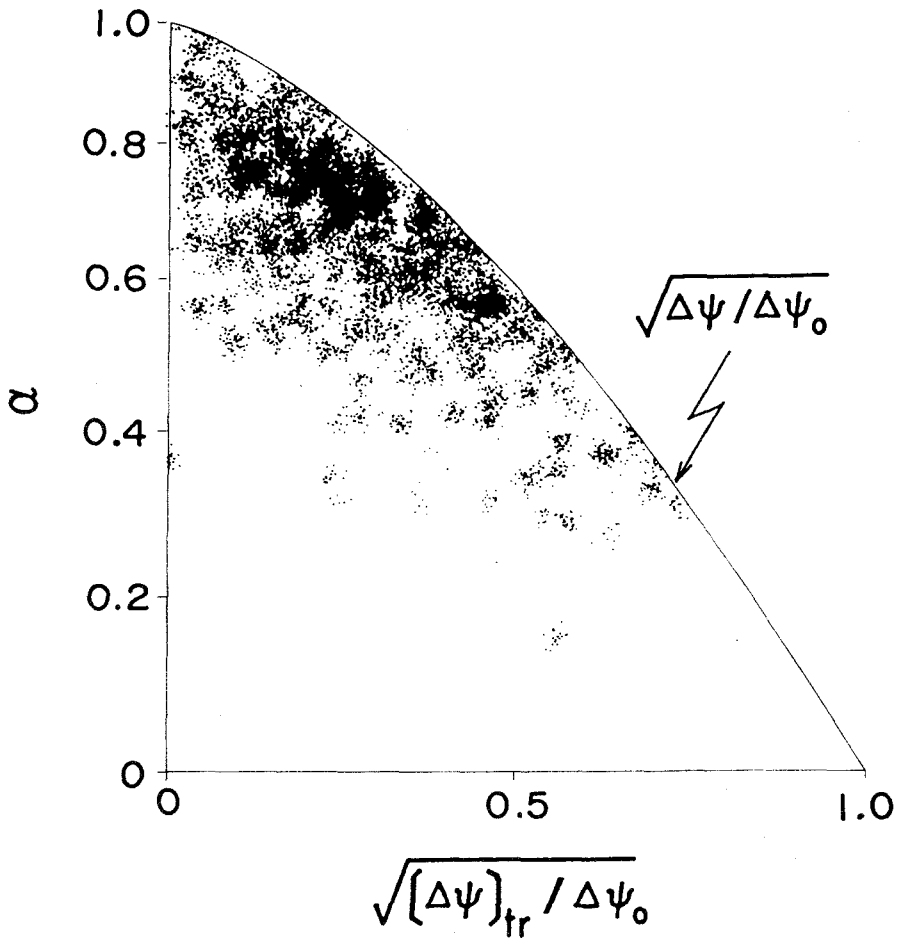

Fig.5-7 Well depth distribution of ripple trapped loss particles.

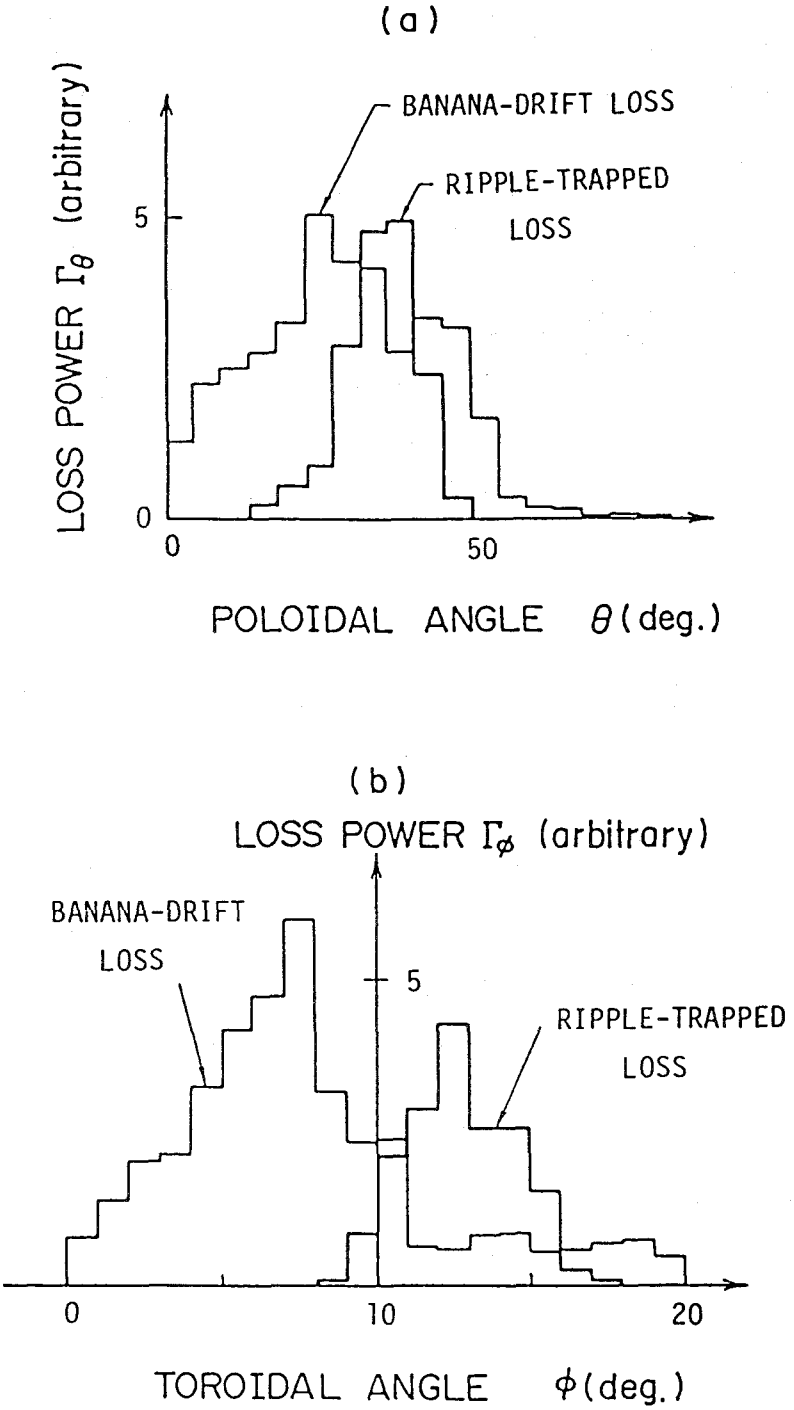

Fig.5-8 Poloidal and toroidal profiles of loss power on plasma surface.

§ 6. Ripple Loss of Suprathermal Alpha Particles during Slowing Down

6-1. Introduction

In the last decade, studies on both prompt[1)-3)] and non-prompt[4)-9)] loss of high-energy charged fusion products were carried out by many authors, and it has been concluded that alpha particles are well confined in an axisymmetric reactor grade tokamak if the contamination of the burning plasma is sufficiently low.

In a real tokamak system, the discrete nature of toroidal field coils produces a small, but finite, field ripple. The effects of the toroidal field ripple on the confinement of fast ions produced by neutral beam injection[10)-13)] and on the transport coefficients of bulk plasma ions[14)-19)] have been investigated extensively, while only a few works[5),20)] are devoted to the confinement of charged fusion products in a rippled toroidal field so that this problem is still unresolved. The design of next generation tokamaks urgently requires a detailed investigation of this problem.

Recently, Goldston *et al.* predicted that there is a critical field ripple which causes the collisionless banana orbit to be ergodic and greatly enhances the banana particle loss[21)]. The allowable toroidal field ripple due to this ergodic loss of banana trapped particles with an energy of 3.5 *MeV* is estimated to be less than 0.3% in a reactor grade tokamak. This fact may substantially affect the reactor concept if the prediction is correct.

Even if the fraction of banana-trapped particles interacting with the toroidal field ripple is large, the loss time of these particles is finite and their energy can be transferred to the plasma via Coulomb collisions. Accordingly, in the present paper, we investigate the ripple effects on the slowing-down process of alpha particles by an orbit-following Monte-Carlo code in which the behavior of fast ions undergoing Coulomb collisions with bulk plasma in a rippled toroidal field is exactly described, and estimate the permissible level of field ripple in a reactor grade tokamak.

6-2. Calculation results and discussions

Numerical investigations are performed for the parameters appropriate to the next generation tokamak (INTOR) which are summarized in Table 6-I. Initially, about 500 test particles are uniformly distributed in a plasma with an energy of 3.5 *MeV* and weighted according to the local fusion reaction rate. We suppose that the distribution of their initial pitch angle is isotropic. After the particles have been launched, we follow them until they all slow down to $\sim 2T_i$.

The model toroidal field coil for the calculation of the field ripple is shown in Fig.6-1 and the constant contours of field ripple δ $(=\tilde{B}_\varphi/B)$ calculated by the method described in § 2-2 are shown in Fig.6-2 for δ_0 = 0.75%. In the presence of $\tilde{B}_r$ and $\tilde{B}_\theta$, the well-known ripple well parameter α is approximately given by eq. (3-1). The boundaries of the ripple well region defined by $|\alpha| = 1.0$ are also shown in Fig.6-2. The lines defined by $|\alpha| = 1.0$ for the case in which both $\tilde{B}_r$ and $\tilde{B}_\theta$ are eliminated from eq. (3-1) are also represented in Fig.6-2 (dashed curves). On the assump-

tion of the usual tokamak ordering, the last two terms in the denominator of eq. (3-1) is much smaller than the first. Therefore, the ripple well region in the self-consistent ripple field covers only a slightly wider area than that in the ripple field $\hat{B}_\varphi$ only.

6-2-1. Prompt loss of alpha particles

Effects of ripple on the prompt loss region in velocity space are investigated by following collisionless guiding center orbits numerically in the ripple field shown in Fig.6-2. Figure 6-3(a), (b) and (c) show the loss region of alphas whose birth points are r/a = 0.9, 0.8 and 0.7 in the mid-plane, respectively. Their initial toroidal angle is set at π/N_t. Collisionless orbits are followed until alpha particles return to the mid-plane or escape to the first wall. It is very interesting that small loss branches appear on both boundaries of the direct ripple-trapping loss cone in the high-velocity region. These branches have not been discovered for fast ions with energy of 100 *keV* at most[12]. Figure 6-3(c) shows a very distorted ripple-trapping loss cone only in the high-velocity region. Generally, the collisionless ripple-detrapping process[12] limits the pitch angle width of the direct ripple trapping loss cone. It must be noted that in the present ripple field any particle trapped at $r/a = 0.7$ in the mid-plane (Fig.6-3(c)) are detrapped from the ripple well without collision on their gradient-B drift path. The particle detrapped in a collisionless fashion starts to make an excursion along a banana orbit. If the particle has a very high velocity like an alpha particle, the banana orbit can intersect the wall. This kind of loss process gives rise to those small

loss branches. The prompt and non-prompt ripple-trapped loss of alpha particles have been investigated theoretically on the assumption that no collisionless ripple-detrapping occurs[5),20)]. The above mentioned loss process will, however, make it very difficult to analytically estimate the energetic-alpha-particle loss in a realistic ripple field.

The boundary of the banana loss cone is also strongly disturbed by ripple, which may enhance the banana orbit loss of alphas.

As is shown in Fig.6-2, the ripple-well region covers a wide area inside the torus. However, no effect of ripple on the loss cone boundary for barely banana-trapped or transit particles is not observed. This indicates that the effect of the ripple inside the torus on fast ion loss may be expected to be small.

The prompt loss depends strongly on the ripple size. The loss fractions in a plasma with parameters summarized in Table 6-I are $\sim$ 2%, 3% and 7% for δ_0 = 0.5%, 1.0% and 1.5%, respectively. If the maximum ripple size is less than 1%, the ripple-induced prompt loss can be neglected.

6-2-2. Non-prompt loss of alpha particles

(1) Evaluation of the Goldston-White-Boozer criterion for fast ion loss

Goldston, White and Boozer have theoretically found a limit on field ripple for particles with large banana size[21)] which is approximately given by

$$\delta_c = \frac{1}{(N_t \pi q/\varepsilon)^{3/2} \rho q'}, \qquad (6\text{-}1)$$

where ρ is the gyroradius, ε the inverse aspect ratio, q the safety factor and $q' = dq/dr$. The particle whose banana tip is in the region

$$\delta > \delta_c$$

is predicted to be lost in a very short time, because of collisionless stochastic orbits. For example, the boundaries of the ergodic loss region $\delta = \delta_c$ are shown in Fig.6-4 for various δ_0 in INTOR with $q_a = 2.5$.

To evaluate the Goldston-White-Boozer criterion, hereafter referred to as G.W.B. criterion, we investigate the loss process of alpha particles which originate at a specific point in the mid-plane ($r_{int} = 0.6a$) with identical pitch angle and energy. Their initial toroidal angle is assumed to be uniformly distributed between 0 and $2\pi/N_t$. First we measure the loss time τ_{ls} which is defined by

$$\tau_{ls} = \frac{N_0}{dN_L/dt \mid_{t=0}},$$

where N_L is the number of loss particles and N_0 is the total particle number. The loss time τ_{ls} in a collisionless plasma is shown in Fig.6-5 by the solid line as a function of the normalized pitch angle ζ/ζ_c, where ζ_c is the critical pitch angle defined by

$$\cos^2\zeta_c = \frac{R_t + r_{int}\cos\theta_c}{R_0 + r_{int}} \qquad (6\text{-}2)$$

with θ_c the poloidal angle at $r = r_{int}$ on the line $\delta = \delta_c$. As is evident from Fig.6-5, the collisionless τ_{ls} shows a very sharp change at $\zeta \sim \zeta_c$ as was predicted by Goldston *et al.* Furthermore, we compare this numerically derived critical pitch angle with theoretical one by changing the gyrora-

dius of the alpha particles. The hatched region in Fig.6-6 is the theoretical ergodic loss region; the numerically derived critical points are shown by crosses. We see that the two results are in a fairly good agreement.

(2) Collisional effects on transport phenomena of banana-trapped alpha particles

Effects of pitch angle scattering of alpha particles by bulk ions are investigated from the following point of view:

1) pitch angle scattering from $\zeta > \zeta_c$ into $\zeta < \zeta_c$ and resultant enlargement of loss region;
2) enhancement of transport of confined banana particles.

The loss time τ_{ls} in the presence of Coulomb collisions is shown in Fig.6-5 by dashed curves. The slowing down time τ_s is about $10^4\tau_b$ (τ_b is the bounce time of 3.5 *MeV* banana-trapped alpha particles), and the deflection time is chosen as $\tau_d/\tau_s \sim 190$ ($Z_{eff} = 1.5$) and $\tau_d/\tau_s \sim 60$ ($Z_{eff} = 5.0$). Other parameters are as the same as those in sub-section 6-2-2 (1). As is shown in this figure, no significant difference is observed between the collisional and collisionless loss time in the region $\zeta < \zeta_c$. The diffusion coefficient which is roughly estimated as $(a - r_{int})^2/\tau_{ls}$ is of the order of 10 m^2/s and approximately agrees with the ripple-plateau diffusion coefficient[17] given by

$$D^{RP} \sim \frac{(\Delta r_m)^2}{\tau_b} \tag{6-3}$$

where Δr_m is the radial displacement described by[21]

$$\Delta r_m = (N_t \pi / \sin\theta_b)^{1/2} (q/\varepsilon)^{3/2} \rho\delta, \qquad (6\text{-}4)$$

with θ_b the poloidal angle of the banana tip. It is very interesting that the collisional effect moderates the change of τ_{ls} near ζ_c and enlarges the loss region effectively. The enlargement of the loss region may be caused by the collision enhanced ergodicity of banana particles with pitch angle $\zeta \sim \zeta_c$ as well as by the scattering of particles from the pitch angle region $\zeta > \zeta_c$ into the collisionless ergodic region $\zeta < \zeta_c$.

Next, we show the diffusion coefficient D^{CB} for (non-ergodic) banana particles confined in a collisionless way with pitch angle $\zeta > \zeta_c$ ($\zeta \sim 1.4\zeta_c$) in Fig.6- 7. The diffusion coefficient is defined as

$$D^{CB} = \frac{1}{2}\frac{d}{dt}\left[\sum_i (r_i - \langle r \rangle)^2 w_i / \sum_i w_i\right] ,$$

where

$$\langle r \rangle = \sum_i r_i w_i / \sum_i w_i .$$

Here, r_i is the radial position of the i^{th} test particle and w_i the particle density weight. It is found that D^{CB} in this region is proportional to the ion collision frequency ν_i and is in the order of 10^{-1} m^2/s which is about 10 $\sim$ 100 times greater than the axisymmetric neoclassical transport coefficient D^{NC} , but much less than D^{RP} .

The pitch-angle change corresponding to the reduction of toroidal angle $\Delta\varphi = \pi/N_t$ of a banana tip can approximately be written as

$$\Delta\zeta_\varphi \sim \frac{r\sin\theta_b}{R_t + r}\frac{\pi}{N_t q}\frac{1}{\sin 2\zeta} \qquad (6\text{-}5)$$

and the effective collision frequency

$$\nu_{eff} = [\pi/(2\Delta\zeta_{\varphi})]^2 \nu_i . \qquad (6\text{-}6)$$

Then the diffusion coefficient for confined banana particles is roughly given by

$$D^{CB} \sim (2\Delta r_m)^2 \nu_{eff}$$

$$\sim \pi (N_t/\sin\theta_b)^3 (q/\varepsilon)^5 \sin^2 2\zeta (\rho\delta)^2 \nu_i . \qquad (6\text{-}7)$$

The solid line in Fig.6-7 is the diffusion coefficient calculated by the above expression. The analytical diffusion coefficient agrees well with the numerical one. It should be noted that D^{CB} has a very strong dependence on (q/ε). The numerically derived diffusion coefficients are shown in Fig.6-8 as a function of the safety factor q_a. These values agree well with the analytical D^{CB} of eq. (6-7) (the solid line in Fig.6-8). This dependence of D^{CB} on q indicates that the plasma current is a very important parameter for the containment of charged fusion products.

(3) Ripple-enhanced power loss of alpha particles

The evolution of the time integrated power loss fraction during slowing down (collisional power loss fraction) is shown in Fig.6-9 by the solid curve. The evolution of the loss fraction in a collisionless plasma (collisionless power loss fraction) is also shown in Fig.6-9 by the dash-dotted curve. Of course, the time derivative of the loss fraction in Fig.6-9 gives the rate of power loss. The collisionless loss rate shows a very slow decay since particles never slow down. On the other hand, the

collisional loss rate shows a very abrupt change in the very early stage of slowing-down ($<0.3\tau_s$) and is reduced to zero. This is due to the decrease of fast ion energy and the consequent shrinking of the ergodic loss region. It should be noted that the initial loss rate in the collisional case is greater than that in the collisionless one. This result is well explained by the collisional effects on the local diffusion coefficient as described in the last sub-section.

The collisional power loss fraction is shown by the solid line in Fig.6-10 as a function of the maximum ripple size δ_0. Evidently, the loss fraction depends strongly on the ripple size. The initial portion of banana-trapped particles is approximately given by

$$<\sqrt{\varepsilon}> = \int_0^a f_b(r)\sqrt{\varepsilon} r dr \Big/ \int_0^a f_b(r) r dr$$

where $f_b(r)$ is the birth profile of the alpha particles. As the field ripple δ_0 decreases, the power loss fraction becomes much smaller than $<\sqrt{\varepsilon}>$.

The power loss fraction for $\delta_0 = 1\%$ for the condition of the next-generation tokamak summarized in Table 6-I is about 13%. Since the loss fraction in the axisymmetric toroidal field is 3%, the ripple-enhanced loss fraction can be considered to amount to only $\sim$ 10%. Even in the presence of ripple, the energy of charged fusion products is well confined in a plasma.

(4) Ripple-enhanced particle loss of alpha particles

From the view point of ash exhaust, ripple-enhanced particle loss is an interesting and important problem. Particle loss fraction are shown by the dashed-curves in Fig.6-9 and 6-10. Figure 6-9 shows that the decay of the particle loss rate is much slower than that of power loss rate and a large number of low energy alphas are continuously lost to the first wall. This is due to the pitch-angle scattering which is very important for slowed-down particles. The particle loss fraction approaches $<\sqrt{\varepsilon}>$ in the limit of high δ_0. For the data of Table 6-I, the fraction of particle loss is 1.5 to 1.8 times as large as that of power loss for a maximum ripple size $0.4\% < \delta_0 < 1.5\%$ as shown in Fig.6-10. The difference between the power and the particle loss fractions probably comes from the effect of slowing-down. This kind of ripple-enhanced alpha particle loss in the slowing down process may alleviate the problem of ash accumulation.

Ripple-associated loss particles can be categorized into two groups[12] : ripple-trapped and banana-drift loss particles. In the present investigations, only a negligible amount of ripple-trapped loss particles is observed. This implies that the ripple-enhanced banana drift dominates the loss process of not only the energetic but also slowed-down alpha particles.

(5) Spatial distribution of loss alpha particles on the first wall

The localized heat load on the first wall caused by the ripple-trapped loss of fast ions produced by neutral beam injection has been studied[22].

Here, we investigate the distribution of heat load due to the ripple-enhanced loss of charged fusion products.

For the convenience of calculations, we consider a first wall which faces the plasma surface without any unevenness like material limiters; the wall radius r_w is assumed to be a. The finite-Larmor-radius modification of the poloidal angle where alpha particles intersect the wall is not taken into account[7]. The two-dimensional distribution of the heat load due to loss alpha particles is shown in Fig.6-11 for $\delta_0 = 1.5\%$. Since the total number of test particles is limited because of the long CPU time, the distribution is very rugged. The peak heat flux, however,is roughly estimated at 1.5 MW/m^2. The average heat load on the first wall is about 0.1 MW/m^2, therefore, the peaking factor is about 15. The maximum heat flux for $\delta_0 = 0.75\%$ is about 0.7 MW/m^2. The linear interpolation indicates that the peak heat load may reach the order of 1 MW/m^2 if δ_0 exceeds 1%. This level of heat load needs some mechanism to remove it from the first wall for the case of long-pulse operation.

It is very noticeable that a large number of loss particles hit the first wall in the vicinity of the mid-plane as shown in Fig.6-11. This kind of poloidal angle distribution characterizes the ripple-enhanced banana drift loss and is very different from that of loss particles in an axisymmetric tokamak which shows a very wide distribution[2),3),7)]. This property of loss alphas might be capable of removing them from the burning plasma by use of a pump limiter outboard, on the mid-plane. It must be noted that the toroidal angle distribution is also uneven as is shown in Fig.6-11. The radial component of the field ripple $\tilde{B}_r$ has a toroidal angle dependence of $\sin N_t\varphi$; therefore, the magnetic surface expands radially in the region $0<\varphi<\pi/N_t$. It can be considered that this makes the toroidal

angle distribution of loss alphas uneven.

6-3. Concluding remarks

The slowing-down process of suprathermal alpha particles in a rippled toroidal field has been investigated by an orbit-following Monte-Carlo code. Conclusions of the present investigation are summarized as follows:

(1) Small prompt-loss branches appear on both boundaries of the direct ripple trapping loss cone owing to the effect of large banana size.

(2) Collisionless ripple loss process of alpha particles is numerically investigated. The G.W.B. criterion for alpha particle loss has been verified numerically.

(3) Although the initial energy of charged fusion products is very high, collisional effects, slowing down as well as pitch angle scattering, are very important for the estimation of their ripple-enhanced particle and power losses.

(4) The ripple-enhanced banana drift dominates the loss process of alpha particles.

(5) The diffusion coefficient D^{CB} for confined banana particles with pitch angle $\zeta > \zeta_c$ is approximately given by eq. (6-7). For the plasma parameters summarized in Table 6-I with $\delta_0 \sim 1\%$, D^{CB} of 3.5 *MeV* alpha particles is of the order of $10^{-1}\ m^2/s$ which is much larger than D^{NC} (axisymmetric neoclassical diffusion) and much less than D^{RP} (ripple-plateau diffusion).

(6) The ripple-enhanced power loss for $\delta_0 = 1\%$ is about 10% of the total

fusion power of charged particles.

(7) The effect of ripple on particle loss is very important for not only energetic but also slowed-down alphas. The fraction of particle loss is about 1.5 to 1.8 times as large as that of power loss for $0.4\% < \delta_0 < 1.5\%$.

(8) The wall heat load due to loss alpha particles is localized and its peak value reaches the order of 1 MW/m^2 if δ_0 exceeds 1%.

The present investigations show that there is a possibility of realizing the design of tokamak reactors with a realistic field ripple of $\delta_0 \sim 1\%$, permitting 10% power loss of alpha particles. Ripple loss of alpha particles, however, depends on their birth profile as well as on the safety factor q. Therefore, calculations should be made for various profiles of plasma parameters including the plasma current in order to provide a satisfactory answer to the questions arising in the design of fusion reactors. These investigations will be reported in a future paper.

References

1) D.G. McAlees: Alpha Particle Energetics and Neutral Beam Heating in Tokamak Plasmas, ORNL-TM-4661 (1974)

2) Ya.I. Kolesnichenko, A.D. Fursa, U.A. Yavorskij: Sov. J. Plasma Phys. 2 (1976) 506.

3) L.M. Hively, G.H. Miley: Nucl. Fusion 17 (1977) 1031.

4) M. Ohnishi, H. Tokunaga, J. Wakabayashi: Nucl. Fusion 16 (1976) 690.

5) T.W. Petrie, G.H. Miley: Nucl. Sci. Eng. 64 (1977) 151.

6) M. Ohnishi, N. AO. J. Wakabayashi: Nucl. Fusion 18 (1978) 859.

7) W. Bauer, K.L. Wilson, C.L. Bisson, L.G. Haggmark, R.J. Goldston: Nucl. Fusion 19 (1979) 93.

8) L.M. Hively, G.H. Miley: Nucl. Fusion 20 (1980) 969.

9) L.M. Hively, G.H. Miley, J.A. Rome: Nucl. Fusion 21 (1981) 1431.

10) G.G. Lister, D.E. Post, R.J. Goldston: *Proc. 3rd Symp. on Plasma Heating in Toroidal Device, Varenna, Italy, 1976* p. 303.

11) K. Tani, H. Kishimoto, S. Tamura: *Proc. 8th Int. Conf. on Plasma Physics and Controlled Nuclear Fusion Research, Brussels, 1980* vol.1, IAEA, Vienna (1981) p. 631.

12) K. Tani, M. Azumi, H. Kishimoto, S. Tamura: J. Phys. Soc. Japan 50 (1981) 1726.

13) R.J. Goldston, H.H. Towner: Journal of Plasma Physics 26 (1981) 283.

14) T.E. Stringer: Nucl. Fusion 12 (1972) 689.

15) J.W. Connor, R.J. Hastie: Nucl. Fusion 13 (1973) 221.

16) K.T. Tsang: Nucl. Fusion 17 (1977) 557.

17) A.H. Boozer: Phys. Fluids 23 (1980) 2283.

18) P.N. Yushmanov: Nucl. Fusion 22 (1982) 315.

19) K.C. Shaing, J.D. Callen: Nucl. Fusion 22 (1982) 1061.

20) D. Anderson, H. Hamnen, M. Lisak: Phys. Fluids 25 (1982) 353.

21) R.J. Goldston, R.B. White, A.H. Boozer: Phys. Rev. Lett. 47 (1981) 647.

22) K. Tani, H. Kishimoto: Nucl. Fusion 22 (1982) 1108.

Table 6-I Plasma parameters

major radius	$R_t = 5.3\ m$
minor radius	$a = 1.2\ m$
toroidal field	$B_t = 5.5\ T$
plasma temperature	$T_e(r) = T_i(r) = T_p(1-(r/a)^2$
	$(T_D(r) = T_T(r) = T_i(r))$
	$T_p = 2.0 \times 10^4\ eV$
plasma density	$n_e(r) = n_p(1-(r/a)^2)$
	$(n_D(r) = n_T(r) = n_i(r))$
	$n_p = 4.0 \times 10^{20}\ m^{-3}$
plasma current	$j_p(r) = j_0(1-(r/a)^2)$
	$j_0 = 3.3/q_a\ \ MA/m^2$
safety factor	$q_a = 2.5$
effective Z	$Z_{eff} = 1.5$ (uniform)
charge number of impurity ion	$Z_{imp} = 8.0$ (oxygen)
number of toroidal field coils	$N_t = 12$

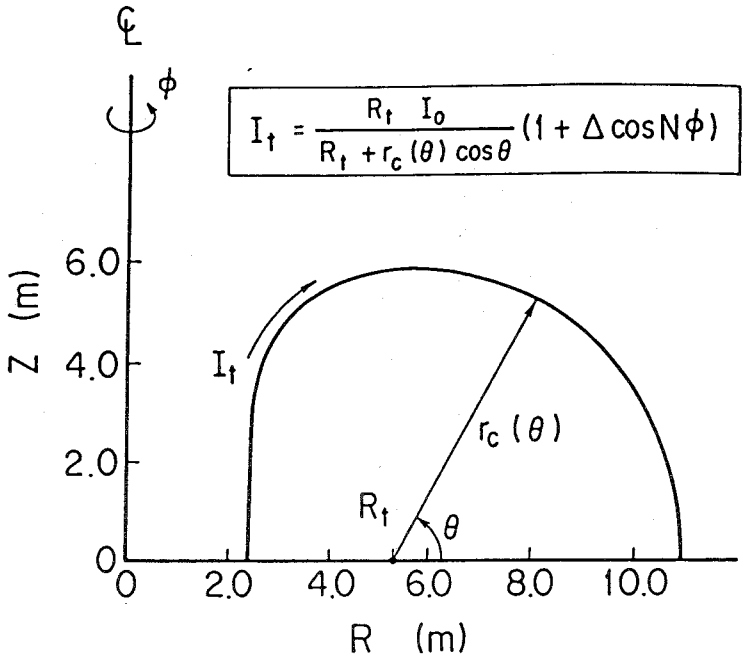

Fig.6-1 Simplified model of toroidal field coil system for calculation of divergence- and curl-free ripple field.

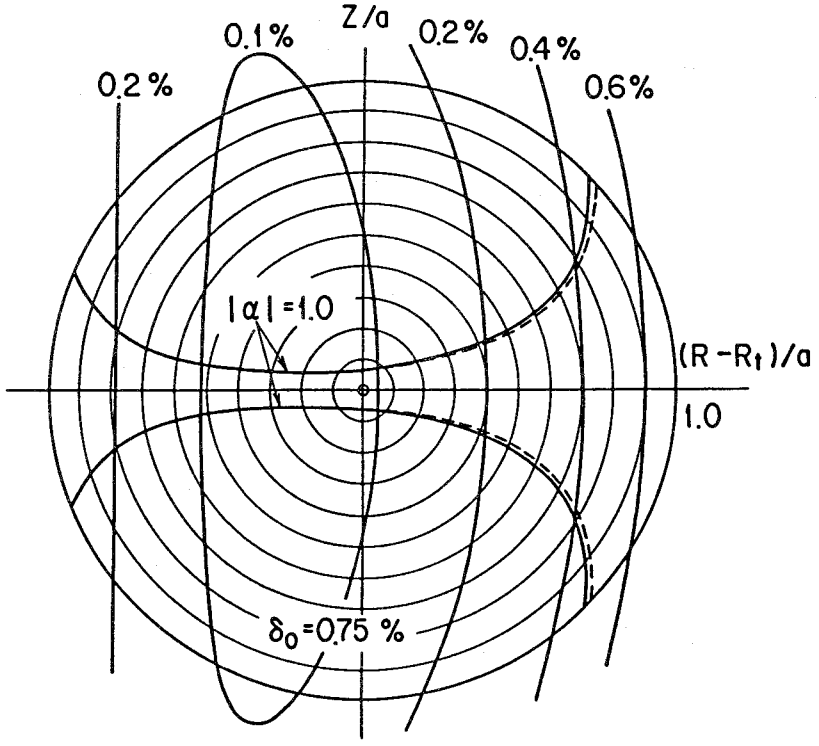

Fig.6-2 Field ripple distribution ($\tilde{B}_\varphi/B$) in the minor cross section for $\delta_0 = 0.75\%$. Ripple-well region in divergence- and curl-free ripple field is shown by the solid lines ; $\tilde{B}_r = \tilde{B}_\theta = 0.0$ ripple field by the dotted.

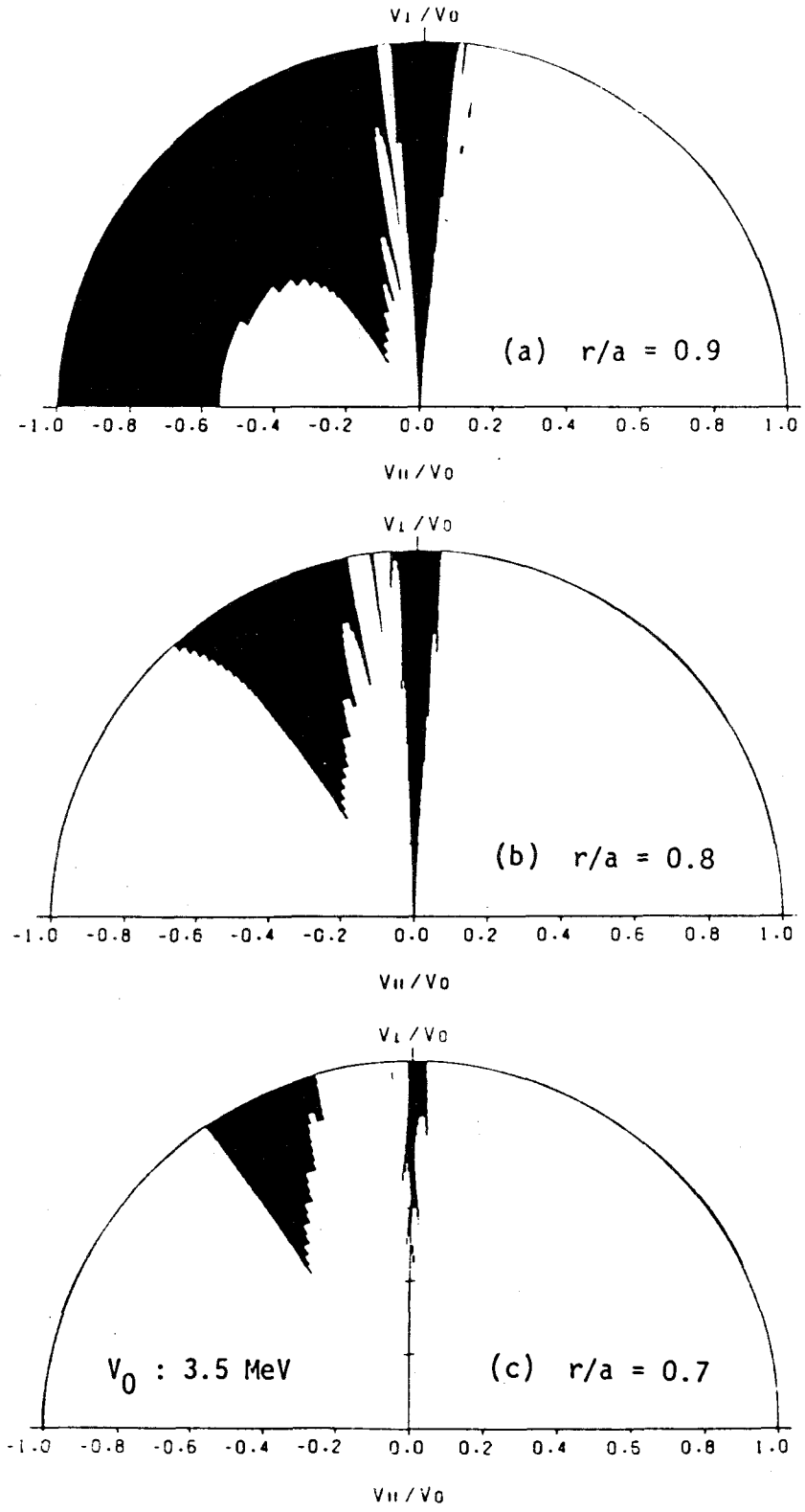

Fig.6-3 Collisionless loss region of alpha particles for δ_0 = 0.75%. Minor radii of starting points are r/a = 0.9(a), 0.8(b) and 0.7(c). Initial θ and φ are set at 0° and 15° , respectively

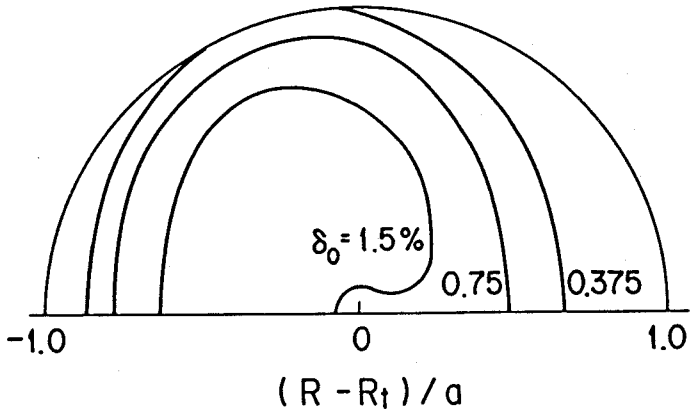

Fig.6-4 Boundary lines of ergodic loss region defined by $\delta = \delta_c$ for various maximum ripple size δ_0.

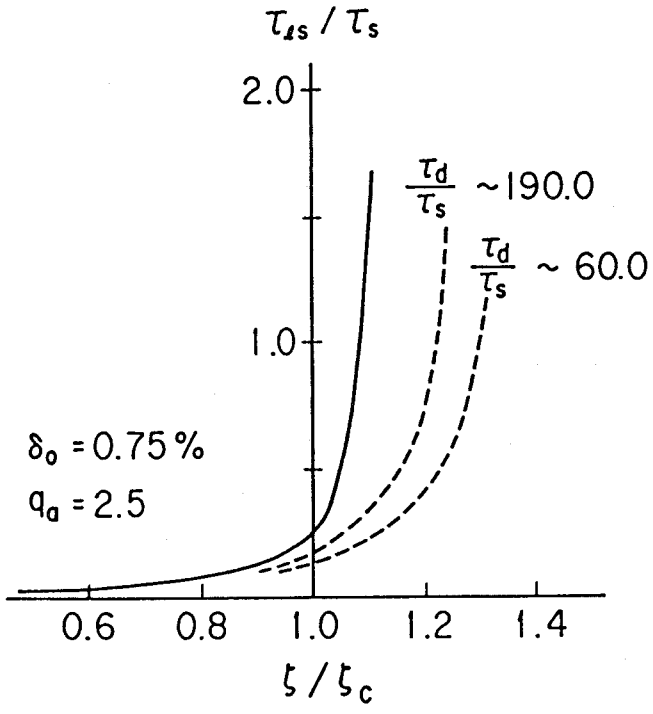

Fig.6-5 Loss time against initial pitch angle for collisionless (——) and collisional plasma (----). Initial position of test particles is set at $r/a = 0.6$ on the mid-plane and $\delta_0 = 0.75\%$. Plasma parameters are uniform in space.

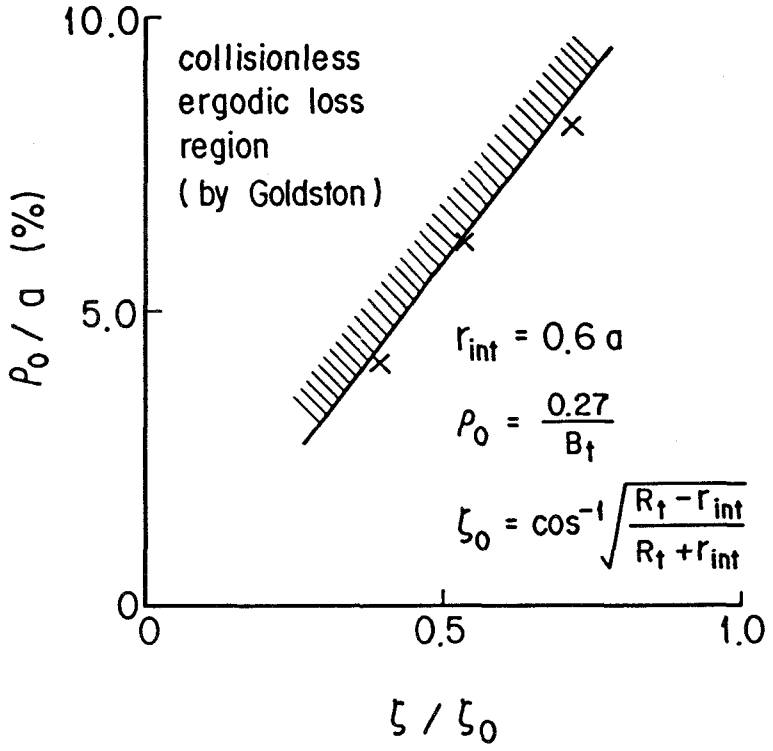

Fig.6-6 Collisionless ergodic loss region in space of gyroradius and initial pitch angle. Numerically derived critical points are shown by crosses. Initial point of test particles is set at r/a = 0.6 in the mid-plane and δ_0 = 0.75%. Plasma parameters are uniform in space.

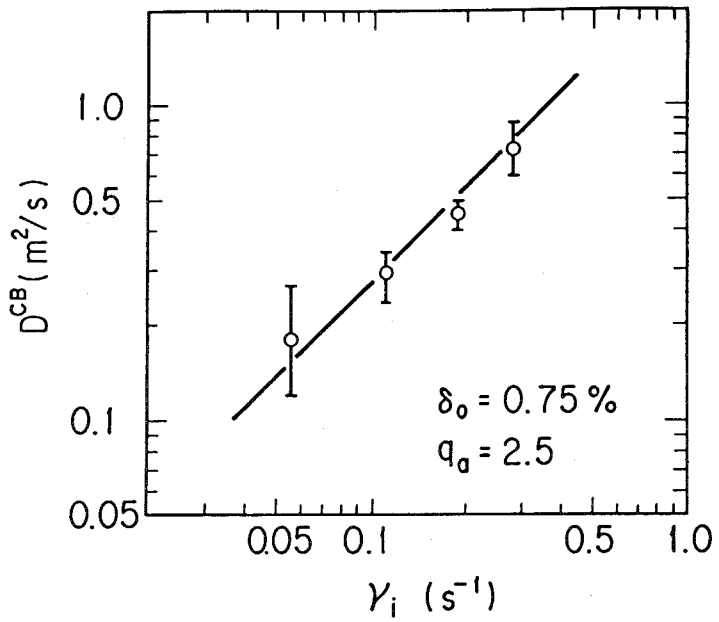

Fig.6-7 Diffusion coefficient D^{CB} versus collisionality for confined banana-trapped alpha particles with $E\sim3.5\,MeV$ at r/a = 0.6. Field ripple δ_0 = 0.75%, safety factor q_a = 2.5.

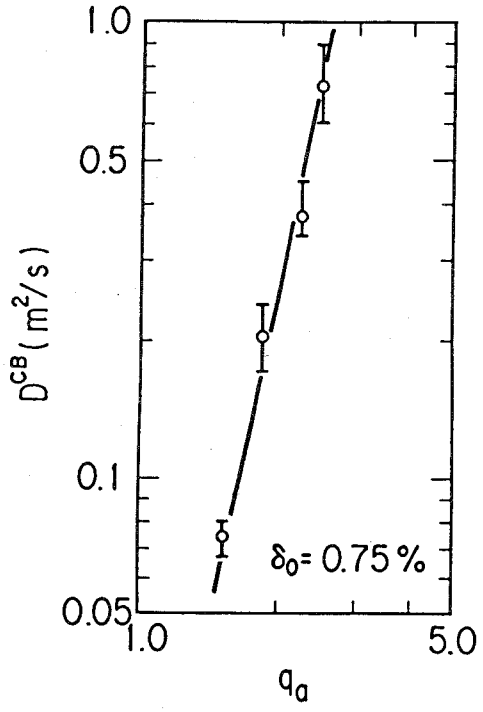

Fig.6-8 Diffusion coefficient D^{CB} versus safety factor q_a for confined banana-trapped alpha particles with $E\sim3.5\,MeV$ at r/a = 0.6. The field ripple δ_0 = 0.75%, collision frequency $\nu_i \sim 0.3$ s^{-1}.

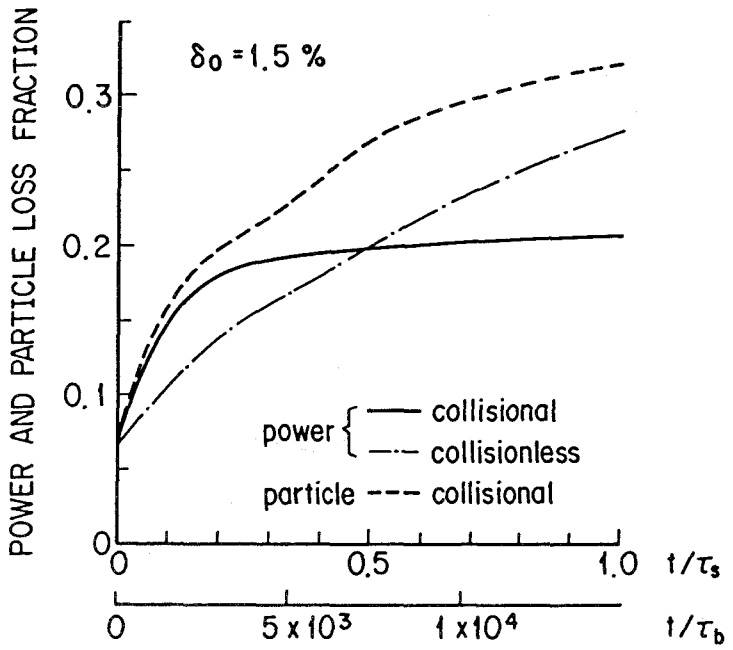

Fig.6-9 Evolution of time integrated power loss fraction of alpha particles during slowing down (——). Dashed line shows particle loss fraction. Power loss fraction in collisionless plasma is shown by dash-dotted curve. Calculation parameters as in Table 6-I with δ_0 = 1.5%.

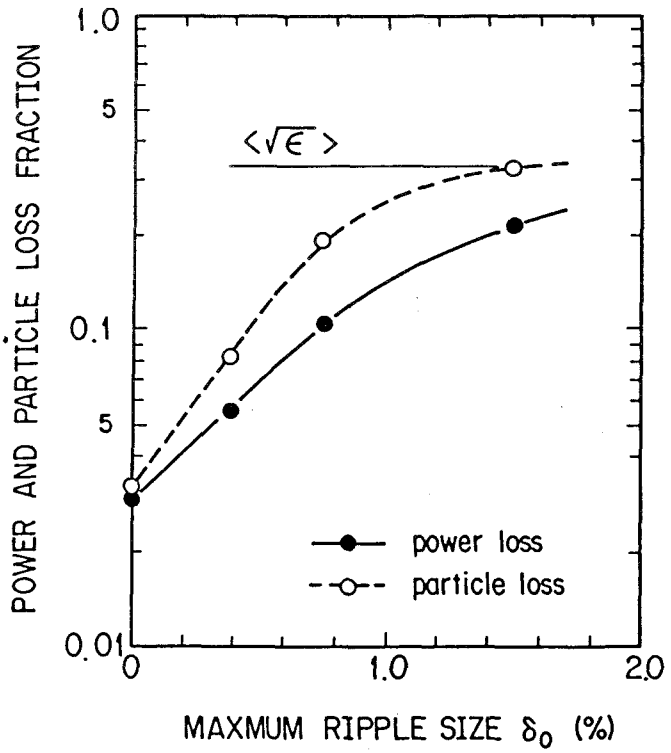

Fig.6-10 Collisional power loss fraction (—●—) and particle loss fraction (--O--) after τ_s as a function of the maximum ripple size δ_0. Calculation parameters as in Table 6-I.

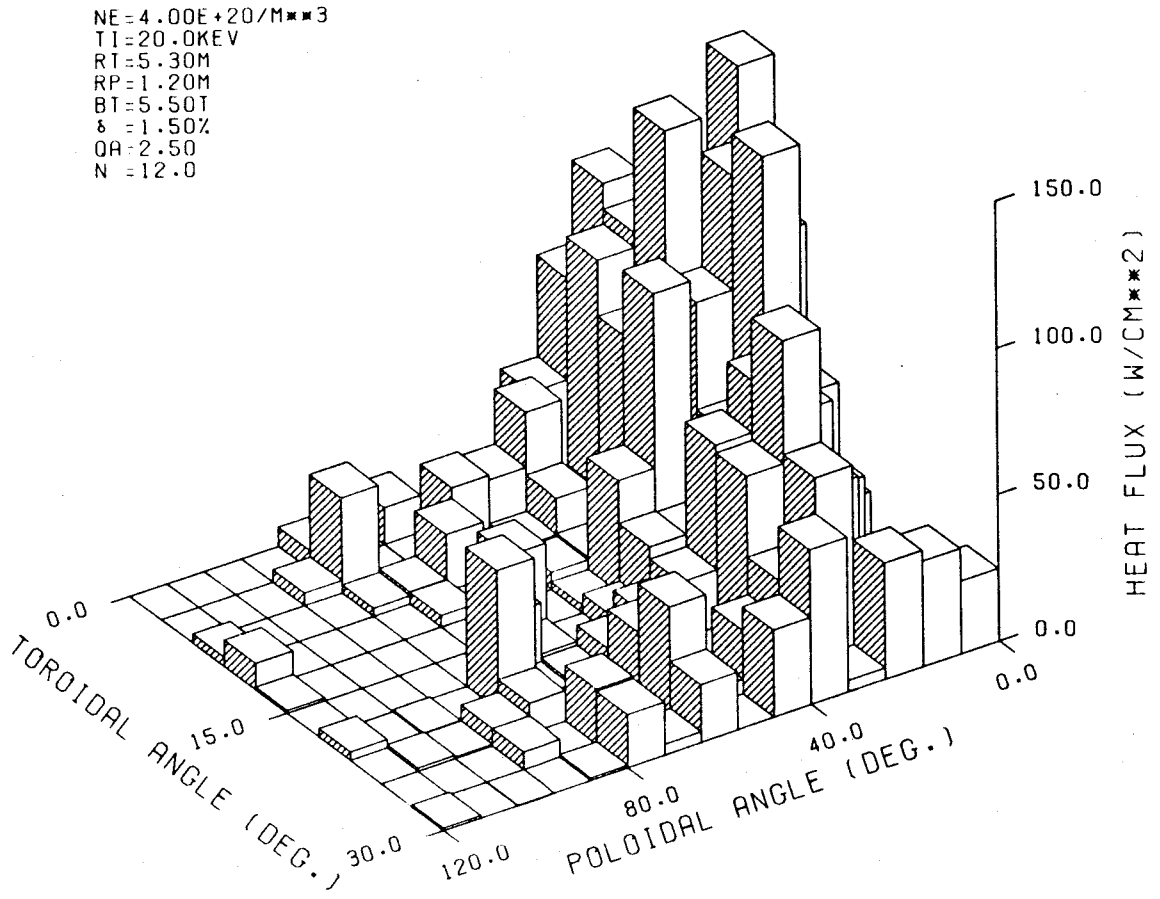

Fig.6-11 Spatial distribution of heat load on first wall due to loss alpha particles for δ_0 = 1.5%.

§ 7. Ripple Diffusion of Bulk Plasma Ions and Burn Control

7-1. Introduction

The discrete nature of toroidal field coils destroys the axisymmetry of a tokamak. This unperfect axisymmetry results in additional neoclassical transport phenomena such as ripple-trapped diffusion, ripple-plateau diffusion and banana-drift diffusion, which are investigated theoretically by a number of authors[1)-3)]. Recently, calculations of the ripple associated ion thermal conductivity have been made by using orbit-following Monte-Carlo code for tokamak[4)], stellarator[5)], and torsatron[6)] magnetic field configurations. Some of these results show that the numerically derived ion thermal conductivity is much smaller than the theoretical prediction, especially in the low collisionality regime.

Concerning the calculation results of tokamak, there have been two assignments for the reason of the small ion thermal conductivity. P.N. Yushmanov has supposed[7)] that this is accounted for the collisionless ripple detrapping which is described in §3-3. Another reason has been considered by K.C. Shaing and his co-worker[8)]. The usual $1/\nu_i$ scaling of ripple-trapped diffusion is valid only for ν_{eff} greater than the toroidal drift frequency ω_d for the energy of $E = 4 \sim 6T_i$ which is much greater than that given in the previous work[1)].

One of the most important problems in the design of a tokamak reactor[9)] is how to control the thermal excursion which may occur after the plasma is ignited. Recently, it has been shown theoretically that the

control of the burning plasma temperature is feasible by using a variable toroidal field ripple (δ_0 from $\sim 0.5\%$ to $\sim 2\%$ at most)[10),11)]. This was based on the assumption that the ripple induced ion thermal conductivity has a temperature dependence of $T_i^{7/2}$ [1)]. However, recent numerical study[4)] does not show that the ripple transport coefficient has such a strong T_i dependence, especially in the low collisionality (high temperature) regime. Therefore, it is doubtful whether this method is effective for burn control.

In the present paper we investigate the ripple diffusion process in detail to find out the conclusive reason for the small ripple ion thermal conductivity. Finally, basing on the numerically derived data for ripple diffusion coefficient, the necessary amount of field ripple to control the burning plasma is estimated.

7-1. Calculation model and assumptions

To evaluate the ion thermal conductivity by using an orbit-following Monte-Carlo code, plasma density and temperatures are given to be uniform in space. The magnetic field ripple in a tokamak can be given by eqs. (2-5-1) $\sim$ (2-5-3). In this section, however, for the convenience to compare the numerical results with analytical ones, we employ an artificial field ripple in which the collisionless ripple trapping nor the collisionless ripple detrapping hardly occurs. Such field ripple can be approximately given by solving the following equation,

$$\frac{\partial \delta}{\partial z} = -\frac{1}{N_t R_t q}\frac{1 - B_p'}{1 - A'(\alpha)} A'(\alpha)\, C(z), \qquad (7\text{-}1)$$

where z is the coordinate vertical to the mid-plane ($= r\sin\theta$), $A(\alpha)$ the function described by eq. (3-4), α the ripple-well parameter defined by eq. (3-1),

$$B_p' = \frac{r}{B_p}\frac{dB_p}{dr},$$

$$A'(\alpha) = \frac{\alpha}{A(\alpha)}\frac{dA(\alpha)}{d\alpha},$$

and

$$C(z) = \begin{cases} (z/\Delta z)^2 & \text{for } |z| < |\Delta z|, \\ 1.0 & \text{for } |z| \geqq |\Delta z|. \end{cases}$$

The solution of eq. (7-1) gives the effective ripple well δ_{eff} ($= 2.0\delta(r,\theta)A(\alpha)$) which is constant on the gradient-B drift trajectory in the region $|z| \geqq |\Delta z|$. The ripple on the mid-plane is given in the form

$$\delta(r,0) = \begin{cases} \delta_0 \left(\dfrac{R - R_b}{R_t + 1 - R_b}\right)^2 & \text{for } R > R_b, \\ 0 & \text{for } R < R_b. \end{cases}$$

With the field ripple derived by eq. (7-1), the toroidal, poloidal and radial components of the magnetic field are given by

$$B_\varphi = B_{\varphi 0}\frac{R_t}{R}\left[\, 1 + \delta(r,\theta)\cos N_t\varphi \,\right], \tag{7-2}$$

$$B_\theta = \frac{R_t}{R}B_p(r), \tag{7-3}$$

$$B_r = -\frac{1}{rR}\int_0^r \frac{\partial}{\partial \varphi}(r' B_\varphi)dr', \qquad (7\text{-}4)$$

respectively.

Note that the model ripple field described by eqs. (7-1) ~ (7-4) is divergence-free, but still non-curl-free. In order to test whether this model field carries validity or not, both ion thermal conductivities in the field with and without $\tilde{B}_r$ component were investigated. For all the plasma parameters in Table 7-I, however, we could not find out any significant difference between those results. The magnitude of the poloidal component of the ripple which makes the field to be curl-free as well as divergence-free, is of the same order with $\tilde{B}_r$. This indicates our model field is enough to describe the ripple transport in a tokamak.

Test particles with pitch angle and energy distribution corresponding to an isotropic Maxwellian are initially set on a specific magnetic surface and launched. The particles which mainly contribute to the ripple induced ion heat conductivity is in the energy range $4T_i < E < 6T_i$ and in the pitch angle region $|\zeta| < \zeta_\alpha$. It must be noted that the fraction of ions in the high energy tail of a Maxwell distribution $E > 4T_i$ is about 0.1 and $\zeta_\alpha \sim 0.2$. This indicates that a large number of test particles are necessary for the Monte-Carlo calculation with good accuracy. In our orbit-following Monte-Carlo code, about 10000 test particles are used. Moreover, for the improvement of calculation accuracy, we employ a kind of importance sampling method, in which test particles are uniformly distributed in the velocity space and weighted according to the local isotropic Maxwellian. With this method, the number of test particles which are effective for the ripple enhanced ion thermal conductivity can be improved by a factor of 4.

Since magnetic surfaces are assumed to be concentric circles, the ion thermal conductivity χ_i can be defined as a time differential coefficient of the minor radius variance, that is,

$$\chi_i = \frac{1}{2}\frac{d}{dt}\left[\sum_j \left(r_j - \langle r \rangle \right)^2 w_j / \sum_j w_j\right] \quad , \tag{7-5}$$

where

$$\langle r \rangle = \sum_j r_j w_j / \sum_j w_j ,$$

w_j is the energy density weigh of the j^{th} test particle.

7-3. Numerical results of ripple transport coefficient

The ion thermal conductivity defined by eq. (7-5) describes the total conductivity χ_i^T. The ripple-associated ion thermal conductivity χ_i^R is assumed to be separated from χ_i^T by

$$\chi_i^R = \chi_i^T - \chi_i^{NC} ,$$

where χ_i^{NC} is the ordinary neoclassical conductivity which is also calculated with the same orbit-following Monte-Carlo code by "switching-off" the ripple terms in the guiding center equations.

It has been considered that there are three kinds of ripple induced transport phenomena, diffusion due to collisional ripple trapping and detrapping, ripple-enhanced banana-drift diffusion and ripple-plateau diffusion, whose ion thermal conductivities are denoted as χ_i^{RT} , χ_i^{BD} , χ_i^{RP} ,

respectively, in the present paper.

Monte-Carlo simulations were performed for parameters of a large tokamak which are summarized in Table 7-I. In Fig.7-1, the numerically derived χ_i^R at $r/a = 0.8$ is plotted as a function of the ion-ion collision frequency ν_i, in which electron and ion temperatures are fixed at 5 keV.

It must be noted that in the ripple field described in §7-2, the ripple well region ($|\alpha| \leqq 1.0$) is congruous precisely to the region $R \geqq R_b$, and neither the ripple well nor the corrugation of B field occurs in the region $R < R_b$. Therefore, the contribution of the particles whose banana tips are out of the ripple-well region to the ripple plateau conductivity χ_i^{RP} can be neglected.

The contribution of banana-drift diffusion to χ_i^R was investigated analytically. For the parameters in Table 7-I, the analytical χ_i^R by Tsang also takes the value in the order of $10^{-3} \sim 10^{-4}$ m^2/s. Therefore, the numerical ion thermal conductivity χ_i^R shown in Fig.7-1 can be considered as the one due to collisional ripple-trapping and detrapping, $\chi_i^R \sim \chi_i^{RT}$.

For comparison, theoretical χ_i^{RT} derived by Connor and Hastie[2] is also shown in Fig.7-1 by the dash-dotted line. It is noticeable that the Monte-Carlo results approximate to the analytical values in the limit of high collisionality and that the difference between the analytical and the numerical results increases as ν_i decreases. The reason of this phenomena will be discussed in the next section in detail.

From the view points of the confinement of high temperature plasma or the control of burning plasma, the most interesting point in the ripple transport is the dependence of χ_i^R on plasma temperature. The numerical χ_i^R against T_i is shown in Fig.7-2. The theoretical χ_i^{RT} ($\propto T_i^{7/2}$) is also plotted in Fig.7-2. In the high temperature region (low collisionality),

the numerical χ_i^R is much less than the theoretical χ_i^{RT} and their difference increasés with T_i, which is the same phenomenon as in Fig.7-1. In the low collisionality regime, the ion thermal conductivity due to ripple-enhanced banana-drift[5] χ_i^{BD} is negligibly small and χ_i^{RP} is also much smaller than χ_i^{RT}. For $T_i < 1\ keV$, however, χ_i^{BD} turns to be greater than χ_i^{RT} and χ_i^{RP} is also in the same order with χ_i^{RT}. We suppose that this makes the numerical χ_i^R somewhat greater than the analytical χ_i^{RT} in the low temperature region. Because of the large error bar, the contributions of χ_i^{BD} and χ_i^{RP} to χ_i^R in this region are still unresolved.

The resulting ripple associated ion thermal conductivity χ_i^R shows a much weaker plasma temperature dependence of T_i^2 at most.

7-4. Reasoning for the small ripple transport coefficient

There have been two assignments for the reason why the numerically derived χ_i^R is much smaller than the theoretical one in the low collisionality regime. P.N. Yushmanov has supposed that this is accounted for the collisionless ripple-detrapping process described in §3. In the present field ripple given in §7-2, however, the collisionless ripple detrapping is sufficiently suppressed. Therefore, the numerically derived small ion thermal conductivity shown in the last section cannot be explained by this reason only. Recently, K. Shaing and J. Callen have pointed out that the particles with energy of $E = 4\sim6\ T_i$ in the tail of the distribution function make dominant contribution to neoclassical ripple transport coefficients. These particles trapped in a ripple well have very high gradient-B drift velocity and can hit the wall without detrapping from the ripple

well. Therefore, the usual $1/\nu_i$ scaling is valid only for $\nu_{eff} > \omega_d(E)$ at $E = 4 \sim 6\ T_i$, where ω_d is the toroidal drift frequency.

Here, we have performed some calculations to make it clear whether above mentioned reason is a conclusive one or not. Keeping the plasma parameters and the ripple distribution unchanged, the numerical ion thermal conductivities are calculated by changing the plasma minor radius, that is, by prolonging the drift time $\Delta r/v_d$ ($= 1/\omega_d$) where Δr is the minor radius difference between the initial magnetic surface to the first wall. The ratio of the numerically derived ion thermal conductivity to the theoretical one is shown in Fig.7-3 against the drift time for ν_i = 80.0 and 200.0. The ion thermal conductivity χ_i^R increases with the drift time to some extent though, it reaches a limit. The limiting values are shown in Fig.7-1 by the dashed curve. As is obvious from Fig.7-1, the limiting values are still much smaller than the theoretical values especially in the low collisionality regime. This indicates that there is another reason for the small ion heat conductivity, which is more important than the former two assignments. As discussed previously the numerical χ_i^R can be considered as χ_i^{RT}, it is inferred from Fig.7-3 that there is another mechanism which make the ripple trapping rate and/or the effective random walk step size to be much smaller than those based on an analytical model given by Stringer[1].

In order to investigate the basic process of ripple diffusion, we have measured the correlation time. For the convenience of calculations, the distribution of ripple is given so that te effective ripple well depth is spatially uniform in the plasma. The energy of the test particles is monocromatic ($E = 5T_i$) and their pitch angle distribution is given to be isotropic. The correlation time is an important measure for the diffusion

process, which is defined by the e-folding time of the correlation function given by

$$f_c(\tau) = \frac{<\xi(t)\xi(t+\tau)>}{<\xi(t)^2>} , \tag{7-6}$$

where $< >$ indicates the time average. Since the correlation time of the ripple diffusion due to ripple-trapping is the average captivity time in a ripple well, we assume the function $\xi(t)$ in eq.(7-6) as

$$\xi(t) = \begin{cases} 1.0 & \text{for the time while particles are trapped in a ripple well,} \\ 0.0 & \text{for the time while they are not.} \end{cases}$$

Here, when the normalized well depth d_w becomes less than unity, we judge that they are captured by ripple. The well depth d_w is defined by

$$d_w = \frac{m_t/2\, v_\parallel{}^2 + \psi(\varphi) - \psi(\varphi_1)}{\Delta\psi} , \tag{7-7}$$

where ψ, $\Delta\psi$ and φ_1 are the same as those in § 5-4.

The correlation time τ_c is shown in Fig.7-4 as a function of the ripple bounce time τ_{rb} (eq.(3-7)), where τ_{rb} and τ_c are normalized by the effective collision time

$$\tau_{eff} \simeq \frac{\delta_{eff}}{\nu_i} . \tag{7-8}$$

and by the average effective collision time

$$<\tau_{eff}> \simeq \frac{\tau_{eff}}{2} , \tag{7-9}$$

respectively. Contrary to the theoretical prediction, the numerical τ_c

shows a strong dependence on τ_{rb} and takes a value much smaller than $<\tau_{eff}>$ in the low collisionality regime. In the high $\tau_{rb}/<\tau_{eff}>$ region, τ_c approximates to $<\tau_{eff}>$, which is also confirmed by the data for stationary orbits in Fig.7-4. The ion thermal conductivity in a ripple field deduced from the Monte-Carlo code shown in Fig.7-1 and 7-2 can be well explained qualitatively by the above mentioned nature of τ_c since

$$\chi_i^{RT} \sim D_i^{RT} \sim \frac{(\upsilon_d \tau_c)^2}{\tau_c} = \upsilon_d{}^2 \tau_c \quad .$$

The theoretical ion thermal conductivity has been derived from a bounce averaged Fokker-Planck equation with the assumption that the bounce frequency of a ripple-trapped particle ω_{rb} is much greater than the effective collision time ν_{eff} ($= 1/\tau_{eff}$). In a rippled toroidal field, however, the Fokker-Planck equation cannot be bounce averaged for the particles with well depth $d_w = 1.0$ (barely ripple-trapped particles), because the residence time of these particles in the vicinity of a ripple peak point $\varphi = \varphi_2$ (see §5-4) diverges. In order to look into this effect, correlation time is calculated for the case (case ①) in which the criterion of normalized well depth for ripple-trapping is artificially reduced, that is, the particles are recognized to be trapped by ripple when their $d_w \leqq S_{trp}$ with $S_{trp} = d_w^* < 1.0$ (case ②). Results are shown in Fig.7-5 by the solid line. The correlation time with an unartificial criterion for ripple-trapping judgement $S_{trp} = 1.0$ and with the well depth $\Delta\psi = d_w^* \Delta\psi^*$ where $\Delta\psi^*$ is the well depth for the case ①, is also plotted in Fig.7-5 by the dashed line. The correlation time with artificial criterion for ripple trapping (case ①) shows a very sharp change near $d_w^* = 1.0$. While, $\tau_c/<\tau_{eff}>$ with an unartificial ripple-trapping criterion (case ②) does not show any signif-

icant change against the well depth. The particle with $d_w = 1.0$ stays extremely long time near a ripple peak point where the potential difference $\psi_t - \psi(\varphi \sim \varphi_2) \ll \Delta\psi$ with ψ_t and $\psi(\varphi)$ given by eq. (5-5) and (5-6), respectively. Consequently, the singular orbit with $d_w = 1.0$ may work as a barrier on a particle to be deeply trapped in a ripple well. This is inferred from the comparison of those two lines shown in Fig.7-5. If particles are prevented to be deeply trapped in a ripple-well, their walk step or the transport coefficient is effectively reduced.

7-5. Burn temperature control using toroidal field ripple

Recently, assuming the theoretical ripple enhanced ion thermal conductivity, feasibility of burn temperature control by using a variable toroidal field ripple is demonstrated by several authors[10),11)]. As discussed in the previous subsections, however, the ripple induced ion thermal conductivity is much smaller than the theoretical prediction especially in the low collisionality regime and has an ion temperature dependence of T_i^2 at most. These results are very favorable for the plasma heating to ignition though, they are unfavorable for the application of ripple transport to the burn control.

In the present section, basing on the numerically derived ion thermal conductivity, the necessary amount of field ripple for the control of burning temperature is estimated by solving a simple power balance with an assumption of a zero-dimensional plasma model. The power balance in a burning plasma can be written in the form

$$P_f - P_{\chi e} - P_{\chi i} - P_\alpha - P_{br} - P_{sy} = 0, \qquad (7\text{-}10)$$

where P_f, $P_{\chi e}$, $P_{\chi i}$, P_α, P_{br} and P_{sy} are the fusion power, the electron conduction loss, the ion conduction loss, the alpha-particle loss due to field ripple, the bremsstrahlung radiation loss[12], and the synchrotron radiation loss[13], respectively. Provided that both spatial distributions of plasma density and temperature are parabolic, the fusion power is given by[14]

$$P_f = 1.8\, \bar{n}_D \bar{n}_T <\sigma v>_{DT} ,$$

where $\bar{n}_D$, $\bar{n}_T$ and $<\sigma v>_{DT}$ are the average deuteron density, the average tritium density and the fusion reaction rate at the average ion temperature ($T_i = \bar{T}_i$). The electron and ion conduction losses $P_{\chi e}$ and $P_{\chi i}$ are estimated at $r = 0.7a$ with electron and ion thermal conductivities

$$\chi_e = \frac{5\times 10^{19}}{\bar{n}_e} \quad m^2/s,$$

and

$$\chi_i = 3\,\chi_i^{NC} + \chi_i^{RT} ,$$

respectively. The theoretical ion heat conductivity in an axisymmetric system[15] is employed for χ_i^{NC} and the numerically derived ion heat conductivity for χ_i^{RT}. The ripple induced alpha-particle loss during slowing-down P_α is also estimated numerically (see §6).

The relation between the burning plasma temperature T_B and the maximum field ripple δ_0 solved by eq. (7-10) is shown in Fig.7-6. The dashed line in Fig.7-6 shows the burning temperature given by eq. (7-10) with theoretical ion thermal conductivity[2], which fairly agrees with the result solved by a detailed one dimensional tokamak simulation code[11]. According to the present numerical study, rather large values of δ_0 ($\sim$ 5%) are required in

order to achieve the appropriate burning temperature T_B ($\sim$ 15keV).

7-6. Concluding remarks

Ripple transport has been investigated numerically by an orbit-following Monte-Carlo code. Conclusions obtained in the present investigations are summarized as follows:

(1) It is found that the collision frequency transition from the collisional ($\chi_i^{RT} \propto 1/\nu_i$) to the collisionless ($\chi_i^{RT} \propto \nu_i$) regime for the numerically derived ion thermal conductivity occurs at a frequency much greater than the theoretical prediction. Consequently, numerical χ^{RT} becomes much smaller than the theoretical one, especially in the low collisionality regime.

(2) The resulting ripple induced ion heat conductivity shows a much weaker temperature dependence of T_i^2 at most.

(3) For the reasons of this small ion heat conductivity in the low collisionality regime, there have been two assignments, the collisionless ripple detrapping and the high drift frequency ω_d for particles with $E = 4$ *to* $6T_i$ which mainly contribute to the ion heat transport. Besides these two reasons, it is found that the singular orbit of barely ripple-trapped particles with $d_w = 1.0$ may prevent them from being deeply trapped in a ripple well and may reduce the ripple transport.

(4) A simple study basing on the power balance of burning plasma with numerically derived ion heat conductivity shows that rather large values of δ_0 ($\sim$ 5%) are required for the control of burning plasma

temperature T_B ($\sim$ 15 keV).

References

1) T.E. Stringer: Nucl. Fusion 12 (1972) 689.

2) J.W. Connor, R.J. Hastie: Nucl. Fusion 13 (1973) 221.

3) K.T. Tsang: Nucl. Fusion 17 (1977) 557.

4) K. Tani, H. Kishimoto, S. Tamura: *Proc. 8th Int. Conf. on Plasma Physics and Controlled Nuclear Fusion Research*, Brussels, 1980 vol.1 IAEA, Vienna (1981) 631.

5) A.H. Boozer, G. Kuo-Petravic: PPPL Report-1703 (1980).

6) R.E. Potok, P.A. Polizer, L.M. Lidsky: Phys. Rev. Lett. 45 (1980) 1328.

7) P.N. Yushmanov: Nucl. Fusion 22 (1982) 315.

8) K.C. Shaing, J.D. Callen: Nucl. Fusion 22 (1982) 1061.

9) INTOR GROUP: International Tokamak Reactor, Zero phase (Rep.Int. Tokamak Reactor Workshop Vienna, 1979), IAEA, Vienna (1980) 247.
INTOR GROUP: International Tokamak Reactor, Phase one (Rep.Int. Tokamak Reactor Workshop Vienna, 1981), IAEA, Vienna (1982) 133.

10) T.W. Petrie, J.M. Rawls: Nucl. Fusion 20 (1980) 419.

11) M. Sugihara, M. Kasai, T. Tazima, T. Tone, K. Maki: J. Nucl. Sci. Technol. 17 (1980) 729.

12) L.J. Spitzer: "*Physics of Fully Ionized Gases*", Interscience Publishers, New York (1962) 149.

13) M.N. Rosenbluth: Nucl. Fusion, 10 (1970) 340.

14) JAERI Fusion Research and Development Center, INTOR Workshop Report,

Group 1, JAERI-M 8621 (1980).

15) A.A. Galeev, R.Z. Sagdeev: Sov. Phys. JETP 26 (1968) 223.

Table 7-I Plasma parameters

major radius	$R_t = 3.03$ m
minor radius	$a = 0.95$ m
toroidal field	$B_t = 4.5$ T
plasma temperature	$T_e(r) = T_{e0}$ (uniform)
	$T_i(r) = T_{i0}$ (uniform)
	$T_{e0}, T_{i0} = 1.0 - 20.0$ keV
plasma density	$n_e(r) = n_{e0}$ (uniform)
	$n_{e0} = 1.0 \times 10^{19} - 5.0 \times 10^{20}$ m^{-3}
plasma current	$j_p(r) = j_0(1-(r/a)^2)$
	$j_0 = 4.73/q_a$ MA/m^2
safety factor	$q_a = 3.5$
plasma ion species	H^+
effective Z	$Z_{eff} = 1.0$ (uniform)
number of toroidal field coils	$N_t = 18$

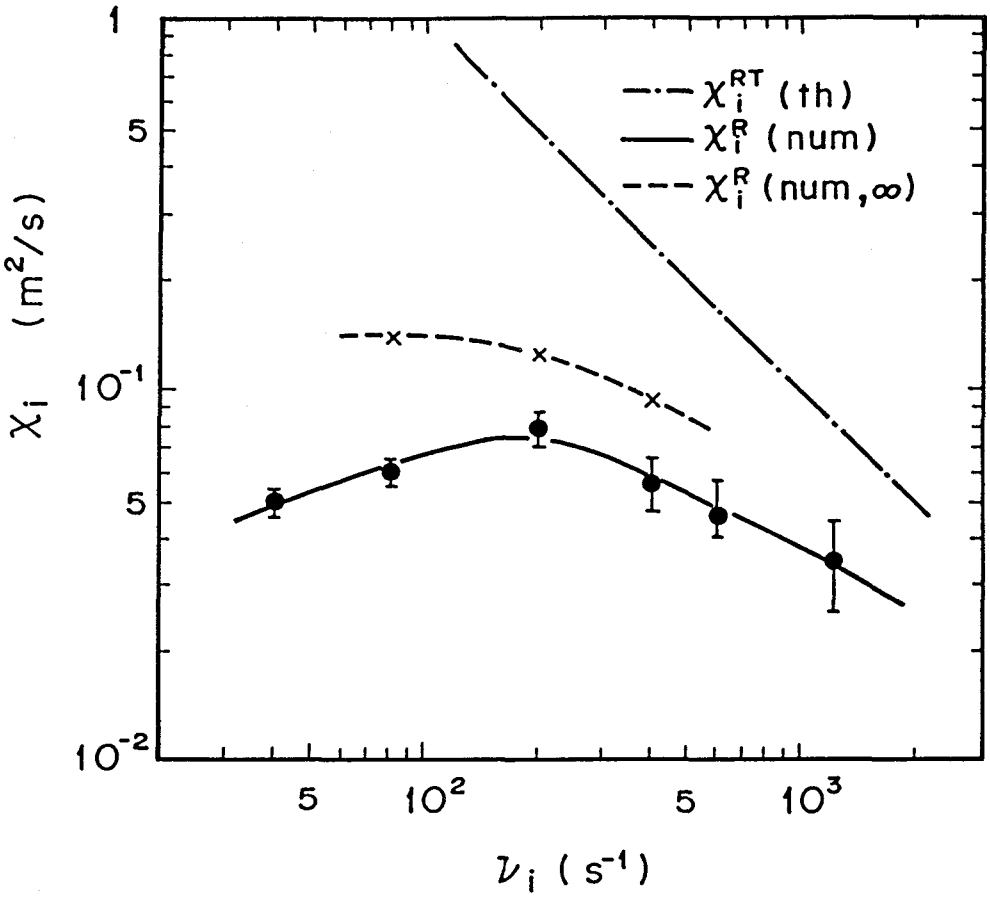

Fig.7-1 Ion thermal conductivity versus collisionality. The solid line is the numerically derived χ_i^R in a plasma with finite minor radius and the dashed curve is the one in the limit of large minor radius. The theoretical χ_i^R is shown by the dash-dotted line. Initial radial position of ions is r/a=0.8, T_i=T_e=5keV and the muximum field ripple δ_0=1%. Other parameters as in Table 7-I.

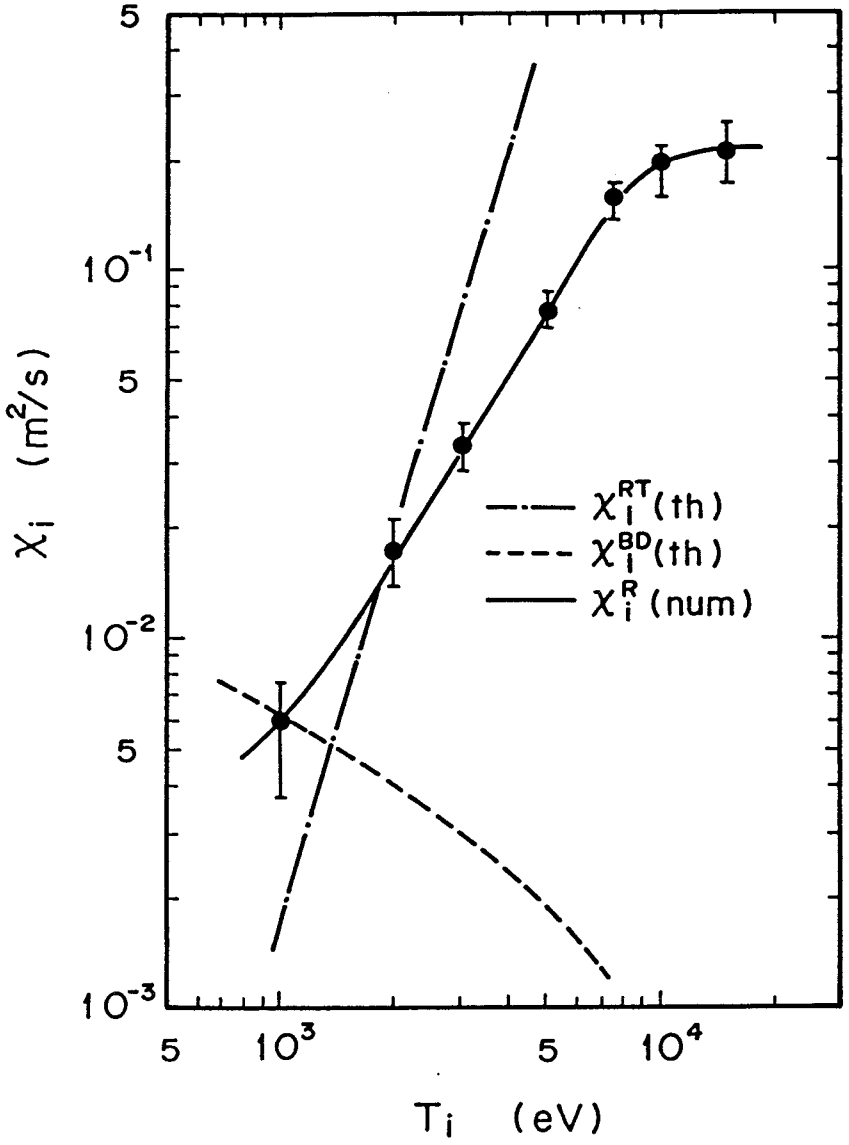

Fig.7-2 Ion thermal conductivity versus plasma ion temperature. The solid line indicates the numerical χ_i^R, and the dash-dotted line the theoretical one. The dashed curve shows the theoretical ion thermal conductivity due to banana drift by Tsang. Initial radial position of ions is r/a=0.8, n_e=5×$10^{19}m^{-3}$ and the muximum field ripple δ_0=1%. Other parameters as in Table 7-I.

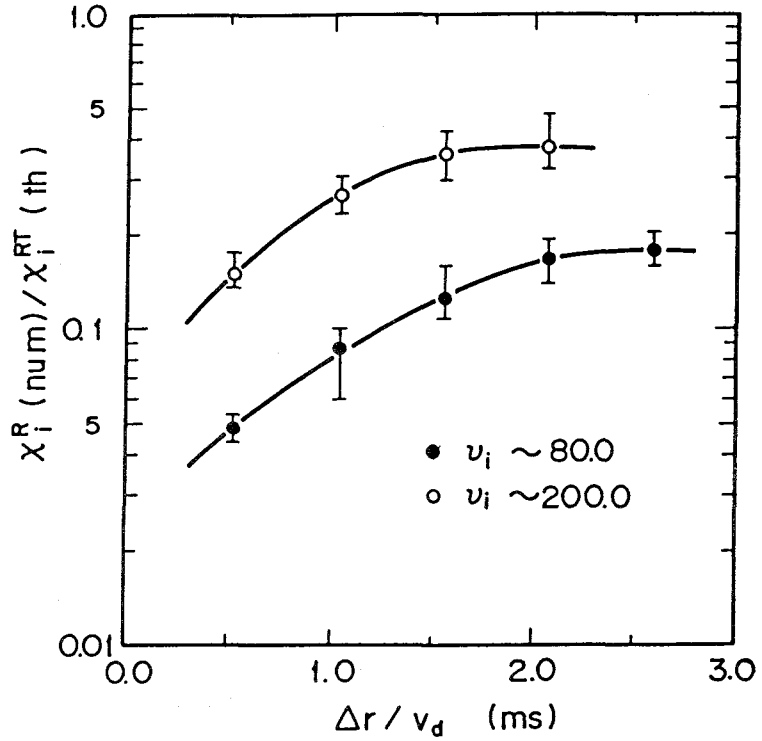

Fig.7-3 Numerical ion thermal conductivity normalized by the theoretical one as a function of the drift time for ν_i = 80.0 and 200.0.

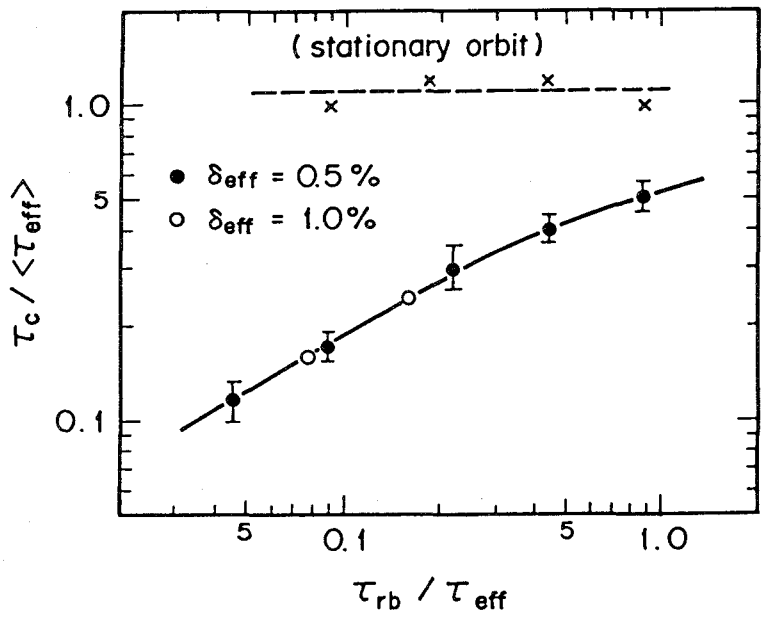

Fig.7-4 Numerically derived correlation time as a function of ripple bounce time. The dashed line shows the results for stationary orbit in which the orbit calculations are "switched-off".

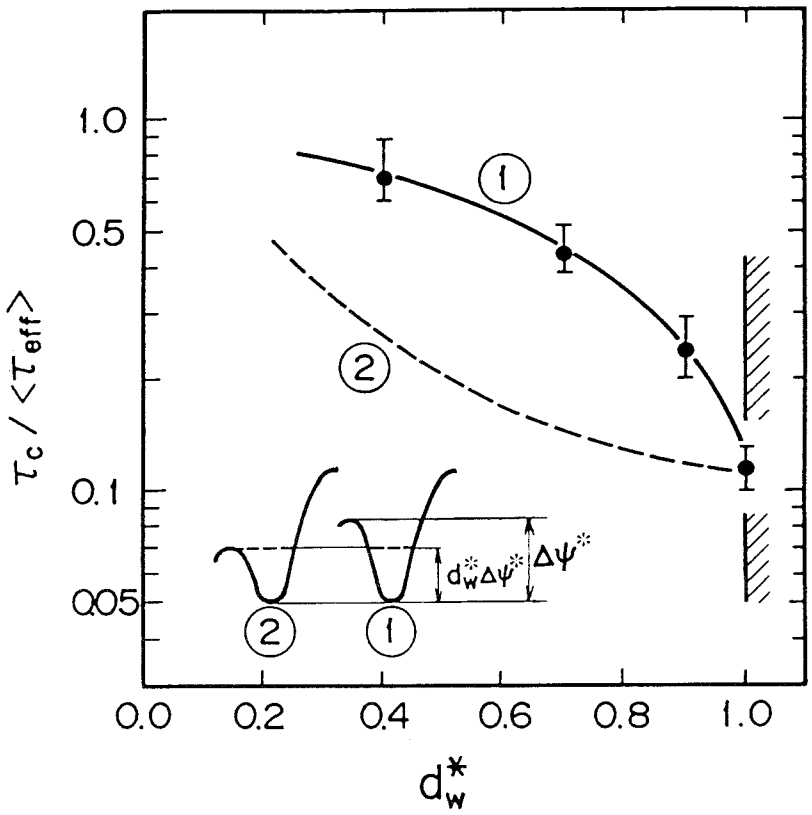

Fig.7-5 Correlation time versus artificial ripple-trapping criterion. (case ①). The dashed line (case ②) is the one with an unartificial criterion.

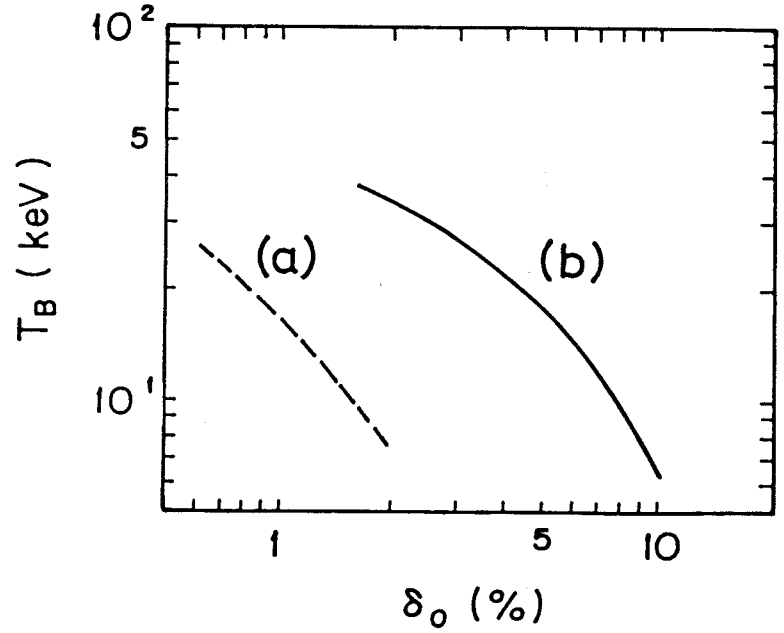

Fig.7-6 Burning temperature versus maximum ripple size with (a) theoretical and (b) numerical χ_i^{RT} .

§ 8. Concluding Remarks

Studies on the confinement of fast ions produced by a quasi-perpendicular neutral beam injection and suprathermal charged fusion products in a rippled toroidal field during slowing down have been extensively performed by means of a newly developed orbit-following Monte-Carlo simulation code. The ripple-associated neoclassical transport coefficient has been also investigated by the same code.

It has been found that the collisionless behaviors of fast ions, the collisionless ripple trapping, collisionless ripple detrapping and the ripple-enhanced banana drift, have essential roles on the loss process of fast ions in a toroidal field ripple. The collisionless ripple trapping occurs in a toroidal field ripple which becomes higher with the displacement vertical to the mid-plane. The pitch-angle width of the collisionless ripple-trapping region is proportional to the gradient-B drift velocity or the banana size of fast ions. The ripple-enhanced banana drift of fast ions is also proportional to their banana size and inversely proportional to the square root of the local field ripple at their banana tip in the region $|\alpha| < 1.0$. The collisionless ripple trapping and the ripple-enhanced banana drift produce a large number of loss bands in the velocity space (in the pitch angle region $|\zeta| < \zeta_\alpha$) and strongly disturb the banana loss cone. It has been considered that the ripple loss cone is the pitch-angle region $|\zeta| < \sqrt{\delta_{eff}}$. However, most of fast ions with pitch angle $|\zeta| < \zeta_\alpha$ are lost in a time interval much shorter than the slowing-down time. Consequently, a kind of loss cone is effectively formed in this

pitch angle region.

Ripple-associated loss dominates the loss of fast ions produced by a quasi-perpendicular neutral beam injection in a reactor-grade tokamak. In order to hold down the ripple loss of fast ions to be less than 10% of the total, $|90 - \theta_{inj}| > 20^{\circ}$ and $\delta_0 < 0.5\%$ for the typical plasma parameters. Banana-drift loss is significantly enhanced by the toroidal field ripple not only in the counter-injection but also in the co-injection. The ripple-trapped loss does not show any pronounced difference between co- and counter-injection. Hence, in the presence of ripple no remarkable advantage of co-injection can be expected in a quasi-perpendicular neutral beam injection.

One of the essential features of the ripple-trapped loss is the localization of the loss particles in a specific area on the first wall. This causes a serious problem of heat loading on the first wall, especially in the long pulse NBI heating. Localized heat load due to ripple-trapped loss ions may reach a magnitude of $1MW/m^2$ for the next-generation tokamak.

Although the initial energy of charged fusion products is very high, collisional effects, the slowing down as well as the pitch angle scattering, dominate their ripple loss. Even in the presence of ripple, the energy of alpha particles is well confined in a plasma. The ripple enhanced power loss for $\delta_0 = 1\%$ is about 10% of the total. The fraction of the particle loss is about $1.5 \sim 1.8$ times as large as that of power loss for $0.4\% < \delta_0 < 1.5\%$. The ripple-enhanced banana drift dominates the loss process of alpha particles and only a trace amount of ripple-trapped loss particles is observed. The diffusion coefficient for confined banana particles with pitch angle $\zeta > \zeta_c$ is approximately given by

$$D^{CB} = \pi (N_t/\sin\theta_b)^3 (q/\varepsilon)^5 \sin^2 2\zeta (\rho\delta)^2 \nu_i .$$

For the plasma parameters of a tokamak reactor with $\delta_0 \sim 1\%$, D^{CB} of 3.5 *MeV* alpha particles is of the order of 10^{-1} m^2/s , which is much greater than the axisymmetric neoclassical diffusion and much less than the ripple-plateau diffusion. It is shown in the present investigation that there is a possibility of realizing the design of tokamak reactors with a realistic field ripple of $\delta_0 \sim 1\%$, permitting 10% power loss of alpha particles.

It is found that the collision frequency transition from the collisional ($\chi_i^{RT} \propto 1/\nu_i$) to the collisionless ($\chi_i^{RT} \propto \nu_i$) regime for the numerically derived ion thermal conductivity occurs at a frequency much greater than the theoretical prediction. Consequently, numerical χ^{RT} becomes much smaller than the theoretical one, especially in the low collisionality regime. The resulting ripple induced ion heat conductivity shows a much weaker temperature dependence of T_i^2 at most. Besides the two reasons of this small ion heat conductivity in the low collisionality regime, the collisionless ripple detrapping and the high drift frequency ω_d for particles with $E = 4$ *to* $6T_i$ which mainly contribute to the ion heat transport, it is found in the present investigation that the singular orbit of barely ripple-trapped particles may prevent them from being deeply trapped in a ripple well and may reduce the ripple transport. A simple study basing on the power balance of burning plasma with numerically derived ion heat conductivity shows that rather large values of δ_0 ($\sim 5\%$) are required for the control of burning plasma temperature T_B ($\sim$ 15 *keV*).

Acknowledgements

The author would like to express his sincere gratitude to Prof. H. Akimune of Kyoto University who introduced him to the field of thermonuclear fusion research and has kept encouraging him. He also wishes to thank Prof. K. Watanabe, Prof. T. Sekiya and Prof. K. Sumita of Osaka University for the helpful advice and guidance during the preparation of this thesis.

The author is also grateful to Dr. Y. Iso, Head of Fusion Research and Development Center in JAERI, Dr. K. Tomabechi, Head of Division of Large Tokamak Development, and Dr. M. Yoshikawa, Deputy Head of Division of Large Tokamak Development, for their continuous encouragement.

The author is greatly indebted to Dr. Kishimoto for the continuing guidance and helpful advice. He also would like to express his special appreciation to Dr. M. Azumi for his original development of the Monte-Carlo code and useful discussions through the course of this work. He wishes to thank Dr. S. Tamura for drawing his attention to this problem. Many fruitful and stimulating discussions with Drs. T. Takizuka, T. Tuda, K. Itoh, T. Takeda and other members of Plasma Theory Laboratory of JAERI are gratefully acknowledged.

He also expresses his gratitude to Prof. K. Miyamoto of University of Tokyo and Dr. M. Ohnishi of Kyoto University for stimulating and useful discussions on the problem of ripple loss of alpha particles. He would like to express his appreciation to Dr. J. Rome of Oak Ridge National Laboratory for his kind suggestion to obtain divergence-free as well as curl-free ripple field. It is a pleasure to acknowledge the hospitality

and encouragement of Drs. S. Seki, Y. Shimomura, T. Hiraoka and all the colleagues of Experiment and Analysis Group of JT-60.

Mr. H. Enomoto, Mrs. T. Toyoda of Kozo Keikaku Engineering Inc. and Mr. T. Osame of Nuclear Data Corporation are acknowledged for their computational support. The author would like to thank Dr. M. Tomiyama of JAERI computer center for his kind support of word processor system (ATF). The most of this work has been made by use of the computer system at JAERI computer center. He would like to express his appreciation to all the stuffs of the computer center.

Appendix: Fast Ion Behavior near Banana Tip in a Toroidal Field Ripple

Provided that $B_\theta \ll B_\varphi$ and $v_\parallel \ll v_\perp$, the guiding center eqs. (2-9-1)-(2-9-4) are represented by

$$\frac{dv_\parallel}{dt} = -\frac{\mu_m}{m_t}\frac{B_t R_t}{R^2}\left[b_\theta \sin\theta - \delta(r,\theta) N_t \sin N_t\varphi\right], \tag{A-1}$$

$$\frac{dr}{dt} = \frac{\mu_m}{e}\frac{\sin\theta}{R}, \tag{A-2}$$

$$\frac{d\theta}{dt} = \frac{\mu_m}{eZ_t}\frac{1}{r^2}\left(1 - R_t/R\right) + \frac{b_\theta}{r}v_\parallel, \tag{A-3}$$

$$\frac{d\varphi}{dt} = \frac{1}{R}v_\parallel, \tag{A-4}$$

By introducing a normalized time $\tau = t/C_t$ where $C_t = \sqrt{2/N_t}R/v_\perp$ and a toroidal angle with the coil pitch periodicity $\Phi = N_t\varphi$, the guiding center eqs. (A-1)-(A-4) can be reduced in the vicinity of a banana tip to

$$\frac{d^2\Phi}{d\tau^2} + c_0 + \varepsilon_0\tau + \varepsilon_1(\Phi - \Phi_0) - \left[c_1 + \varepsilon_2\tau + \varepsilon_3(\Phi - \Phi_0)\right]\sin\Phi = 0, \tag{A-5}$$

where

$$c_0 = b_\theta \sin\theta,$$

$$c_1 = N_t\delta(r,\theta),$$

$$\varepsilon_0 = \frac{R_t}{R^2}\left(\frac{1}{q} - r\frac{dq}{dr}\sin^2\theta\right)v_d C_t,$$

$$\varepsilon_1 = \frac{R_t}{R^2}\frac{r}{N_t q^2}\cos\theta,$$

$$\varepsilon_2 = N_t \left(\frac{\partial \delta}{\partial r} \sin\theta + \frac{\partial \delta}{\partial \theta} \frac{\cos\theta}{r} \right) v_d C_t ,$$

$$\varepsilon_3 = \frac{\partial \delta}{q \partial \theta} , \quad \text{and}$$

$$v_d = \frac{E}{e Z_t R_t B_t} .$$

The solution of eq. (A-5) is approximately given by

$$\tau(\Phi) = Sn \int_{\Phi_0}^{\Phi} d\Phi / \sqrt{2\,[U(\Phi_0) - U(\Phi)]} , \qquad (A\text{-}6)$$

where

$$U(\Phi) = c_0\Phi + c_1\cos\Phi + \varepsilon_0 \Lambda_1(\Phi, \Phi_0) + \varepsilon_1 (\Phi^2/2 - \Phi_0\Phi)$$

$$- \varepsilon_2 \Lambda_2(\Phi, \Phi_0) - \varepsilon_3 [\sin\Phi - \sin\Phi_0 - (\Phi - \Phi_0)\cos\Phi] ,$$

$$\Lambda_1(\Phi, \Phi_0) = \int_{\Phi_0}^{\Phi} \tau^*(\Phi)\, d\Phi ,$$

$$\Lambda_2(\Phi, \Phi_0) = \int_{\Phi_0}^{\Phi} \tau^*(\Phi) \sin\Phi \, d\Phi$$

$$\tau^*(\Phi) = \int_{\Phi_0}^{\Phi} d\Phi / \sqrt{2\,[U^*(\Phi_0) - U^*(\Phi)]} ,$$

$$U^*(\Phi) = c_0\Phi + c_1\cos\Phi + \varepsilon_1 (\Phi^2/2 - \Phi_0\Phi) - \varepsilon_3 [\sin\Phi - \sin\Phi_0 - (\Phi - \Phi_0)\cos\Phi] ,$$

$Sn = 1.0$ for $\Phi > \Phi_0$ and -1.0 for $\Phi < \Phi_0$, and Φ_0 is the toroidal angle at the banana tip.

The pitch-angle band width $\Delta\zeta$ for collisionless ripple-trapping is approximately given by

$$\Delta\zeta \simeq \frac{1}{2}(b_\theta \sin\theta_b - N_t \delta \sin\Phi_b)\Delta\Phi \cos\zeta, \qquad (A\text{-}7)$$

where ζ is the pitch angle of fast ion and $\Delta\Phi$ is the toroidal angle difference between the banana tips with and without banana size as shown in Fig.A-1. In case of small $|\alpha|$ ($|\alpha| \ll 1.0$), $\Delta\Phi$ can be described by

$$\Delta\Phi \simeq (\varepsilon_0\kappa_1 - \varepsilon_2\kappa_2)/[\sqrt{c_1}u(\Phi)], \qquad (A\text{-}8)$$

where

$$u(\Phi) = dU(\Phi)/d\Phi$$

$$\kappa_1 = \sqrt{c_1}\Lambda_1(\Phi_s, \Phi_b), \text{ and}$$

$$\kappa_2 = \sqrt{c_1}\Lambda_2(\Phi_s, \Phi_b).$$

Here, Φ_s and Φ_b are the toroidal angles satisfying the following conditions:

$$U(\Phi) = 0, \quad \text{and} \quad U(\Phi_s) = U(\Phi_b).$$

For a large value of the safety factor q, the parameter ε_1 and ε_3 become sufficiently small and κ_1 and κ_2 are described as functions of α only.

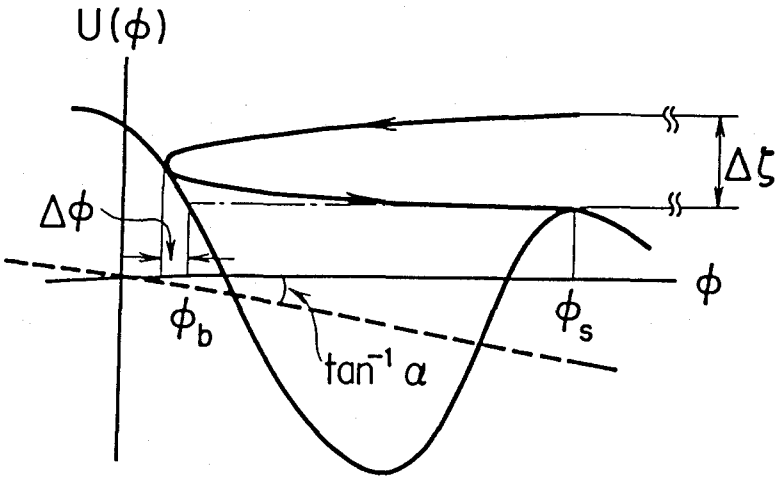

Fig.A-1 Fast ion orbit near banana tip in a ripple field

List of Publications

(1) K. Tani, H. Kishimoto, S. Tamura: "*Ripple Loss of Fast Ions in a Large Tokamak*", Proc. 9th European Conf. on Contolled Fusion and Plasma Physics, Oxford, Vol 1 (1979) 157.

(2) K. Tani, H. Kishimoto, S. Tamura: "*Toroidal Ripple Effects on Fast Ion Behavior and Burn Control in Tokamaks*", Proc. 8th Int. Conf. on Plasma Physics and Controlled Nuclear Fusion Research, Brussels, 1980 Vol.1 IAEA, Vienna (1981) 631.

(3) K. Tani, M. Azumi. H. Kishimoto, S. Tamura: "*Effects of Toroidal Field Ripple on Fast Ion Behavior in a Tokamak*", J. Phys. Soc. Japan 50 (1981) 1726.

(4) T. Tone, T. Yamamoto, K. Tani, K. Kitamura: "*Effects of Toroidal Field Ripple on the Loss of Energetic Injected Ions and Toroidal Coil Configuration in a Tokamak Reactor*", J. Nucl. Sci. Technol. 18 (1981) 684.

(5) K. Tani, H. Kishimoto: "*Localized Heat Deposition on Tokamak First Wall due to Ripple-Trapped Loss of Suprathermal Ions Produced by NBI*", Nucl. Fusion 22 (1982) 1108.

(6) K. Miyamoto, M. Sugihara, K. Ueda, S. Yamamoto, M. Maeno, S. Sengoku, N. Suzuki, S. Kasai, M. Nagami, T. Tuda, K. Tani, M. Okamoto. and N. Fujisawa: "*Japanese Contributions to IAEA INTOR Workshop, Phase IIA Chapter IV : Plasma Confinement and Control*", JAERI-M 82-171 (1982).

(7) K. Tani, T. Takizuka, M. Azumi, H. Kishimoto: "*Ripple Loss of Suprathermal Alpha Particles during Slowing Down in a Tokamak Reactor*", Nucl. Fusion 23 (1983) 657.